

RAPID DETECTION OF POLYCYCLIC AROMATIC HYDROCARBONS FROM COOKING
OIL USING ON-CHIP ULTRA-THIN LAYER CHROMATOGRAPHY WITH SURFACE
ENHANCED RAMAN SPECTROSCOPY

by

JING CHEN

(Under the Direction of YAO-WEN HUANG)

ABSTRACT

Polycyclic aromatic hydrocarbons (PAHs) are a class of potent environmental pollutants which exhibit carcinogenic, mutagenic, and teratogenic properties. High levels of PAHs are found in food products cooked at high temperatures, such as fried foods and repeatedly used or illicitly recycled oils. Screening and detection of PAH compounds are an urgent demand to ensure cooking oil safety, but current techniques require labor-intensive and time-consuming sample preparation procedures. To shorten the detection time and avoid complicated sample pretreatment, a new technique combining ultra-thin layer chromatography (UTLC) and surface enhanced Raman spectroscopy (SERS) has been proposed and evaluated for rapid screening of PAHs in oil samples. The UTLC-SERS method utilizes the nanoporous and Raman enhancing properties of the silver nanorod (AgNR) substrates for chromatographic separation of mixture samples directly on the sensing surface within minutes.

In this dissertation, the UTLC-SERS principles were demonstrated using model Raman reporter molecules, and subsequently applied in the detection of PAHs. The AgNR substrate was modified with mercaptoethanol (ME), which served as the stationary phase in UTLC. The

mobile phase was optimized for the separation of three representative PAHs, benz(a)anthracene (BaA), benzo(a)pyrene (BaP), and pyrene (P).

PAHs were extracted from artificially contaminated vegetable oil samples through a 1-min acetonitrile extraction procedure, and the organic phase was directly used for UTLC-SERS without further treatment. The UTLC process served to elute target PAHs from the oil matrix to near the solvent front, where the SERS signal of BaA, BaP, and P could be identified at concentrations as low as 50 μg PAH/mL oil.

The UTLC-SERS approach was demonstrated to rapidly identify BaA, BaP, and P from vegetable oil at relatively high contamination levels without complicated sample preparation. To achieve lower detection limits and more efficient separation among the PAHs, more in-depth work is needed on improving the UTLC solvent migration as well as refining the sample preparation protocols.

INDEX WORDS: Polycyclic aromatic hydrocarbons, Surface enhanced Raman spectroscopy, Ultra-thin layer chromatography, Silver nanorod arrays, Rapid detection methods

RAPID DETECTION OF POLYCYCLIC AROMATIC HYDROCARBONS FROM COOKING
OIL USING ON-CHIP ULTRA-THIN LAYER CHROMATOGRAPHY WITH SURFACE
ENHANCED RAMAN SPECTROSCOPY

by

JING CHEN

B.S., Shanghai Jiao Tong University, Shanghai, China, 2006

M.S., Shanghai Jiao Tong University, Shanghai, China, 2010

A Dissertation Submitted to the Graduate Faculty of The University of Georgia in Partial

Fulfillment of the Requirements for the Degree

DOCTOR OF PHILOSOPHY

ATHENS, GEORGIA

2014

© 2014

Jing Chen

All Rights Reserved

RAPID DETECTION OF POLYCYCLIC AROMATIC HYDROCARBONS FROM COOKING
OIL USING ON-CHIP ULTRA-THIN LAYER CHROMATOGRAPHY WITH SURFACE
ENHANCED RAMAN SPECTROSCOPY

by

JING CHEN

Major Professor: Yao-wen Huang

Committee: Mark A. Harrison
Fanbin Kong
Bosoon Park

Electronic Version Approved:

Julie Coffield
Interim Dean of the Graduate School
The University of Georgia
August 2014

ACKNOWLEDGEMENTS

I would like to express my sincere gratitude to my advisor Dr. Yao-wen Huang for his kind support and academic guidance during my Ph.D. study. I am especially thankful for his continuous financial support and encouragements in participating in teaching and academic exchange activities. I would also like to express my deep appreciation for Dr. Yiping Zhao, who continuously provided scientific insights and guidance, experimental materials, and partial financial support for my research. I sincerely thank my other advisors, Dr. Bosoon Park, Dr. Mark Harrison, and Dr. Fanbin Kong, for providing me with research opportunities and equipment in their labs, and for serving in my committee and offering invaluable guidance to me. Dr. Xibo Li is acknowledged for his instructions on DFT calculation in this dissertation. I thank Mr. Yuntao Wang for providing old oil samples. My genuine gratitude goes to my fellow lab members and friends for their much help and moral support over the years: Mr. Xiaomeng Wu, Dr. Justin Abell, Dr. Chunyuan Song, Dr. Caiqin Han, Dr. Cunlan Guo, Dr. Gareth Sheppard, Mr. Yizhuo He, Mr. George Larsen, Mr. Manoj Manjare, Mr. Weijie Huang, Mr. Rui Cheng, Ms. Whitney Ingram, Mr. Layne Bradley, Ms. Lu Zhu, Mr. Funing Chen, Mr. Pradip Basnet, Ms. Qian Liu, Ms. Chong Ma, Ms. Huitong Yan, Ms. Linshan Li, Dr. Chi-Ching Lee, Ms. Winnie Lim, Ms. Chao Xu, and many others whose names are not shown on this short page. Finally, I would also like to thank the kind and professional support provided by Ms. Karen Simmons, Ms. Lisa Cash, Ms. Lisa Porterfield, and Ms. Beth Knight from the Department of Food Science and Technology.

TABLE OF CONTENTS

	Page
ACKNOWLEDGEMENTS	iv
LIST OF TABLES	vii
LIST OF FIGURES	viii
CHAPTER	
1 INTRODUCTION	1
2 LITERATURE REVIEW	4
3 ON-CHIP ULTRA-THIN LAYER CHROMATOGRAPHY AND SURFACE ENHANCED RAMAN SPECTROSCOPY	36
4 CHARACTERIZATION OF POLYCYCLIC AROMATIC HYDROCARBONS USING RAMAN AND SURFACE ENHANCED RAMAN SPECTROSCOPY	61
5 TOWARDS ULTRA-THIN LAYER CHROMATOGRAPHY AND SURFACE ENHANCED RAMAN SPECTROSCOPY DETECTION OF POLYCYCLIC AROMATIC HYDROCARBONS	85
6 DETECTION OF POLYCYCLIC AROMATIC HYDROCARBONS FROM COOKING OIL USING ULTRA-THIN LAYER CHROMATOGRAPHY AND SURFACE ENHANCED RAMAN SPECTROSCOPY	113
7 CONCLUSIONS AND FUTURE WORK	138
APPENDICES	

A ON-CHIP ULTRA-THIN LAYER CHROMATOGRAPHY AND SURFACE ENHANCED RAMAN SPECTROSCOPY SUPPLEMENTARY INFORMATION	142
B CHARACTERIZATION OF POLYCYCLIC AROMATIC HYDROCARBONS USING RAMAN AND SURFACE ENHANCED RAMAN SPECTROSCOPY SUPPLEMENTARY INFORMATION	145
C TOWARDS ULTRA-THIN LAYER CHROMATOGRAPHY AND SURFACE ENHANCED RAMAN SPECTROSCOPY DETECTION OF POLYCYCLIC AROMATIC HYDROCARBONS SUPPLEMENTARY INFORMATION.....	165
D DETECTION OF POLYCYCLIC AROMATIC HYDROCARBONS FROM COOKING OIL USING ULTRA-THIN LAYER CHROMATOGRAPHY AND SURFACE ENHANCED RAMAN SPECTROSCOPY SUPPLEMENTARY INFORMATION.....	181

LIST OF TABLES

	Page
Table 2.1: 16 priority PAHs identified by the U.S. EPA.....	33
Table 4.1: PAH compounds used in this study and their corresponding SERS limits of detection (LODs) and lowest detectable mass (LDMs).....	81
Table B.1: Band assignments for DFT-Raman, experimental Raman and SERS spectra of ACP....	149
Table B.2: Band assignments for DFT-Raman, experimental Raman and SERS spectra of ACY	150
Table B.3: Band assignments for DFT-Raman, experimental Raman and SERS spectra of ANT	151
Table B.4: Band assignments for DFT-Raman, experimental Raman and SERS spectra of BaP	152
Table B.5: Band assignments for DFT-Raman, experimental Raman and SERS spectra of BaA	153
Table B.6: Band assignments for DFT-Raman, experimental Raman and SERS spectra of F ...	155
Table B.7: Band assignments for DFT-Raman, experimental Raman and SERS spectra of P ...	156
Table C.1: Spreading area, migration distance, and drying speed of solvents on the AgNRs	171
Table C.2: Retention factors of BaA, BaP, and P on unmodified AgNRs	177

LIST OF FIGURES

	Page
Figure 2.1: Simplified Jablonski diagrams of Rayleigh scattering, Stokes Raman scattering, and anti-Stokes Raman scattering.....	34
Figure 2.2: Silver nanorod (AgNR) substrates fabricated by oblique angle deposition (OAD)....	35
Figure 3.1: Schematic representation of the ULTC-SERS process	57
Figure 3.2: SERS spectra of the analytes used in the four- and two-component mixtures.....	58
Figure 3.3: Separation of MO, CR, BPE, and MV with UTLC-SERS in methanol (a and b) and acetonitrile (c and d)	59
Figure 3.4: Separation of melamine and Rhodamine 6G (R6G): (a) and (b) equimolar mixture of melamine and R6G (1:1); (c) and (d) 100:1 mixture of melamine and R6G.....	60
Figure 4.1: DFT-calculated Raman spectra of seven PAH compounds	82
Figure 4.2: Bulk Raman spectra of BaA, BaP, F, ACP, and P after vector normalization.....	83
Figure 4.3: SERS spectra of seven PAH compounds on the AgNR substrates and the solvent (methanol) control.....	84
Figure 5.1: Water contact angle on (a) ME (b) MH (c) PT and (d) OCT modified AgNR substrates.....	106
Figure 5.2: SERS spectra of blank substrates after thiol modification.....	107
Figure 5.3: SERS intensity of 200 $\mu\text{g/mL}$ BaA, BaP, and P on (a) ME (b) MH (c) PT and (d) OCT modified substrates.....	108

Figure 5.4: UTLC separation of BaA, BaP, and P on (a) 10 μM ME (b) 100 μM ME (c) 10 μM MH and (d) 100 μM MH modified AgNR substrates.....	109
Figure 5.5: UTLC separation of BaA, BaP, and P on unmodified AgNR substrates using methanol and water mixed at different ratios.....	110
Figure 5.6: R_f values and (b) chromatographic band widths of BaA, BaP, and P developed by mixtures of methanol and water on unmodified AgNR substrates	111
Figure 5.7: UTLC separation of BaA, BaP, and P on 10 μM ME modified AgNR substrates using methanol: water 95:5 (v/v).....	112
Figure 6.1: Averaged (a) Raman and (c) SERS spectra of edible oil products	132
Figure 6.2: (a) SERS intensity of P dissolved in neat and oil-saturated acetonitrile (ACN) before and after UTLC in methanol (b)-(d) Correlation between the SERS peak intensity of P and actual P concentration in neat (b) and oil-saturated ACN before (c) and after (d) UTLC development in methanol.....	133
Figure 6.3: Effect of extraction solvents on the PAH extraction.....	134
Figure 6.4: Effect of extraction solvent (ACN) volume and solvent evaporation on the SERS intensity of P	135
Figure 6.5: UTLC-SERS detection of PAHs using methanol: water (95:5, v/v) on 10 μM ME modified substrates.....	136
Figure 6.6: UTLC-SERS detection of PAH from oil extract using methanol: water 80:20 (v/v) on 10 μM ME modified substrates.....	137
Figure A.1: SERS spectra of AgNR substrates pre-treated with mobile phase solvents	142
Figure A.2: Spatially-resolved SERS intensity map of (a) melamine (700 cm^{-1}) and (b) R6G (610 cm^{-1})	143

Figure A.3: Point-to-point fluctuation of the AgNR array substrates.....	144
Figure B.1: DFT-calculated molecular structure of acenaphthene (ACP).....	145
Figure B.2: DFT-calculated molecular structure of acenaphthylene (ACY).....	146
Figure B.3: DFT-calculated molecular structure of anthracene (ANT).....	146
Figure B.4: DFT-calculated molecular structure of benz(a)anthracene (BaA).....	147
Figure B.5: DFT-calculated molecular structure of benzo(a)pyrene (BaP).....	147
Figure B.6: DFT-calculated molecular structure of fluorene (F).....	148
Figure B.7: DFT-calculated molecular structure of pyrene (P)	148
Figure B.8: (a) SERS spectra of ACP at different concentrations in methanol (b) Corresponding intensities at specific peaks	158
Figure B.9: (a) SERS spectra of ACY at different concentrations in methanol (b) Corresponding intensities at specific peaks	159
Figure B.10: (a) SERS spectra of ANT at different concentrations in methanol (b) Corresponding peak intensities at 755 cm^{-1}	160
Figure B.11: (a) SERS spectra of BaA at different concentrations in methanol (b) Corresponding peak intensities at 724 cm^{-1}	161
Figure B.12: (a) SERS spectra of BaP at different concentrations in methanol (b) Corresponding peak intensities at 1384 cm^{-1}	162
Figure B.13: (a) SERS spectra of F at different concentrations in methanol (b) Corresponding peak intensities at 725 cm^{-1}	163
Figure B.14: (a) SERS spectra of P at different concentrations in methanol (b) Corresponding peak intensities at 593 cm^{-1}	164

Figure C.1: SERS spectra of (a) BaA, (b) BaP, and (c) P on difference concentrations of ME modified substrates	166
Figure C.2: SERS spectra of (a) BaA, (b) BaP, and (c) P on difference concentrations of MH modified substrates	167
Figure C.3: SERS spectra of (a) BaA, (b) BaP, and (c) P on difference concentrations of PT modified substrates	168
Figure C.4: SERS spectra of (a) BaA, (b) BaP, and (c) P on difference concentrations of OCT modified substrates	169
Figure C.5: SERS spectra of common lab solvents on the AgNR substrate.....	173
Figure C.6: UTLC separation of BaA, BaP, and P on unmodified AgNR substrates using single solvent systems	178
Figure C.7: UTLC separation of BaA, BaP, and P on unmodified AgNR substrates using binary mobile phases.....	179
Figure D.1: Effect of partitioning conditions on the SERS intensity of extracted P	181
Figure D.2: UTLC-SERS detection of PAHs using methanol on 10 μ M ME modified substrates... ..	182
Figure D.3: UTLC-SERS detection of PAHs using methanol: water (80:20, v/v) on unmodified substrates.....	183

CHAPTER 1

INTRODUCTION

In recent years, the safety of edible oil has attracted wide attention due to intensive media coverage on cooking oil products intentionally adulterated with recycled waste oil [1]. During repeated cooking, hazardous substances, especially lipophilic contaminants tend to accumulate in the oil. Polycyclic aromatic hydrocarbons (PAHs) are a group of lipophilic compounds that form during cooking at high temperatures, which, at excessive levels, can be used as an indicator of recycled waste oil. PAHs are also found to exhibit carcinogenic, mutagenic, and teratogenic effects in human [2]. Therefore, the identification of PAHs is critical to ensure the safety of oil products.

Traditionally, PAHs are identified using liquid chromatography (LC) or gas chromatography (GC) coupled with fluorescence detection or mass spectrometry [3]. Despite high sensitivity provided by LC and GC, these techniques require labor-intensive and time-consuming sample preparation, which has limited their application in routine inspection. Particularly, there is a great challenge in extracting highly lipophilic PAHs from fatty food matrices, such as cooking oil [4]. Hence, there remains a demand for alternative analytical techniques capable of handling PAH detection in oil samples.

Surface enhanced Raman spectroscopy (SERS) is an ultra-sensitive technique for trace detection. The subtle molecular vibrational fingerprints are captured thanks to the enhanced electromagnetic field provided by nanostructured metal surfaces (*i.e.*, SERS substrates) [5].

SERS has been proposed for the detection of a myriad of chemical and biological agents, and single molecule detection has been achieved [6]. However, SERS detection in mixture samples is challenging due to the spectral interference from non-target components co-existing in the same matrix. Although post-spectroscopic chemometric analyses have been demonstrated to differentiate samples, inherent drawbacks in statistical model construction have largely limited their use in real samples [7].

In this dissertation, a different strategy for SERS detection in mixture samples is proposed. This new technique enables ultra-thin layer chromatographic (UTLC) separation directly on the SERS-active substrate prior to SERS measurements, which allows for improved spectral differentiation between co-existing sample components. In addition, because the interference from food matrix may also be mitigated, and the SERS substrates are disposable, sample preparation becomes less demanding for chromatography. A proof-of-principle study was conducted using Raman reporter molecules (Chapter 3), and then the new UTLC-SERS approach was applied to the detection of PAHs from oil samples. For UTLC-SERS detection of PAHs, the Raman and SERS characteristics of selective PAH compounds were first obtained (Chapter 4). Then the surface of the SERS-active substrates was functionalized and the mobile phase solvent system was optimized for improved UTLC performance using PAH standard solutions (Chapter 5). Finally, the established UTLC-SERS method was adjusted and used in the detection of PAHs from real oil samples (Chapter 6). Conclusions and remarks on future work can be found in Chapter 7.

References

1. Lu, F. and X. Wu, *China food safety hits the "gutter"*. Food Control, 2014. **41**:134-138.
2. Scientific Committee on Food, European Commission, *Opinion of the scientific committee on food on the risks to human health of polycyclic aromatic hydrocarbons in food*, 2002, European Commission (EC): Brussel.
3. Plaza-Bolanos, P., A.G. Frenich, and J.L.M. Vidal, *Polycyclic aromatic hydrocarbons in food and beverages. Analytical methods and trends*. Journal of Chromatography A, 2010. **1217**(41):6303-6326.
4. Moret, S. and L.S. Conte, *Polycyclic aromatic hydrocarbons in edible fats and oils: occurrence and analytical methods*. Journal of Chromatography A, 2000. **882**(1-2):245-253.
5. Fleischmann, M., P.J. Hendra, and A.J. McQuillan, *Raman spectra of pyridine adsorbed at a silver electrode*. Chemical Physics Letters, 1974. **26**(2):163-166.
6. Kneipp, K., H. Kneipp, S. Abdali, R.W. Berg, and H. Bohr, *Single molecule Raman detection of enkephalin on silver colloidal particles*. Spectroscopy: An International Journal, 2004. **18**(3):433-440.
7. Chen, J., J. Abell, Y.W. Huang, and Y.P. Zhao, *On-Chip Ultra-Thin Layer Chromatography and Surface Enhanced Raman Spectroscopy*. Lab on a Chip, 2012. **12**(17):3096-3102.

CHAPTER 2

LITERATURE REVIEW

Safety of Cooking Oil

Oils and fats constitute an important component in both Eastern and Western diets, frequently used in frying, baking, and other forms of food preparation to provide aroma, taste, texture, and nutrition to the food. In East Asian countries, oil is a primary ingredient used for stir frying and deep frying, and has an equivalent status as staple foods. In recent years, there is a growing concern on the safety of cooking oils, primarily as a result of the Chinese “gutter oil” scandal. Gutter oil is a broad term used in China for oil collected from gutters, sewage lines, grease traps of restaurants, or processed from slaughter house wastes [1]. In the developed countries, such oil wastes are typically recycled and used for biofuel or biodiesel generation. Historically, highly refined waste oil was also allowed in animal feed, but recycled waste oil is strictly banned in the production of human foods [2-4]. However, in developing countries where oil safety laws and regulations are lacking, waste oil has been found to be intentionally adulterated into edible oil products for short term economic profits. Gutter oil is reprocessed rudimentarily using boiling, filtration, and coarse refining techniques, and then adulterated into fresh cooking oil. It is estimated that two million tons of gutter oil is consumed annually in China [5]. Since 2010, the illicit reuse of gutter oil has been disclosed by the news media, triggering large scale public outrage over oil safety. On the other hand, in the Western countries, deep fried foods such as French fries and fried chickens are consumed at large quantities, yet there is a large

variation in the standard operating procedures for deep fryer oil disposal and reuse. Food safety is also at stake if deep fryer oil is not replaced at appropriate frequencies.

A number of hazardous substances have been identified in gutter oil and repeatedly used deep fryer oil, for example, oxidation products of triglycerides (free radicals, peroxides and epoxides), hydrolysis products (free fatty acids), trans-fatty acids, and polycyclic and heterocyclic aromatic hydrocarbons. Other carcinogens such as mycotoxins, acrylamide, heavy metals (lead, cadmium), and pesticides (arsenic, organophosphates, and organochlorides), and pathogenic microorganisms have also been found in gutter oil. Symptoms associated with gutter oil consumption range from diarrhea and abdominal pain to more severe health effects like intoxication, damage to the gut epithelial cells, anemia, hypertension, cardiovascular diseases, diabetes, hepatitis, and cancers in the stomach, intestines, liver, and kidneys [6-9].

To prevent used oil products from entering the edible oil market, there is an urgent demand for reinforced inspection throughout the production chain. To date, several techniques targeting at a variety of waste oil indicators have been proposed for gutter oil detection. For instance, a few studies have revealed a correlation between conductivity and the freshness (or purity) of cooking oil, and significantly higher conductivity is found in gutter oil compared to pure cooking oil [10]. Since waste oils often contain animal fat from previous cooking processes, Zhang *et al* (2006) developed a method based on gas chromatography (GC) to determine the cholesterol content of edible oils, thereby differentiating slaughter house waste oils and recycled restaurant cooking oils from fresh plant oils [11]. Quan *et al* (2004) applied static headspace and gas chromatography/ mass spectroscopy (GC/MS) to the analysis of volatile compounds of refined gutter oil, and found that large amounts of hexanals were present in gutter oil [12]. In addition, arsenic [13], heavy metals [14, 15], polar compounds [16], and sodium dodecylbenzene

sulfonate [17] have also been targeted in oil authentication. Nonetheless, detection of gutter oil remains largely ineffective, since gutter oil can be mixed with fresh oil at relatively low ratios such that general indicators (peroxide value, acid value, conductivity, iodine value, *etc.*) are still kept below positive thresholds.

The complexity of gutter oil remains another obstacle in gutter oil detection, since the composition can vary to a great extent depending on the source of waste oil. Carefully selected indicators thus become crucial in successful detection. Polar compounds such as ketones and aldehydes are by far the most widely proposed gutter oil indicators, and are relatively easy to detect [12, 16]. However, they are also easy to remove from waste oil, which enables crudely refined gutter oil to escape from detection. On the contrary, polycyclic aromatic hydrocarbons are more persistent contaminants in lipid environments. They are also considered the most hazardous components in gutter oil risk analysis [18]. The non-polar fractions of repeatedly used deep-frying oil have been shown to exhibit increased mutagenicity [8], which implies a correlation between polycyclic aromatic hydrocarbons and repeated use of cooking oil. Therefore, these non-polar hazardous compounds may be a better indicator of waste cooking oil.

Polycyclic Aromatic Hydrocarbons and Detection Techniques

Polycyclic aromatic hydrocarbons (PAHs) are a large group of compounds with fused aromatic rings but do not contain heteroatoms or substitution groups. PAHs may contain four-, five-, six-, or seven-membered rings, but those with five- or six-membered rings are most common. Some common PAHs and their chemical structures can be found in Table 2.1. PAHs originate mainly from incomplete combustion of organic compounds at high temperatures (500 -

700 °C), though formation can also occur in fossil fuels at low temperatures (100 - 150 °C) but requires a period on the geological time scale [19].

The hazardous health effects of PAHs have long been recognized. Seven PAH compounds, benz(a)anthracene, benzo(a)pyrene, benzo(b)fluoranthene, benzo(k)fluoranthene, chrysene, dibenz(a,h)anthracene, and indeno(1,2,3-c,d)pyrene are classified by the U.S. Environmental Protection Agency (EPA) as probable human carcinogens, while others may act as carcinogenic synergists. Furthermore, some PAHs can form adducts with DNA or proteins and exhibit mutagenic or teratogenic properties. Studies have indicated that prenatal exposure to PAHs may lead to adverse birth outcomes, low IQ, childhood asthma, anxiety, and depression, etc [20, 21].

For non-smokers, exposure to PAHs is mainly through inhalation of polluted air and ingestion of contaminated food. As a ubiquitous environmental pollutant, PAH compounds are released into the atmosphere through fossil fuel burning and conversion of coal, whereas in food, they are formed during industrial food processing as well as domestic preparation. Cooking at high temperatures, such as grilling, roasting, smoking, and deep frying, has been linked to increased levels of PAHs in processed meats. The average benzo(a)pyrene concentration is estimated between 0.1 µg/kg and 1.2 µg/kg in smoked fishery products [22]. Drying is another process that can introduce significant amounts of PAHs to the diet. As fresh produce (coffee beans, tea, nuts, seeds, etc.) is dried, the combustion gases generated from the heat source may come into contact with the food material and cause PAHs to deposit on the food surface. Food contamination caused by environmental pollution, such as seafood contaminated during an oil spillage, or produce grown in a heavily industrialized region, has also been reported [19]. Though contaminated drinking water is also a possible source of PAHs, it is usually considered a

minor exposure route because of the sparing solubility of PAHs in water. In contrast, vegetable oils and fats are a significant source of PAHs as they readily dissolve in lipid environments. PAHs are introduced in vegetable oils mainly during the drying processes of oil-bearing seeds [23], but can also accumulate through repeated use of oil, such as those in recycled deep fryer oil. In waste oils and minimally refined gutter oils, the PAH content is expected to increase compared to refined oil products [24].

Legal standards and regulations of PAHs have been developed for occupational safety and environmental protection purposes. The EPA has established a list of priority organic pollutants which includes 16 PAH compounds (*i.e.*, 16 EPA PAHs, see Table 2.1); meanwhile, the European Union (EU) also developed a list of 15 PAHs in its monitoring studies. The EPA has set maximum contamination levels in the workplace for occupational exposure, ranging from 0.0001 to 0.0004 mg/L for representative PAHs, and a maximum contaminant level of 0.2 parts per billion (ppb) for benzo(a)pyrene in drinking water [25]. Though food is a major route of non-occupational exposure, the U.S. Food and Drug Administration (FDA) has not established standards to govern the PAH contents in foodstuffs. On the other hand, since PAHs are rarely present in food individually but rather in mixtures, there have been controversies and debates on the selection of indicator PAH compounds. In the past, benzo(a)pyrene (BaP) was used as a sole indicator the presence of PAHs. In Germany, Austria, and Poland, a legal limit of 1 µg/kg was adopted for BaP in smoked foods. However, the European Food Safety Authority (EFSA) later pointed out that the supposition that BaP was a good indicator of any PAH contamination was uncertain. Consequently, new maximum levels were established by the EU for the sum of BaP, benz(a)anthracene (BaA), benzo(b)fluoranthene (BbFA), and chrysene (CHR), or the so-called PAH4 to replace BaP as indicator substances. Currently, the EU has established the maximum

allowed levels of 2 $\mu\text{g}/\text{kg}$ for BaP and 10 $\mu\text{g}/\text{kg}$ for PAH4 in oils and fats intended for direct human consumption or use as an ingredient in food [26].

Historically, the detection of PAHs evolved from paper chromatography and thin-layer chromatography (TLC) followed by ultra-violet (UV) or fluorescence spectroscopy to higher resolution liquid chromatography (LC) or gas chromatography (GC) coupled to UV detection. More recently, fluorescence detectors (FLD) with various excitation and emission wavelengths have largely replaced UV as the detection system of choice for its higher selectivity and sensitivity. A number of PAH compounds have been detected using high performance liquid chromatography (HPLC) in a wide range of matrices including fresh [27] and grilled meats [28], edible oils [29-31], processed foods [32], barbecued foods [29], spirit [33], vegetables and fruits [34].

HPLC is the preferred technique in the analysis of PAHs for its shorter runtime compared with GC. Still, GC has an inherent advantage over HPLC when low-molecular-weight PAHs are concerned. Moreover, LC/FLD can show a lack of selectivity, particularly in the presence of alkylated PAHs which exhibit similar fluorescence responses to the unsubstituted PAHs. In such cases, GC/MS is used to confirm the positive results. Numerous reports on GC/MS or GC/MS/MS analysis of PAHs are available in the literature, which encompass detection in fresh [35] and smoked fish [36], animal feed [37], and fruits and vegetables [38, 39]. However, MS cannot be used for identifying large amounts of unresolved components. In this case, FLD represents the only means of quantitating PAHs of unknown identity [24].

A capillary zone electrophoresis method was also developed to detect PAHs from edible oils, with limits of quantification (LOQs) ranging from 10 to $> 1000 \mu\text{g}/\text{L}$ [40]. Other techniques, mainly optical and spectroscopic methods, have been employed for PAH

identification. Nevertheless, to this date, chromatography based techniques are the only validated methods for PAH detection in real samples, in part due to the need to identify coexisting PAHs in the same sample. Sample preparation methods for HPLC and GC remain an area of intense research. Traditional means of separating PAHs from interfering food components involve extraction using organic solvents, evaporation of solvents, cleanup of co-extracted matrix components. This can be a lengthy, complicated, and expensive process with large solvent consumption and waste generation [41]. Recent developments in sample preparation have achieved shortened extraction time and reduced use of extraction solvents, but challenges persist for PAH detection in fatty matrices including edible oils due to the difficulties in removing co-extracted triglycerides [24, 42].

Raman Scattering and Surface Enhanced Raman Scattering (SERS)

In essence, Raman scattering is the inelastic scattering of light, *i.e.*, events associated with energy changes between the scattering molecule and the scattered light. As light encounters a molecule, the photons may be absorbed or scattered by the molecule. As illustrated in Figure 2.1, during scattering, the molecule is excited to a virtual energy state. The majority of the excited molecules relax back to its initial vibrational state (*i.e.*, Rayleigh scattering), in which case there is no energy loss or gain. However, a small fraction of the excited molecules can relax back to a higher or a lower vibrational state after interacting with the incident photons, corresponding to Stokes and anti-Stokes Raman scattering, respectively. This process causes the scattered light to shift to a lower or higher frequency compared to the incident light. Consequently, the frequency shifts in the Raman spectra become unique fingerprints of different vibrational modes within the molecule.

Raman spectra are typically acquired using a monochromatic laser (usually in the visible, near infrared, or near ultraviolet range) as the source light, after the intense Rayleigh scattered light is filtered out. From a quantum chemical perspective, the number of scattered photons is proportional to the size of the bond. For instance, π bonds are generally larger scatterers than small single bonds; hence molecules rich in π systems often have stronger Raman intensity compared to those with only small single bonds. Therefore, the intrinsic scattering properties of the molecule (*i.e.*, the Raman cross section) strongly affect the Raman intensity. In addition, the Raman intensity is proportional to the intensity of the incident light and the number of molecules in the laser beam, and inversely proportional to the 4th power of the incident light wavelength.

Raman spectra can be used to observe vibrational, rotational, and other low-frequency modes in a system and provide molecular information that is complementary to that obtained by infrared (IR) spectroscopy. Because the Raman signal is not interfered by the presence of moisture, water can be used as a solvent during the analysis. This is particularly attractive in the analysis of biological or environmental samples, since most of these samples can only be maintained in aqueous systems. However, spontaneous Raman scattering is typically very weak: approximately only 1 in 10^8 incident photons are inelastically scattered. This has undoubtedly limited the application of Raman spectroscopy in analytical chemistry. Fortunately, other variations of Raman scattering techniques have emerged with enhanced Raman intensity, including resonance Raman scattering, tip-enhanced Raman scattering, and surface enhanced Raman scattering (SERS).

In the early 1970s, Fleischmann *et al* (1974) discovered that pyridine adsorbed on roughened silver electrodes yielded unusually intense Raman signal [43]. This observation led to a new branch of Raman spectroscopy—SERS. The SERS effect occurs when the test analyte is

placed near nanostructured (1 - 100 nm) surfaces of gold, silver, or copper (these nanostructures are thus called SERS-active or SERS substrates). The strong local electromagnetic field provided by the metal nanostructures is a major factor that contributes to the enhanced Raman signal. Additionally, many molecules, particularly those with a lone pair of electrons, can not only physically adsorb onto the SERS-active substrates but also chemically bond to the metal surface. In such scenarios, charge transfer between the metal surface and the chemically adsorbed molecule can further increase the magnitude of signal enhancement. Overall, the Raman scattering signal can be enhanced up to 10^6 - 10^{12} times under SERS conditions, and because of the strong signal enhancement, SERS can be used to detect single molecules [44, 45].

SERS-Active Substrates and Silver Nanorod Arrays

Center to the SERS phenomenon is the SERS-active substrate. A myriad of substrates have been made available for SERS analysis, with dispersed silver or gold nanoparticles (AgNPs or AuNPs) being the most prevailing. Colloidal gold and silver (10 - 30 nm individual nanoparticles) are easy and inexpensive to prepare, without the demand for sophisticated equipment, and can provide high SERS enhancement factors (up to 10^{13}) when the so-called SERS “hot spots” form at inter-particle junctions after the nanoparticles aggregate into 60-80 nm nanoparticle clusters. However, aggregation of nanoparticles also leads to non-uniform particle distribution and poor signal reproducibility. More recently, silver film over nanosphere (AgFON) and substrates fabricated by e-beam lithography (EBL) have demonstrated high uniformity and signal reproducibility. Unfortunately, fabrication of uniform nanostructures over a large area remains technically problematic or expensive [46].

In this regard, silver nanorod (AgNR) array substrates are an attractive alternative to colloidal SERS substrates. The AgNRs are fabricated by a physical vapor deposition process named oblique angle deposition (OAD). In OAD, clean glass slides or silicon wafers are loaded onto the substrate holder in the deposition chamber. Under high vacuum conditions ($< 10^{-6}$ Torr), electron beam is generated to vaporize the source material (silver), which then condenses on the cold glass surface and forms a thin (~ 200 nm) film at normal incident angle. However, when the glass slides are rotated to an oblique angle (Fig. 2.2a), the initially formed silver islands or nuclei will act as shadowing centers which prevent incoming vapor flux from nucleating in the shadowed areas (Fig. 2.2b). As the source material continues to evaporate and condense, the individual nuclei form nanospheres which eventually elongate into nanorods. Since the evaporation rate, duration of deposition, and vapor flux angle in relative to the substrate normal are all controllable parameters, the geometry and morphology of the resultant AgNRs can be fine-tuned [47]. A typical OAD process performed at 86° with respect to the substrate normal generates a film of tilted and aligned Ag nanorods (AgNRs) with 868 ± 95 nm rod length, and 99 ± 29 nm rod diameter, with a tilting angle of approximately 73° with respect to the substrate normal. (Fig. 2.2 c) The average density of AgNRs on the substrate is estimated to be 13 ± 0.5 rods/ μm^2 [48].

Due to the highly uniform distribution and morphology of the nanorods, SERS signal obtained with the AgNR substrates exhibits superior reproducibility, with a relative standard deviation (RSD) of less than 8% over a large area of 1 inch^2 [49]. Such high reproducibility is comparable to the EBL-fabricated substrates, but with a lower cost and higher SERS enhancement factors (up to 10^9 higher than normal Raman intensity) [50]. By far, the AgNR substrates have been demonstrated to detect a wide range of chemicals as well as biological

species, including aflatoxins [51], antibiotics [52], miRNAs [53], foodborne pathogens [54, 55], and respiratory viruses [56].

SERS Detection of PAHs

SERS has demonstrated wide applications in the detection of heavy metals [57], explosives [58], dyes, environmental pollutants [59], drugs [60, 61], toxins, DNA/RNA [62], disease biomarkers [63, 64], pathogenic bacteria [65], and viruses [66, 67], *etc.* A handful of studies have reported detecting PAH compounds using SERS. However, due to the low adsorption rates of PAHs onto metallic surfaces, numerous efforts have been devoted to surface-functionalization of the SERS substrates to improve the adsorption rates. Surface modification agents including alkanethiols [68], per-6-deoxy-(6-thio)- β -cyclodextrin [69], humic acid [70], poly-N-isopropylacrylamide [71], viologens [72], dithiocarbamate calix[4]arene [73], and mercapto-cyclodextrin [74] were anchored onto the SERS-active surface (by soaking the substrates into modification agents) before test PAHs were applied to the modified substrate. These modifications resulted in PAH detection limits as low as ~ 10 nM (or 20 ppb), but they usually involved an incubation step in which the modified substrates were “conditioned” with the PAH solution for a pre-determined period of time, so that the PAHs can partition to the SERS active surface.

In the meantime, the spectra of several PAHs (*e.g.*, naphthene, anthracene, fluorene, pyrene, phenanthrene, tetracene, and chrysene) have been documented very early on (in the 1970s and 1980s) using conventional Raman, Fourier transform Raman, coherent anti-Stokes Raman, and resonance Raman techniques. PAHs exhibit strong signal at the low to mid wavenumber regions ($300 - 2000 \text{ cm}^{-1}$) due to their C=C rich structures. The vibrational modes

in this region involve those caused by the C-C skeleton structure, ring breathing, in-plane and out-of-plane bending and deformations. The strongest peaks usually appear below 1700 cm^{-1} [75, 76].

Ultra-Thin Layer Chromatography (UTLC) and UTLC-SERS

Challenges in SERS Detection from Mixtures

In general, the reported SERS detection methods can be categorized as either extrinsic or intrinsic. In extrinsic SERS, detection specificity relies on the use of recognition elements, such as antibodies or aptamers, which specifically bind to the detection target. A reporting moiety labeled with the recognition unit and Raman reporter molecules is used in conjunction with the capture moiety, and the detection is usually performed in a sandwich format, such that the binding event can be signaled by the characteristic SERS spectra of the reporter. Extrinsic detection yields straightforward negative/ positive test results, and can be particularly facile for detecting biological macromolecules or organisms, such as large proteins and bacterial cells [77, 78]. However, its applicability is limited by the availability and cost of antibodies or aptamers. Information on the molecular and chemical composition of the targeted analyte is also sacrificed since only the signal from Raman labels is observed.

Alternatively, intrinsic SERS signal of the probed molecule can be directly registered to obviate the use of antibodies or aptamers and external Raman labels, which can in turn simplify the assay and reduce detection cost. For this reason, label-free intrinsic methods remain a hot topic and a future trend in SERS analysis. However, as only one SERS spectrum can be generated from each scan, it becomes difficult to extract spectral information of individual components from mixture samples. In intrinsic SERS detection, the most common practice to

achieve specificity is to treat the spectral data with multivariate statistical analyses, such as principle component analysis (PCA), hierarchical cluster analysis, and independent component analysis [79-81]. Unfortunately, several inherent drawbacks have limited the adoption of these analyses in real-world scenarios. For instance, multivariate analysis requires establishing prediction models based on the spectra of known analytes, and the models are not only sensitive to the type of analytes involved, but also to their relative abundance. Construction of spectral libraries to encompass infinite possibilities is highly unrealistic. On the other hand, as an ultra-sensitive technique, SERS is subject to the spectral interference from both the environment (*e.g.*, airborne cross-contamination) and the matrix in which the targeted analytes are dispersed. Consequently, the majority of intrinsic SERS detection methods are only demonstrated in relatively simple matrices (*e.g.*, water or pure organic solvents) but rarely in real food, environmental, or biological samples. Though the matrix effect can be mitigated through sample dilution, the target concentration is also undesirably reduced, which can lead to compromised detection sensitivity.

Ultra-Thin Layer Chromatography

In chemical or biochemical assays, to resolve issues of signal interference, purification or separation of the target analyte from its matrix is often required prior to the actual detection. Chromatography is a useful technique frequently adopted for such purposes. In chromatography, individual compounds in a mixture sample are physically separated before detection. Thin-layer chromatography (TLC) is a type of chromatography technique conducted on a thin layer of porous materials (*i.e.*, TLC plate). In TLC, the components in a mixture equilibrate at different

locations on the TLC plate according to their varying affinities to the stationary phase and mobile phase.

The TLC technique requires two essential components: a mobile phase and a stationary phase. The mobile phase is a liquid which carries the solutes across the surface of the stationary phase *via* capillary action. It usually consists of a mixture of organic solvents. The stationary phase in TLC is immobilized on a porous bed of the supporting material, and counteracts the effect of the mobile phase by retaining the analyte molecules and preventing them from moving with the mobile phase. Stationary phase can be solid (*i.e.*, the porous material itself), a thin film of liquid formed on the surface of the solid support, or an element (such as a cation or an antibody) that is covalently bonded to the solid support. Because the interactions between the solute and the stationary and mobile phases are determined by the molecule's chemical structure, different analytes can equilibrate at different locations on the TLC plate.

TLC can adopt different separation mechanisms, with the most common being partition chromatography and adsorption chromatography. In partition chromatography, a liquid film coated on the solid support material acts as the stationary phase (*e.g.*, water held by silica), and is immiscible with the mobile phase. The distribution of the solute between the stationary and mobile phase liquids determines the chromatographic separation. Ideally, the solid support is inactive in the retention of the solute. In reality, retention is often a result of both partition chromatography and adsorption chromatography mechanisms, though the former plays a major role [82]. The basic principle of solute retention in adsorption chromatography is its distribution between the sorbent (stationary phase) and the mobile phase. In contrast to partition chromatography where the stationary phase is a continuous film of liquid, in adsorption chromatography the solute directly interacts with the active centers (*e.g.*, hydroxyl groups in

silica gel) on the solid sorbent material. Sorbent activity is the sorbent's ability to interact with the solute, and is affected by the sorbent's specific area, density of the unoccupied active centers per unit of surface area, and the energy of intermolecular interactions between a solute molecule and a given sorbent active center.

In both mechanisms of TLC, individual components are differentiated using the retention factor R_f , which is expressed as

$$R_{fi} = \frac{d_i}{L}$$

where d_i is the distance travelled by the i th component in the mixture, and L is the distance travelled by the solvent from the original sample spots. Qualitative identification in TLC is based on comparing the R_f of an unknown component with that of a known standard, which is usually eluted in parallel to the test samples. The identity of TLC bands may be further confirmed by more sophisticated techniques such as mass spectroscopy (MS) [83], nuclear magnetic resonance (NMR) [84], and infrared spectroscopy (IR) [85]. Coupling between TLC and these techniques can be a time-consuming and laborious process, as the developed TLC bands are often scraped off the plate, extracted from the matrix material through repeated rinsing and centrifugation, chemically derivatized, and then finally dissolved in instrument-compatible solvents.

UTLC-SERS

As an ultra-sensitive detection technique, SERS has been utilized to provide additional molecular information to the separated TLC bands. In most reports, the mixture components were subject to conventional TLC separation on silica gel plates, and silver or gold nanoparticles were applied onto the TLC spots before SERS measurements [86, 87]. Inevitably in this format, a large number of detection targets in the bulk of the stationary phase are not exposed to

nanoparticles or the incident Raman light, and only the analyte molecules on the top layer are detected. On the other hand, while the nanoparticles can bring remarkable enhancement to the SERS signal through aggregation and formation of hot spots, the signal reproducibility is severely affected by decreased substrate uniformity.

A potential alternative for coupling TLC with SERS is revealed in recent publications by Bezuidenhout and Brett *et al* (2010) [88] and Jim *et al* (2010) [89], in which ultra-thin layer chromatography (UTLC) separation of dye mixtures was achieved on thin films of SiO₂ nanostructures fabricated using a physical vapor deposition process similar to OAD. Since the AgNRs possess similar porous properties to the reported SiO₂ nanostructures, it is also possible to achieve UTLC directly on the SERS-active structures. In fact, Abell *et al* (2012) [90] have demonstrated that a composition gradient of two Raman reporters could be generated on highly uniform AgNR SERS substrates, and the two reporters could be differentiated with the help of independent component analysis. This finding has partially supported the hypothesis that components in mixtures can spatially re-distribute on the AgNR substrates, which could lead to novel coupling of TLC and SERS on the ultra-thin surface. Ultimately, issues and challenges in the intrinsic SERS detection of mixture samples may be resolved.

References

1. Lu, F. and X. Wu, *China food safety hits the "gutter"*. Food Control, 2014. **41**:134-138.
2. Brown, R., *Cooking oil recycling projects are moving into the mainstream*, in *Chemical Market Reporter*1998, Reed Business Information Limited.8.
3. Bowling, D., *From waste oil to resource*, in *Hospitality*2010, Reed Business Information / Australia.28-30.
4. Anonymous, *Health fears bring ban on cooking oil*, in *Farmers Weekly*2002, Reed Business Information Limited.34.
5. Anonymous, *In the gutter*, in *The Economist*2011: London.
6. Leong, X.F., A. Aishah, U. Nor Aini, S. Das, and K. Jaarin, *Heated palm oil causes rise in blood pressure and cardiac changes in heart muscle in experimental rats*. Archives of Medical Research, 2008. **39**(6):567-572.
7. Kitts, D.D., *Toxicity and safety of fats and oils*. Bailey's Industrial Oil and Fat Products, 1996.
8. Hageman, G., R. Kikken, F. Ten Hoor, and J. Kleinjans, *Assessment of mutagenic activity of repeatedly used deep-frying fats*. Mutation Research/Genetic Toxicology, 1988. **204**(4):593-604.
9. Grootveld, M., C.J. Silwood, P. Addis, A. Claxson, B.B. Serra, and M. Viana, *Health effects of oxidized heated oils*. Foodservice Research International, 2001. **13**(1):41-55.
10. Hu, X.-h., Z.-j. Liu, X.-y. Zheng, H.-z. Pan, and L.-t. Liang, *Research on electroconductivity detection of hogwash fat*. Food Science, 2007. **28**(11):482-484.

11. Zhang, R., L.-y. Zu, T. Fan, and K.-p. Zhao, *Distinguishing hogwash oil in edible vegetable oil by determination of cholesterol content*. Chinese Oils and Fats, 2006. **31**(5):65-67.
12. Quan, C.-c., P.-h. Yin, L. Zhao, X.-z. Shan, X. Zhang, and H.-h. Yu, *Assay on the harmful volatile components of the refined waste edible oil gained from the restaurant sewer by static headspace and gas chromatography/mass spectrometry*. Food Science, 2004. **25**(4):128-134.
13. Chu, Y. and S. Jiang, *Speciation analysis of arsenic compounds in edible oil by ion chromatography-inductively coupled plasma mass spectrometry*. Journal of Chromatography A, 2011. **1218**(31):5175-5179.
14. Ismail, I.J. and E.H. Abdel-Hakiem, *Quality assessment of edible vegetable oils for presence of some toxic heavy metals*. Assiut Veterinary Medical Journal, 2009. **56**(124):36-45.
15. Pehlivan, E., G. Arslan, F. Gode, T. Altun, and M.M. Özcan, *Determination of some inorganic metals in edible vegetable oils by inductively coupled plasma atomic emission spectroscopy (ICP-AES)*. Grasas y Aceites (Sevilla), 2008. **59**(3):239-244.
16. Huang, J., H. Xiong, X.-Q. Xiong, and Z.-L. Chen, *Study on polar compounds of hogwash oil with thin-layer chromatography and column chromatography*. Food Science, 2008. **29**(12):568-571.
17. Liu, W., P.-h. Yin, and L. Zhao, *Distinguishing hogwash fat by determination of sodium dodecylbenzene sulfonate with fluorescence spectrum analysis*. Chinese Oils and Fats, 2005. **30**(5):24-26.

18. Anonymous. *Chemistry of gutter oil*. July 14, 2014]; Available from: <http://wenku.baidu.com/view/206382f9700abb68a982fb62.html>.
19. Scientific Committee on Food, European Commission, *Opinion of the scientific committee on food on the risks to human health of polycyclic aromatic hydrocarbons in food*, 2002, European Commission (EC): Brussel.
20. Dejmek, J., I. Solanský, I. Benes, J. Lenčák, and R.J. Srám, *The impact of polycyclic aromatic hydrocarbons and fine particles on pregnancy outcome*. Environmental Health Perspectives, 2000. **108**(12):1159.
21. Nisbet, I.C. and P.K. LaGoy, *Toxic equivalency factors (TEFs) for polycyclic aromatic hydrocarbons (PAHs)*. Regulatory Toxicology and Pharmacology, 1992. **16**(3):290-300.
22. Karl, H. and M. Leinemann, *Determination of polycyclic aromatic hydrocarbons in smoked fishery products from different smoking kilns*. Zeitschrift Fur Lebensmittel-Untersuchung Und-Forschung, 1996. **202**(6):458-464.
23. Speer, K., E. Steeg, P. Horstmann, T. Kuhn, and A. Montag, *Determination and distribution of polycyclic aromatic-hydrocarbons in native vegetable-oils, smoked fish products, mussels and oysters, and bream from the river elbe*. Journal of High Resolution Chromatography, 1990. **13**(2):104-111.
24. Moret, S. and L.S. Conte, *Polycyclic aromatic hydrocarbons in edible fats and oils: occurrence and analytical methods*. Journal of Chromatography A, 2000. **882**(1-2):245-253.
25. EPA. *Technical Factsheet on: polycyclic aromatic hydrocarbons (PAHs)*. April 29, 2014]; Available from: <http://www.epa.gov/ogwdw/pdfs/factsheets/soc/tech/pahs.pdf>.

26. European Commission, *Commission Regulation (EU) No 835/2011 amending Regulation (EC) No 1881/2006 as regards maximum levels for polycyclic aromatic hydrocarbons in foodstuffs*, E. Commission, Editor 2011, EFSA.
27. Janoszka, B., *HPLC-fluorescence analysis of polycyclic aromatic hydrocarbons (PAHs) in pork meat and its gravy fried without additives and in the presence of onion and garlic*. Food Chemistry, 2011. **126**(3):1344-1353.
28. Ince, M. and M. Yaman, *High performance liquid chromatography-mass spectrometry for determination of benzo[a]pyrene in grilled meat foods*. Asian Journal of Chemistry, 2012. **24**(8):3391-3395.
29. Dost, K. and C. İdeli, *Determination of polycyclic aromatic hydrocarbons in edible oils and barbecued food by HPLC/UV-Vis detection*. Food Chemistry, 2012. **133**(1):193-199.
30. Ye, Y.U., J. Qinze, and W. Xing Guo, *Rapid assay of polycyclic aromatic hydrocarbons in edible oils by HPLC with FLD detection without clean-up*. Journal of Chemical & Pharmaceutical Research, 2013. **5**(10):409-414.
31. Zhao, W.J., X.B. Chen, L. Fang, C.L. Li, and D.Y. Zhao, *Determination of light-medium-heavy polycyclic aromatic hydrocarbons in vegetable oils by solid-phase extraction and high-performance liquid chromatography with diode array and fluorescence detection*. Journal of Agricultural and Food Chemistry, 2013. **61**(8):1804-1809.
32. Kumosani, T.A., S.S. Moselhy, A.M. Asseri, and A.H. Asseri, *Detection of polycyclic aromatic hydrocarbons in different types of processed foods*. Toxicology and Industrial Health, 2013. **29**(3):300-304.

33. Tfouni, S.A.V., R.M.D. Machado, M.C.R. Camargo, S.H.P. Vitorino, E. Vicente, and M.C.F. Toledo, *Determination of polycyclic aromatic hydrocarbons in cachaca by HPLC with fluorescence detection*. Food Chemistry, 2007. **101**(1):334-338.
34. Zhao, X.N., X.J. Liu, Z.X. Zhao, C.J. Huang, M.H. Zhang, H.L. Wang, and X.D. Wang, *Homogeneous liquid-liquid extraction combined with high performance liquid chromatography-fluorescence detection for determination of polycyclic aromatic hydrocarbons in vegetables*. Journal of Separation Science, 2009. **32**(12):2051-2057.
35. Sapozhnikova, Y. and S.J. Lehotay, *Multi-class, multi-residue analysis of pesticides, polychlorinated biphenyls, polycyclic aromatic hydrocarbons, polybrominated diphenyl ethers and novel flame retardants in fish using fast, low-pressure gas chromatography-tandem mass spectrometry*. Analytica Chimica Acta, 2013. **758**:80-92.
36. Ghasemzadeh-Mohammadi, V., A. Mohammadi, M. Hashemi, R. Khaksar, and P. Haratian, *Microwave-assisted extraction and dispersive liquid-liquid microextraction followed by gas chromatography-mass spectrometry for isolation and determination of polycyclic aromatic hydrocarbons in smoked fish*. Journal of Chromatography A, 2012. **1237**:30-36.
37. Nacher-Mestre, J., R. Serrano, T. Portoles, M.H.G. Berntssen, J. Perez-Sanchez, and F. Hernandez, *Screening of pesticides and polycyclic aromatic hydrocarbons in feeds and fish tissues by gas chromatography coupled to high-resolution mass spectrometry using atmospheric pressure chemical ionization*. Journal of Agricultural and Food Chemistry, 2014. **62**(10):2165-2174.
38. Calderon-Preciado, D., C. Jimenez-Cartagena, G. Penuela, and J.M. Bayona, *Development of an analytical procedure for the determination of emerging and priority*

- organic pollutants in leafy vegetables by pressurized solvent extraction followed by GC-MS determination.* Analytical and Bioanalytical Chemistry, 2009. **394**(5):1319-1327.
39. Dobrinas, S., S. Birghila, N. Matei, and V. Coatu, *Determination of PAHs and organochlorine pesticides in tomato and green pepper.* Revista De Chimie, 2004. **55**(12):942-944.
40. Ferey, L., N. Delaunay, D.N. Rutledge, C.B.Y. Cordella, H. This, A. Huertas, Y. Raoul, and P. Gareil, *Optimizing separation conditions of 19 polycyclic aromatic hydrocarbons by cyclodextrin-modified capillary electrophoresis and applications to edible oils.* Talanta, 2014. **119**:572-581.
41. Fromberg, A., A. Hojgard, and L. Duedahl-Olesen, *Analysis of polycyclic aromatic hydrocarbons in vegetable oils combining gel permeation chromatography with solid-phase extraction clean-up.* Food Additives and Contaminants, 2007. **24**(7):758-767.
42. Anastassiades, M., S.J. Lehotay, D. Stajnbaher, and F.J. Schenck, *Fast and easy multiresidue method employing acetonitrile extraction/partitioning and "dispersive solid-phase extraction" for the determination of pesticide residues in produce.* Journal of AOAC International, 2003. **86**(2):412-431.
43. Fleischmann, M., P.J. Hendra, and A.J. McQuillan, *Raman spectra of pyridine adsorbed at a silver electrode.* Chemical Physics Letters, 1974. **26**(2):163-166.
44. Kneipp, K., H. Kneipp, S. Abdali, R.W. Berg, and H. Bohr, *Single molecule Raman detection of enkephalin on silver colloidal particles.* Spectroscopy: An International Journal, 2004. **18**(3):433-440.

45. Le Ru, E.C., M. Meyer, and P.G. Etchegoin, *Proof of single-molecule sensitivity in surface enhanced raman scattering (SERS) by means of a two-analyte technique*. The Journal of Physical Chemistry B, 2006. **110**(4):1944-1948.
46. Fan, M., G.F. Andrade, and A.G. Brolo, *A review on the fabrication of substrates for surface enhanced Raman spectroscopy and their applications in analytical chemistry*. Analytica Chimica Acta, 2011. **693**(1):7-25.
47. Fu, J.X., A. Collins, and Y.P. Zhao, *Optical properties and biosensor application of ultrathin silver films prepared by oblique angle deposition*. The Journal of Physical Chemistry C, 2008. **112**(43):16784-16791.
48. Liu, Y.J. and Y.P. Zhao, *Simple model for surface-enhanced Raman scattering from tilted silver nanorod array substrates*. Physical Review B, 2008. **78**(7).
49. Chen, J., J. Abell, Y.W. Huang, and Y.P. Zhao, *On-chip ultra-thin layer chromatography and surface enhanced Raman spectroscopy*. Lab on a Chip, 2012. **12**(17):3096-3102.
50. Liu, Y.J., H.Y. Chu, and Y.P. Zhao, *Silver nanorod array substrates fabricated by oblique angle deposition: morphological, optical, and sers characterizations*. The Journal of Physical Chemistry C, 2010. **114**(18):8176-8183.
51. Wu, X., S. Gao, J.-S. Wang, H. Wang, Y.-W. Huang, and Y. Zhao, *The surface-enhanced Raman spectra of aflatoxins: spectral analysis, density functional theory calculation, detection and differentiation*. Analyst, 2012. **137**(18):4226-4234.
52. Han, C., J. Chen, X. Wu, Y.-w. Huang, and Y. Zhao, *Detection of metronidazole and ronidazole from environmental samples by surface enhanced Raman spectroscopy*. Talanta, 2014. **128**(0):293-298.

53. Abell, J.L., J.M. Garren, J.D. Driskell, R.A. Tripp, and Y. Zhao, *Label-free detection of micro-RNA hybridization using surface-enhanced Raman spectroscopy and least-squares analysis*. Journal of the American Chemical Society, 2012. **134**(31):12889-12892.
54. Chu, H., Y. Huang, and Y. Zhao, *Silver nanorod arrays as a surface-enhanced Raman scattering substrate for foodborne pathogenic bacteria detection*. Applied Spectroscopy, 2008. **62**(8):922-931.
55. Wu, X., C. Xu, R.A. Tripp, Y.-w. Huang, and Y. Zhao, *Detection and differentiation of foodborne pathogenic bacteria in mung bean sprouts using field deployable label-free SERS devices*. Analyst, 2013. **138**(10):3005-3012.
56. D. Driskell, J., S. Shanmukh, Y. Liu, S. B. Chaney, X.J. Tang, Y.P. Zhao, and R. A. Dluhy, *The use of aligned silver nanorod arrays prepared by oblique angle deposition as surface enhanced Raman scattering substrates*. The Journal of Physical Chemistry C, 2008. **112**(4):895.
57. Ding, X., L. Kong, J. Wang, F. Fang, D. Li, and J. Liu, *Highly sensitive SERS detection of Hg²⁺ ions in aqueous media using gold nanoparticles/graphene heterojunctions*. ACS Applied Materials & Interfaces, 2013. **5**(15):7072-7078.
58. Yang, L., L. Ma, G. Chen, J. Liu, and Z.-Q. Tian, *Ultrasensitive SERS detection of TNT by imprinting molecular recognition using a new type of stable substrate*. Chemistry – A European Journal, 2010. **16**(42):12683-12693.
59. Alvarez-Puebla, R.A., J.D.S. dos Santos, and R.F. Aroca, *SERS detection of environmental pollutants in humic acid-gold nanoparticle composite materials*. Analyst, 2007. **132**(12):1210-1214.

60. Reipa, V. and J.J. Horvath, *Surface-enhanced Raman: study of benzylpenicillin*. Applied Spectroscopy, 1992. **46**(6):1009-1013.
61. Horváth, E., J. Mink, and J. Kristóf, *Surface-enhanced Raman spectroscopy as a technique for drug analysis*, in *Progress in Fourier Transform Spectroscopy*, J. Mink, G. Keresztury, and R. Kellner, Editors. 1997, Springer Vienna.745-746.
62. Cao, Y.C., R. Jin, and C.A. Mirkin, *Nanoparticles with Raman spectroscopic fingerprints for DNA and RNA detection*. Science, 2002. **297**(5586):1536-1540.
63. Cho, H., B.R. Baker, S. Wachsmann-Hogiu, C.V. Pagba, T.A. Laurence, S.M. Lane, L.P. Lee, and J.B.H. Tok, *Aptamer-based SERRS sensor for thrombin detection*. Nano Letters, 2008. **8**(12):4386-4390.
64. Volkan, M., D.L. Stokes, and T. Vo-Dinh, *Surface-enhanced Raman of dopamine and neurotransmitters using sol-gel substrates and polymer-coated fiber-optic probes*. Applied Spectroscopy, 2000. **54**(12):1842-1848.
65. Jarvis, R.M. and R. Goodacre, *Characterisation and identification of bacteria using SERS*. Chemical Society Reviews, 2008. **37**(5):931-936.
66. Isola, N.R., D.L. Stokes, and T. Vo-Dinh, *Surface-enhanced Raman gene probe for HIV detection*. Analytical chemistry, 1998. **70**(7):1352-1356.
67. Shanmukh, S., L. Jones, J. Driskell, Y. Zhao, R. Dluhy, and R.A. Tripp, *Rapid and sensitive detection of respiratory virus molecular signatures using a silver nanorod array sers substrate*. Nano Letters, 2006. **6**(11):2630-2636.
68. Jones, C.L., K.C. Bantz, and C.L. Haynes, *Partition layer-modified substrates for reversible surface-enhanced Raman scattering detection of polycyclic aromatic hydrocarbons*. Analytical and Bioanalytical Chemistry, 2009. **394**(1):303-311.

69. Xie, Y.F., X. Wang, X.X. Han, X.X. Xue, W. Ji, Z.H. Qi, J.Q. Liu, B. Zhao, and Y. Ozaki, *Sensing of polycyclic aromatic hydrocarbons with cyclodextrin inclusion complexes on silver nanoparticles by surface-enhanced Raman scattering*. *Analyst*, 2010. **135**(6):1389-1394.
70. Qu, L.L., Y.T. Li, D.W. Li, J.Q. Xue, J.S. Fossey, and Y.T. Long, *Humic acids-based one-step fabrication of SERS substrates for detection of polycyclic aromatic hydrocarbons*. *Analyst*, 2013. **138**(5):1523-1528.
71. Mueller, M., M. Tebbe, D.V. Andreeva, M. Karg, R.A. Alvarez-Puebla, N. Pazos-Perez, and A. Fery, *Large-area organization of pNIPAM-coated nanostars as SERS platforms for polycyclic aromatic hydrocarbons sensing in gas phase*. *Langmuir*, 2012. **28**(24):9168-9173.
72. Guerrini, L., J.V. Garcia-Ramos, C. Domingo, and S. Sanchez-Cortes, *Building highly selective hot spots in Ag nanoparticles using bifunctional viologens: application to the SERS detection of PAHs*. *The Journal of Physical Chemistry C*, 2008. **112**(20):7527-7530.
73. Kwon, Y.H., K. Sowoidnich, H. Schmidt, and H.D. Kronfeldt, *Application of calixarene to high active surface-enhanced Raman scattering (SERS) substrates suitable for in situ detection of polycyclic aromatic hydrocarbons (PAHs) in seawater*. *Journal of Raman Spectroscopy*, 2012. **43**(8):1003-1009.
74. Xie, Y.F., X. Wang, X.X. Han, W. Song, W.D. Ruan, J.Q. Liu, B. Zhao, and Y. Ozaki, *Selective SERS detection of each polycyclic aromatic hydrocarbon (PAH) in a mixture of five kinds of PAHs*. *Journal of Raman Spectroscopy*, 2011. **42**(5):945-950.
75. Asher, S.A., *Ultraviolet resonance Raman spectrometry for detection and speciation of trace polycyclic aromatic hydrocarbons*. *Analytical Chemistry*, 1984. **56**(4):720-724.

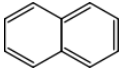
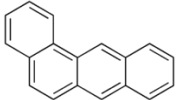
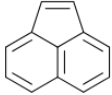
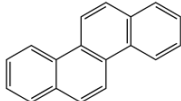
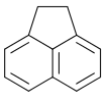
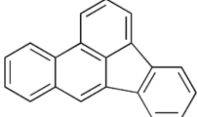
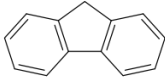
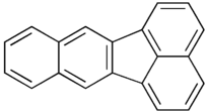
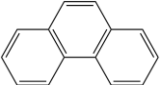
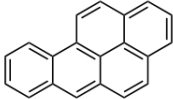
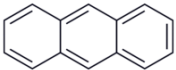
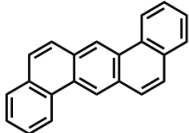
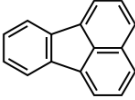
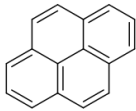
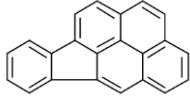
76. Maddams, W. and I. Royaud, *The characterization of polycyclic aromatic hydrocarbons by Raman spectroscopy*. Spectrochimica Acta Part A: Molecular Spectroscopy, 1990. **46**(2):309-314.
77. Wang, Y.L., S. Ravindranath, and J. Irudayaraj, *Separation and detection of multiple pathogens in a food matrix by magnetic SERS nanoprobos*. Analytical and Bioanalytical Chemistry, 2011. **399**(3):1271-1278.
78. Bizzarri, M., A. Rita, and M. Cannistraro, *SERS detection of thrombin by protein recognition using functionalized gold nanoparticles*. Nanomedicine: Nanotechnology, Biology and Medicine, 2007. **3**(4):306-310.
79. Abell, J.L., J. Lee, Q. Zhao, H. Szu, and Y. Zhao, *Differentiating intrinsic SERS spectra from a mixture by sampling induced composition gradient and independent component analysis*. Analyst, 2012. **137**(1):73-76.
80. Hennigan, S.L., J.D. Driskell, R.A. Dluhy, Y.P. Zhao, R.A. Tripp, K.B. Waites, and D.C. Krause, *Detection of mycoplasma pneumoniae in simulated and true clinical throat swab specimens by nanorod array-surface-enhanced Raman spectroscopy*. Plos One, 2010. **5**(10):e13633.
81. Patel, I.S., W.R. Premasiri, D.T. Moir, and L.D. Ziegler, *Barcoding bacterial cells: A SERS based methodology for pathogen identification*. Journal of Raman Spectroscopy, 2008. **39**(11):1660-1672.
82. Kowalska, T., *Theory and Mechanism of Thin-Layer Chromatography*, in *Handbook of Thin-Layer Chromatography*, S. Joseph and F. Bernard, Editors. 1996, Marcel Dekker, Inc.: New York.

83. Stoll, M.S., E.F. Hounsell, A.M. Lawson, W. Chai, and T. Feizi, *Microscale sequencing of O-linked oligosaccharides using mild periodate oxidation of alditols, coupling to phospholipid and TLC-MS analysis of the resulting neoglycolipids*. *European Journal of Biochemistry*, 1990. **189**(3):499-507.
84. Bonnett, R., F. Czechowski, and L. Latos-Grazynski, *Metalloporphyrins in coal. 4. TLC-NMR of iron porphyrins from coal: the direct characterization of coal hemes using paramagnetically shifted proton NMR spectroscopy*. *Energy and Fuels*, 1990. **4**(6):710-716.
85. Fuller, M.P. and P.R. Griffiths, *Diffuse reflectance measurements by infrared Fourier transform spectrometry*. *Analytical Chemistry*, 1978. **50**(13):1906-1910.
86. Caudin, J.P., A. Beljebbar, G.D. Sockalingum, J.F. Angiboust, and M. Manfait, *Coupling FT Raman and FT SERS microscopy with TLC plates for in situ identification of chemical compounds*. *Spectrochimica Acta Part A: Molecular and Biomolecular Spectroscopy*, 1995. **51**(12):1977-1983.
87. Brosseau, C.L., A. Gambardella, F. Casadio, C.M. Grzywacz, J. Wouters, and R.P. Van Duyne, *Ad-hoc surface-enhanced Raman spectroscopy methodologies for the detection of artist dyestuffs: thin layer chromatography-surface enhanced Raman spectroscopy and in situ on the fiber analysis*. *Analytical Chemistry*, 2009. **81**(8):3056-62.
88. Bezuidenhout, L.W. and M.J. Brett, *Ultrathin layer chromatography on nanostructured thin films*. *Journal of Chromatography A*, 2008. **1183**(1-2):179-185.
89. Jim, S.R., M.T. Taschuk, G.E. Morlock, L.W. Bezuidenhout, W. Schwack, and M.J. Brett, *Engineered anisotropic microstructures for ultrathin-layer chromatography*. *Analytical Chemistry*, 2010. **82**(12):5349-5356.

90. Abell, J.L., J. Lee, Q. Zhao, H. Szu, and Y.P. Zhao, *Differentiating intrinsic SERS spectra from a mixture by sampling induced composition gradient and independent component analysis*. *Analyst*, 2012. **137**(1):73-76.

Tables

Table 2.1 16 priority PAHs identified by the U.S. EPA

Chemical Name	Structure	Chemical Name	Structure
Naphthalene		Benz(a)anthracene	
Acenaphthylene		Chrysene	
Acenaphthene		Benzo(b)fluoranthene	
Fluorene		Benzo(k)fluoranthene	
Phenanthrene		Benzo(a)pyrene	
Anthracene		Dibenz(a,h)anthracene	
Fluoranthene		Benzo(g,h,i)perylene	
Pyrene		Indeno(1,2,3-cd)pyrene	

Figures

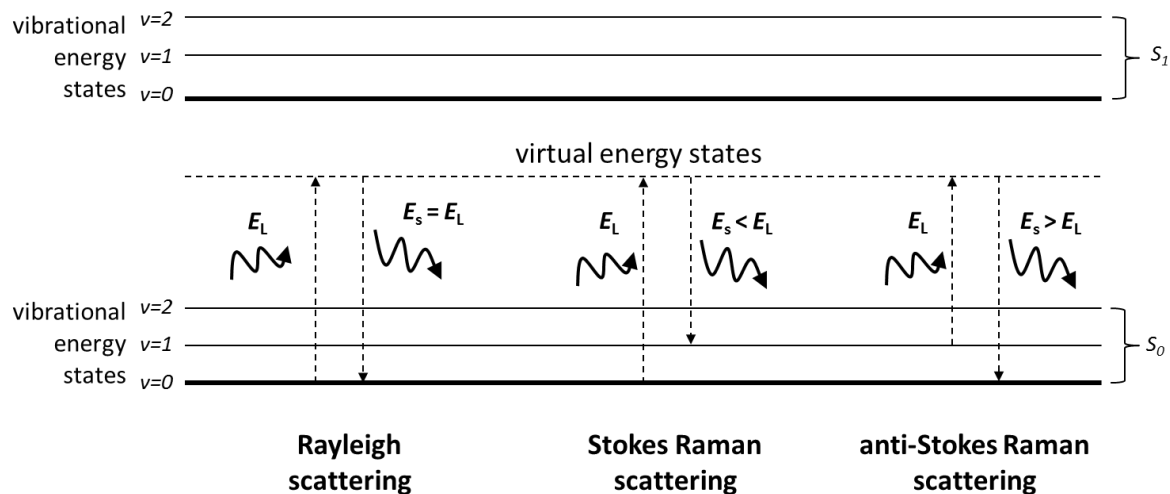


Figure 2.1 Simplified Jablonski diagrams of Rayleigh scattering, Stokes Raman scattering, and anti-Stokes Raman scattering. Solid horizontal lines indicate vibrational energy states ($v = 0, 1,$ and 2) of the ground (S_0) and first excited (S_1) electronic energy states. When an incident photon with an energy of E_L strikes the molecule, the molecule can be excited to a virtual energy state (indicated by the dashed horizontal line) and then relax back to the same vibrational energy state (Rayleigh scattering), a higher vibrational energy state (Stokes Raman scattering), or a lower vibrational energy state (anti-Stokes Raman scattering). In these events, the energy of the photon (E_s) will remain the same as the incident photon (Rayleigh scattering), or become lower (Stokes Raman) or higher (anti-Stokes Raman) than the incident photon.

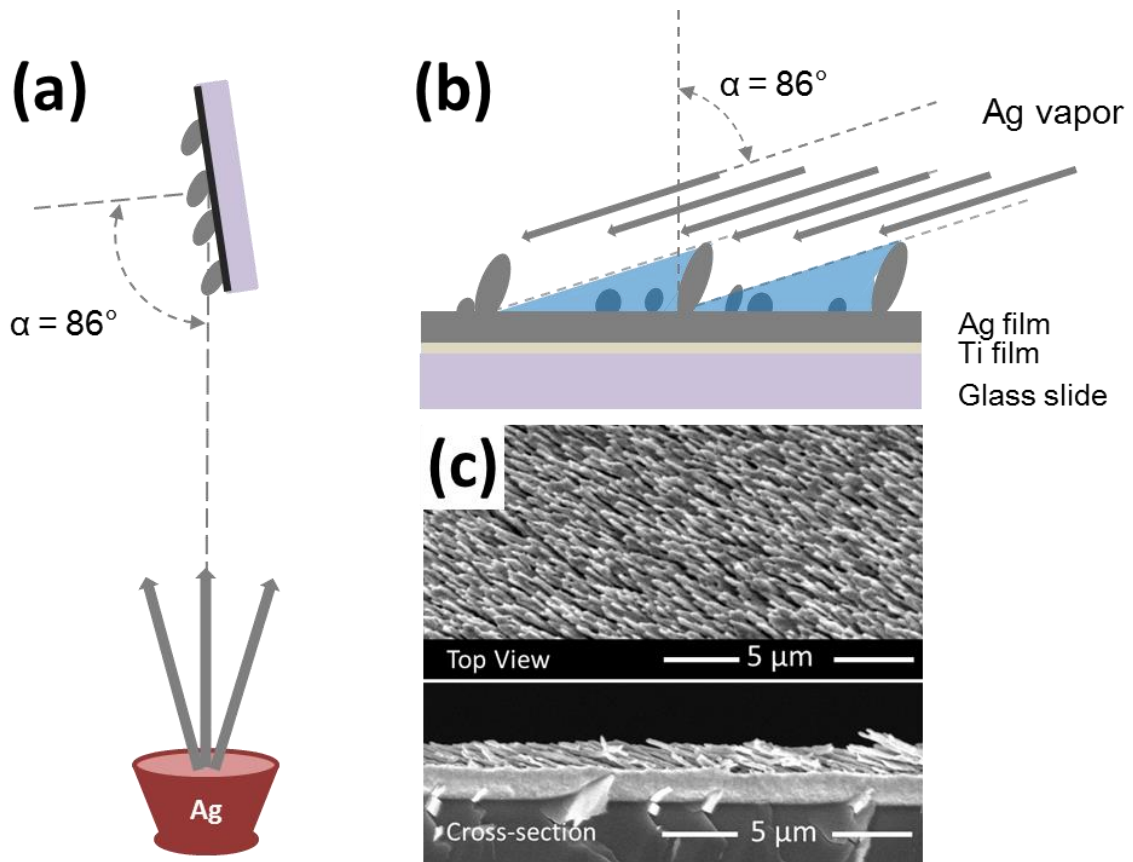


Figure 2.2 Silver nanorod (AgNR) substrates fabricated by oblique angle deposition (OAD) (a) Illustration of the OAD process (b) Shadowing effect. (c) SEM images of AgNRs

CHAPTER 3
ON-CHIP ULTRA-THIN LAYER CHROMATOGRAPHY AND SURFACE ENHANCED
RAMAN SPECTROSCOPY¹

¹ Jing Chen, Justin Abell, Yao-wen Huang, and Yiping Zhao. 2012. *Lab on a Chip*. 12: 3096–3102 - Reprinted with permission of The Royal Society of Chemistry.

Abstract

We demonstrate that silver nanorod (AgNR) array substrates can be used for on-chip separation and detection of chemical mixtures by combining ultra-thin layer chromatography (UTLC) and surface enhanced Raman spectroscopy (SERS). The UTLC-SERS plate consists of a AgNR array fabricated by oblique angle deposition. The capability of the AgNR substrates to separate different compounds in a mixture was explored using a mixture of four dyes, and a mixture of melamine and Rhodamine 6G at varied concentrations with different mobile phase solvents. After UTLC separation, spatially-resolved SERS spectra were collected along the mobile phase development direction and the intensities of specific SERS peaks from each component were used to generate chromatograms. The AgNR substrates demonstrate the potential of separating the test dyes with plate heights as low as 9.6 μm . The limits of detection are between 10^{-5} - 10^{-6} M. Furthermore, we show that the coupling of UTLC with SERS improves the SERS detection specificity, as small amounts of target analytes can be separated from the interfering background components.

Introduction

Surface enhanced Raman spectroscopy (SERS) has proven to be a highly sensitive detection platform for chemical and biological agents due to the enhancement of the electromagnetic field in close vicinity (<10 nm) of nanostructured metal surfaces [1-3]. SERS analysis is attractive in part due to the wealth of information ascertained about the chemical and molecular composition of a sample. On the other hand, such an abundance of spectral information makes extracting individual spectral components from that of a mixture a challenging obstacle for applying SERS in real-world scenarios. In this regard, multivariate

analyses, e.g., principle component analysis (PCA), hierarchical cluster analysis (HCA), and independent component analysis (ICA), are commonly utilized to classify complex SERS spectra and/or distinguish individual components from mixtures [4-7]. This strategy faces several challenges with regards to SERS detection: (i) Classification of unknown samples is based on models established with known analytes, and these models may be sensitive to the ratio of individual components, and establishing a complete library of all possible combinations of analytes of interest would be unfeasible; (ii) As a highly sensitive tool, SERS analysis is subject to interference from environmental contaminants that adsorb onto the SERS-active surface during fabrication, handling, sampling, and measurement. The variation introduced by such contamination would further impede library construction; (iii) Thus far, most reported SERS-based assays are conducted in a relatively simple background, e.g., water or other pure solvents. In more realistic situations, the signal of target analytes is likely to be overwhelmed by the spectral background from components that are naturally abundant in the sample. In order to reduce this interference, the samples are often diluted before SERS measurement. This process also artificially reduces the concentration of the target analyte and lowers the detection sensitivity; (iv) The ability of molecules to adsorb onto a metal surface varies significantly. In the context of SERS analysis, this implies that only those molecules that can readily adsorb to the metal surface can be detected; the signal from weak adsorbants is likely either not to be captured, or to be buried in the signal from strongly adsorbed molecules. Ultimately, to address the aforementioned challenges for real-world applications, a simple means to physically separate the components of a mixture sample prior to SERS detection is necessary.

Thin-layer chromatography (TLC) has been used for decades to separate components from mixtures [8, 9]. This well-established method is simple and can be used to process multiple

samples and standards simultaneously. In TLC the test sample is first spotted onto a thin layer of porous stationary phase (e.g., SiO₂ gel) and allowed to dry. During plate development, the mobile phase (*i.e.*, mixture of organic solvents) propagates along the TLC plate via capillary action, allowing the individual components to migrate along the solvent migration direction and spatially redistribute as a function of their varying affinity between the stationary and mobile phases. With the emergence of high-performance TLC (HPTLC) and ultra-thin layer chromatography (UTLC), the efficiency of separation and the sensitivity of detection have been further improved [10].

Qualitative identification of samples in TLC is based on characteristic colors or fluorescence produced by a specific detection reagent combined with retention factor (R_f) values. Often the developed TLC spots are scraped off the plate, extracted from the SiO₂ gel matrix by means of repeatedly rinsing and centrifugation, and further examined by gas chromatography (GC) [11], infrared spectroscopy (IR) [12], nuclear magnetic resonance (NMR) [13], or mass spectrometry (MS) [14] for further identification, which are time-consuming and labor-intensive. SERS has previously been used in conjunction with TLC to overcome the poor sensitivity, and to provide more molecular information about the detected analytes [15-18]. In most reports, silver or gold nanoparticles are added onto the pre-separated TLC component bands, and SERS spectra collected from each band are rather an indication of surface concentration of the analytes, which means the full sensitivity of SERS will be compromised due to large amount of analytes left inside the bulk of the stationary phase. In addition, the multi-step treatment increases the complexity of the assay processing and data analysis. Moreover, the dramatically increased SERS enhancement brought about by silver nanoparticle aggregation is unfortunately cancelled

out by the lack of uniform SERS response across the entire sampling region, making quantitation impossible.

Here, we propose that UTLC-SERS can be directly performed on a uniform SERS-active surface with proper porosity for the sample components to be separated based on their affinity to the surface material. Bezuidenhout *et al* (2008) [19-21] reported a series of novel SiO₂ ULTC plates fabricated by glancing angle deposition with controllable nanostructure geometry and dimensions, and demonstrated the capability of effective separation of four dyes. Similar to these SiO₂ nanostructures, silver nanorod (AgNR) arrays fabricated by oblique angle deposition (OAD) have anisotropic nanoporous structures with the nanorod diameters under 100 nm in at least two dimensions, and can be readily used as SERS-active substrates [22-26]. Therefore, they possess the requisite characteristics to be utilized as a platform for simultaneous separation and detection of components in complex mixtures. In this feasibility study, we tested the practicality of using the OAD-fabricated AgNR arrays as novel on-chip UTLC plates and SERS-active substrates for both separation and detection purposes.

Materials and Methods

Materials

Methyl Orange (4-dimethylaminoazobenzene-4'-sulfonic acid sodium acid, MO) and Cresol Red (o-Cresolsulfonephthalein, CR), were obtained from Alfa Aesar (Ward Hill, MA). Trans-1,2-bis(4-pyridyl)ethylene (BPE) was purchased from Fluka (Buchs, Switzerland). Melamine (1,3,5-triazine-2,4,6-triamine), Rhodamine 6G (R6G), acetonitrile, and methylene violet 2B (MV) were from Sigma-Aldrich (St. Louis, MO). Methanol was obtained from J. T. Baker (Phillipsburg NJ). Silver (99.999%) and titanium (99.995%) were obtained from Kurt L.

Lesker (Clairton, PA).

UTLC-SERS Plate Fabrication

The SERS-active UTLC plates were fabricated using the OAD technique in a custom-built electron beam evaporation system as previously described [23, 24, 27-29]. Briefly, microscopic glass slides were cleaned with Piranha solution (80% sulfuric acid, 20% hydrogen peroxide), rinsed with deionized (DI) water, and dried with compressed nitrogen gas before being loaded into the deposition system. A 20-nm Ti layer and a 200-nm Ag thin-film were first deposited onto the glass substrates at normal incidence angle at the rates of 0.2 nm/s and 0.3 nm/s, respectively. The substrate surface normal was then rotated to an oblique angle of 86° with respect to the vapor incident direction with the continued Ag deposition at a rate of 0.3 nm/s. The chamber maintained a pressure of 10^{-6} Torr throughout the deposition process. The last OAD step generated a film of tilted and aligned Ag nanorods (AgNRs) with 868 ± 95 nm rod length, and 99 ± 29 nm rod diameter, with a tilting angle of approximately 73° with respect to the substrate normal [24, 28, 30]. The AgNR arrays have been demonstrated to be highly reproducible SERS-active substrates with intra-substrate relative standard deviations $< 15\%$, [28, 31] and using a 0.1 mM mercaptophenol solution we have further shown that the point-to-point fluctuation of our substrates is $< 8\%$ (See Appendix Fig. A.3).

UTLC Process

The as-deposited AgNR substrates were cleaned for 2 min using a custom made inductively-coupled RF plasma chamber operating at 40 W under a constant flow of ultra-pure argon with a chamber pressure < 1 Torr. Argon plasma cleaning allowed the removal of carbonaceous and organic contaminants during fabrication and storage of the substrates [32]. To ensure the mobile phase solvents do not induce spectral interference to the target samples, these

solvents were applied to the plasma-cleaned substrates and SERS spectra were recorded after the solvents completely vaporized.

After plasma cleaning, 0.1 μL of the samples were spotted near the edge of the substrate as indicated in Fig. 3.1A, and corresponding SERS spectra were recorded immediately after the droplets were dried under ambient conditions (Fig. 3.1B). Initially, a small amount of mobile phase solvent ($\sim 3\text{-}5\text{ mL}$) was placed into a glass beaker which was then covered with a glass lid to pre-saturate the beaker volume with solvent vapor. The substrate was then carefully placed upright into the beaker containing the mobile phase reservoir. Care was taken to assure that the sample spots were in proximity to the mobile phase, but did not contact the meniscus. The development process took approximately 5 min for each plate, during which the beaker remained covered to minimize mobile phase evaporation from the AgNR surface (Fig. 3.1C).

When UTLC development was completed, the solvent front position was marked immediately after the substrates were taken out of the beaker. After gently drying in nitrogen flow, spatially-resolved SERS measurements were performed on the developed substrate plate (Fig. 3.1D).

Limit of detection (LOD) for single components was tested using serial dilutions of pure BPE, CR, MO, MV, melamine, and R6G from 10^{-4} M to 10^{-7} M , both before and after UTLC development. Two sets of UTLC experiments were performed: (a) separation of 4 mixed dyes consisting of BPE, CR, MO, and MV, and (b) a mixture of R6G and melamine. In experiment (a), the concentration for each compound in the final mixture was $2.5 \times 10^{-5}\text{ M}$, whereas in experiment (b), two concentrations of melamine ($5 \times 10^{-3}\text{ M}$ and $5 \times 10^{-5}\text{ M}$) were used to create mixtures of melamine and R6G at different ratios (100:1, and 1:1). Methanol and acetonitrile were used as the mobile phase solvents in the four-component test, whereas methanol was used for the

separation of melamine and R6G.

SERS Measurement

SERS spectra were acquired using a HRC-10HT Raman analyzer system (Enwave Optronics, Irvine, CA) equipped with a 785 nm diode laser, a spectrometer, an integrated Raman probe for both excitation and signal collection. The focal length of the Raman probe was approximately 6 mm and the diameter of the laser beam is $\sim 100 \mu\text{m}$. The laser power used in all measurements was 30 mW at the sample, as monitored by a power meter. The spectrum collection time for each measurement was 1 to 10 s.

Before UTLC, nine spectra were collected from each sample spot at the origin. After UTLC, spectra were acquired at a spatial interval of 0.5 mm along the plate developing direction, starting from 5 mm below the sample origin line until approximately 5 mm beyond the visually identified solvent front.

Data Analysis

The collected SERS spectra were analyzed with WiRE 2.0 (Renishaw, Hoffman Estates, IL) and Origin 8.0 (OriginLab, Northampton, MA) software. Specific signature peaks for each sample component are identified and fit with a Gaussian and/or Lorentzian function to obtain corresponding baseline-corrected peak intensity values I , which are used as indicators of local analyte concentration. To verify the accuracy of the chromatograms and rule out false chromatographic bands introduced by distortions resulting from the peak fitting, several signature peaks are fitted for each component, and only the locations in which all the peaks are not equal to zero are considered as positive for this particular component. Intensity data from one of the fitted peaks were used for subsequent analyses.

For each sample component, the peak intensities at various locations r along the

development direction are divided by the highest peak intensity found in that component, resulting in a series of normalized peak intensities I_N , which are plotted against the developing distance r to generate the corresponding chromatograms. R_f value for each component is represented by the ratio of the distance between the sample origin and the location with the highest peak intensity for that component and the solvent migration distance (L). Plate height (H) is calculated accordingly as an indication of UTLC separation efficiency: $H = LW^2/16D^2$, where W is the width of the UTLC band, and D is the distance between sample origin and the center of the band [33].

Results and Discussion

Solvent Background Characterization

SERS spectra of the AgNR substrates pre-treated with the mobile phase solvents were first collected (Appendix Fig. A.1) to verify that the background spectra did not contain any significant Raman peaks. After argon plasma cleaning, the blank substrates exhibit a low spectral background, with no significant spectral features observed. Low intensity peaks at $\Delta\nu = 690\text{ cm}^{-1}$, 765 cm^{-1} , 810 cm^{-1} , 877 cm^{-1} , 958 cm^{-1} , and 1004 cm^{-1} are found in the spectra of acetonitrile and methanol. The presence of these same spectral features with other organic solvents (acetone, isopropanol, dichloromethane, and chloroform) suggests that these features result from subtle contaminant residues on the substrate surface adsorbed to the silver surface. In the spectrum of DI water, additional peaks at $\Delta\nu = 855\text{ cm}^{-1}$, 1051 cm^{-1} , 1136 cm^{-1} , 1229 cm^{-1} , 1275 cm^{-1} , 1330 cm^{-1} , and 1607 cm^{-1} are identified. Nonetheless, since the intensity of the background peaks is trivial compared to the analyte peaks, there is little or no interference to the analyte spectra after chromatogram development.

SERS of Single Components

Fig. 3.2 shows the molecular structures and corresponding SERS spectra of BPE, CR, MO, MV, R6G, and melamine. Asterisks indicate the signature peaks for each component. Specifically, the peak intensities at $\Delta\nu = 495\text{ cm}^{-1}$, 600 cm^{-1} , and 702 cm^{-1} are used to represent melamine; the $\Delta\nu = 1309\text{-}1360\text{ cm}^{-1}$ double peak and the $\Delta\nu = 1510\text{ cm}^{-1}$ peak are chosen for R6G; the $\Delta\nu = 1344\text{ cm}^{-1}$ single peak and $\Delta\nu = 1609\text{-}1640\text{ cm}^{-1}$ double peak for BPE; the $\Delta\nu = 430\text{-}447\text{ cm}^{-1}$ double peak for CR; the $\Delta\nu = 1365\text{-}1447\text{ cm}^{-1}$ quadruple peak for MO; and the $\Delta\nu = 418\text{ cm}^{-1}$ and 904 cm^{-1} peaks are selected for MV. The intensity of peaks at $\Delta\nu = 1609\text{ cm}^{-1}$ (BPE), 442 cm^{-1} (CR), 1420 cm^{-1} (MO), 904 cm^{-1} (MV), 1360 cm^{-1} (R6G), and 702 cm^{-1} (melamine) is used for chromatogram generation.

UTLC Separation

UTLC-SERS of CR, MO, BPE, and MV Mixture

For the UTLC-SERS substrates developed using two different mobile phases (methanol and acetonitrile), chromatograms are generated by plotting the normalized intensity of specific peaks against distance from sample origin (Fig. 3.3 (a) and (c)). MV and BPE are separable from MO and CR, as well as from each other after 5 min of UTLC development using methanol as the mobile phase. The solvent front migrates approximately 7.5 mm beyond the sample origin spots. The highest measured intensity values are obtained at 2.5 mm, 1.5 mm, 6.5 mm, and 7.0 mm for MO, CR, BPE, and MV, respectively, which correspond to retention factors (R_f s) of 0.36, 0.20, 0.87, and 0.93. When acetonitrile is used as the mobile phase, the most intense locations are at 2.0 mm, 1 mm, 1.5 mm, and 4.5 mm for MO, CR, BPE, and MV, respectively, with R_f s being 0.4, 0.2, 0.3, and 0.9. Different R_f s in acetonitrile compared with methanol indicate different partitioning ratios of these four analytes in the mobile phase solvents and on the silver surface,

which serves as the stationary phase.

In multiple experiments, we found that the solvent migration distance on the AgNR substrates varied between 3.5 and 10.5 mm from the sample origin, which is comparable to Brett *et al*'s observation on the GLAD-fabricated SiO₂ films [20]. However, our AgNR plate has a lower and more variable efficiency, with theoretical plate heights ranging from 9.6 μm to 861 μm, whereas the GLAD-fabricated SiO₂ films has a theoretical plate of 12 to 28 μm. The low resolution of the AgNR UTLC-SERS plate is primarily due to the restriction of our current spotting equipment. The large sample volume (0.1 μL, applied by hand) compared to that used in most UTLC (10-25 nL, applied robotically) resulted in an average spreading area of ~1 mm in diameter. Given the low concentration used, the analyte molecules are expected to form an unsaturated monolayer on the silver surface, and the spots to maintain constant spatial coverage as the components are carried along with the mobile phase. In the face of limited migration distance of UTLC, the inevitable overlapping of chromatographic bands could ultimately undermine the resolution of the plate in conventional UTLC, in which the characterization of individual components is based upon comparison of R_f values.

In contrast, at locations where more than one component are present, the high spectral resolution of SERS is nonetheless able to capture the spectral features of all components involved, thereby compensating for the loss in spatial resolution. For example, Fig. 3.3 (b) shows the spatially-resolved SERS spectra of the plate developed with methanol. At 1.5 mm from sample origin, the spectrum is dominated by CR, but features near the 1365-1447 cm⁻¹ region indicate the presence of a small amount of MO.

UTLC-SERS of Melamine and R6G Mixture

Since R6G has significantly higher solubility in methanol (400 g/L at 20 °C) than

melamine (<1 g/L), at low concentrations (5×10^{-5} M) these two components can be easily separated with methanol as demonstrated in Fig. 3.4 (a) and (b). After the solvent front has migrated 0.5-1.0 mm, the melamine signal remains localized to the original sample spot, whereas the R6G signal is only detected near the solvent migration front. In another scenario, the mixture consisting of 5×10^{-3} M melamine and 5×10^{-5} M R6G exhibits only the melamine spectrum before UTLC, as more melamine molecules tend to out-compete the R6G molecules for binding sites on the silver surface. During UTLC, however, the weakly bound R6G molecules are carried with the migration front. Without having to compete with melamine for adsorption, R6G spectra can more readily access and adsorb to the Ag surface. SERS spectra also confirm the presence of this zone (Fig. 3.4 (c) and (d)). At the sample origin, because of the extremely high concentration, melamine molecules are likely to form multilayers, where only a portion of molecules are directly adsorbed to the AgNR surface, and the rest reside unadsorbed on top of this layer. During UTLC, the excess melamine molecules are carried by the migrating solvent flow, and become adsorbed onto the available adsorption sites of the AgNRs along the migration direction, yielding an undesired tailing effect (Fig. 3.4 (c) and Appendix Fig. A.2). In contrast, as the concentration is decreased to 5×10^{-5} M, nearly all of the molecules are adsorbed onto the silver, and form a single layer. As the number of molecules available to migrate with the mobile phase significantly decreases, the tailing effect is eliminated. This result clearly demonstrates that UTLC could improve the LOD in a mixed solution by displaying the analytes spatially.

LODs for pure BPE, CR, MO, MV, melamine, and R6G were investigated using pure analytes serially diluted in DI water, both before and after UTLC development in methanol. Before development, SERS is able to detect BPE and R6G with concentrations as low as 10^{-6} M, equivalent to 182 ng/mL and 479 ng/mL in original sample solution. Considering the small

sample volume (0.1 μL) and measurement area (100 μm in diameter), this corresponds to 1 fmole of analytes. LODs for CR, MO, and MV are found to be 10^{-5} M, equivalent to 4.04×10^3 ng/mL, 3.27×10^3 ng/mL, and 3.94×10^3 ng/mL before development, respectively. Melamine has a higher LOD of 10^{-4} M (1.26×10^4 ng/mL). After developing the plate with methanol, the LODs for all the analytes remain unaffected. Lower LODs for BPE and R6G than other dyes result from its larger Raman cross section. The LOD for melamine is higher than the FDA tolerance level (2.5 mg/L) and that observed in our previous study on direct SERS measurement of melamine (0.1 mg/L) [34], possibly due to the smaller surface coverage resulted from the much lower sample volume. Because the detection sensitivity is directly determined by the SERS enhancement factor (EF), further modification to the UTLC-SERS chip through more versatile substrate fabrication techniques (e.g., glancing angle deposition) could be attempted to achieve even higher EFs, as different morphologies of the resulted silver nanostructure could lead to higher enhancement factors in SERS. For example, we have demonstrated recently the SERS enhancement factor can be further improved 2-4 times by bending the Ag nanorods [35, 36]. The LODs could also be improved by employing a micro-Raman system with a cooled charge coupled device (CCD).

Although the exact mechanisms for different partitioning behaviors of individual analytes between AgNR surface and the mobile phase solvents is not yet completely understood, it is likely to involve the same two major principles of standard TLC: the molecule's affinity to stationary phase (*i.e.* silver nanorod surface), and its solubility in the mobile phase. The affinity to the silver surface is further dependent on the binding strength of the molecule onto silver surface (physical adsorption, covalent or non-covalent bonding), and available binding sites on the AgNR surface. Unlike conventional UTLC adsorbent material (SiO_2 or Al_2O_3), the binding

sites can be chemically active to target analytes in the test sample as well as undesirable contaminants. Therefore, it is necessary to remove all adsorbed material from AgNRs before samples are loaded onto the substrate with effective argon plasma cleaning, and freeing up adsorption sites. The removal of organic impurities from the surface of the AgNRs also improves the hydrophilic character of the SERS plate. Molecules with thiol or triazole moieties that tend to form strong bonds with silver are expected to have a low retention factor, which is confirmed by the behavior of melamine in our experiments. Changing mobile phase solvents resulted in altered R_f s in some molecules, implying that optimum separation could potentially be achieved given adequate knowledge of the analytes, including its interactions with both the stationary (silver) and mobile phases.

Conclusion

In this pilot study we have demonstrated the potential of using OAD-fabricated AgNR array substrates to serve as on-chip UTLC and SERS plates for mixtures of dyes and Raman reporters without the need for extra processing steps beyond initial development. Despite the limited spatial separation resolution of these SERS-UTLC plates, which results primarily from our sample application/spotting equipment, the incorporation of SERS is nonetheless capable of capturing spectral differences at locations where components are not fully separated, thus compensating for low resolution. The analyte separation could be further explored by optimizing mobile phase solvents to achieve maximum efficiency, and the limit of detection can reach as low as 10^{-6} M. Meanwhile, the sensitivity of SERS can also be improved in conjunction with the UTLC process, as demonstrated by the successful detection of R6G at a low concentration, whose SERS signal is otherwise blocked by the predominant melamine spectra. This could be

particularly useful in the real-world scenarios in which the target analytes are likely to be scarce compared to the complex matrix, such as food, urine, sputum, and blood. Although silver is not as chemically inert as the commonly used TLC stationary phases, e.g., SiO_2 and Al_2O_3 , and the possibility for the analyte molecules to react with silver could not be precluded, we have recently demonstrated that the silver nanorod surface could be coated with a thin layer of inert material (e.g., gold or SiO_2) through chemical modification or atomic vapor deposition techniques such that the chemical reactions between the analytes and silver do not occur [37, 38]. In addition, thanks to the shorter migration distance in UTLC compared to conventional TLC, the size of the UTLC-SERS chip could be significantly reduced, and the platform could be further modified or incorporated into other miniaturized (microscale) devices for rapid, on-site, and high throughput screening of target analytes.

Acknowledgements

This work is supported by USDA CSREES Grant #2009-35603-0551, and is also partially supported by National Science Foundation under the contract number CMMI-0824728 and the University of Georgia College of Agricultural & Environmental Sciences College Experimental Station.

References

1. Schatz, G.C., *Theoretical studies of surface enhanced Raman scattering*. Accounts of Chemical Research, 1984. **17**(10):370-376.
2. Wang, Y., K. Lee, and J. Irudayaraj, *Silver nanosphere SERS probes for sensitive identification of pathogens*. The Journal of Physical Chemistry C, 2010. **114**(39):16122-16128.
3. Kneipp, K., Y. Wang, R.R. Dasari, and M.S. Feld, *Approach to single molecule detection using surface-enhanced resonance Raman scattering (SERRS): a study using Rhodamine 6G on colloidal silver*. Applied Spectroscopy, 1995. **49**(6):780-784.
4. Naja, G., P. Bouvrette, S. Hrapovich, Y. Liu, and J.H.T. Luong, *Detection of bacteria aided by immuno-nanoparticles*. Journal of Raman Spectroscopy, 2007. **38**(11):1383-1389.
5. Patel, I.S., W.R. Premasiri, D.T. Moir, and L.D. Ziegler, *Barcoding bacterial cells: A SERS based methodology for pathogen identification*. Journal of Raman Spectroscopy, 2008. **39**(11):1660-1672.
6. Abell, J.L., J. Lee, Q. Zhao, H. Szu, and Y. Zhao, *Differentiating intrinsic SERS spectra from a mixture by sampling induced composition gradient and independent component analysis*. Analyst, 2012. **137**(1):73-76.
7. Hennigan, S.L., J.D. Driskell, R.A. Dluhy, Y.P. Zhao, R.A. Tripp, K.B. Waites, and D.C. Krause, *Detection of mycoplasma pneumoniae in simulated and true clinical throat swab specimens by nanorod array-surface-enhanced Raman spectroscopy*. Plos One, 2010. **5**(10):e13633.

8. Skipski, V.P., A.F. Smolowe, R.C. Sullivan, and M. Barclay, *Separation of lipid classes by thin-layer chromatography*. *Biochimica et Biophysica Acta - Lipids and Lipid Metabolism*, 1965. **106**(2):386-396.
9. Scott, P., J. Lawrence, and W. Van Walbeek, *Detection of mycotoxins by thin-layer chromatography: application to screening of fungal extracts*. *Applied Microbiology*, 1970. **20**(5):839.
10. Hauck, H.E., O. Bund, W. Fischer, and M. Schulz, *Ultra-thin layer chromatography (UTLC)—A new dimension in thin-layer chromatography*. *Journal of Planar Chromatography-Modern TLC*, 2001. **14**(4):234-236.
11. Berkov, S., J. Bastida, M. Nikolova, F. Viladomat, and C. Codina, *Rapid TLC/GC-MS identification of acetylcholinesterase inhibitors in alkaloid extracts*. *Phytochemical Analysis*, 2008. **19**(5):411-419.
12. Fuller, M.P. and P.R. Griffiths, *Diffuse reflectance measurements by infrared Fourier transform spectrometry*. *Analytical Chemistry*, 1978. **50**(13):1906-1910.
13. Bonnett, R., F. Czechowski, and L. Latos-Grazynski, *Metalloporphyrins in coal. 4. TLC-NMR of iron porphyrins from coal: the direct characterization of coal hemes using paramagnetically shifted proton NMR spectroscopy*. *Energy & Fuels*, 1990. **4**(6):710-716.
14. Stoll, M.S., E.F. Hounsell, A.M. Lawson, W. Chai, and T. Feizi, *Microscale sequencing of O-linked oligosaccharides using mild periodate oxidation of alditols, coupling to phospholipid and TLC-MS analysis of the resulting neoglycolipids*. *European Journal of Biochemistry*, 1990. **189**(3):499-507.
15. Caudin, J.P., A. Beljebbar, G.D. Sockalingum, J.F. Angiboust, and M. Manfait, *Coupling FT Raman and FT SERS microscopy with TLC plates for in situ identification of chemical*

- compounds*. Spectrochimica Acta Part A: Molecular and Biomolecular Spectroscopy, 1995. **51**(12):1977-1983.
16. Wang, Y., J. Zhang, and X. Ma, *TLC-FT-SERS study on a pair of optic isomers in ephedra*. Spectroscopy and Spectral Analysis, 2004. **24**(11):1373-1375.
 17. Brosseau, C.L., A. Gambardella, F. Casadio, C.M. Grzywacz, J. Wouters, and R.P. Van Duyne, *Ad-hoc surface-enhanced Raman spectroscopy methodologies for the detection of artist dyestuffs: thin layer chromatography-surface enhanced Raman spectroscopy and in situ on the fiber analysis*. Analytical Chemistry, 2009. **81**(8):3056-62.
 18. Geiman, I., M. Leona, and J.R. Lombardi, *Application of Raman spectroscopy and surface-enhanced Raman scattering to the analysis of synthetic dyes found in ballpoint pen inks*. Journal of Forensic Sciences, 2009. **54**(4):947-952.
 19. Bezuidenhout, L.W. and M.J. Brett, *Ultrathin layer chromatography on nanostructured thin films*. Journal of Chromatography A, 2008. **1183**(1-2):179-185.
 20. Brett, M.J., S.R. Jim, M.T. Taschuk, G.E. Morlock, L.W. Bezuidenhout, and W. Schwack, *Engineered anisotropic microstructures for ultrathin-layer chromatography*. Analytical Chemistry, 2010. **82**(12):5349-5356.
 21. Oko, A.J., S.R. Jim, M.T. Taschuk, and M.J. Brett, *Analyte migration in anisotropic nanostructured ultrathin-layer chromatography media*. Journal of Chromatography A, 2011. **1218**(19):2661-7.
 22. Shanmukh, S., Les Jones, J. Driskell, Y. Zhao, R. Dluhy, and R.A. Tripp, *Rapid and sensitive detection of respiratory virus molecular signatures using a silver nanorod array SERS substrate*. Nano Letters, 2006. **6**(11):2630-2636.

23. Fu, J.X., A. Collins, and Y.P. Zhao, *Optical properties and biosensor application of ultrathin silver films prepared by oblique angle deposition*. The Journal of Physical Chemistry C, 2008. **112**(43):16784-16791.
24. Chaney, S.B., S. Shanmukh, R.A. Dluhy, and Y.P. Zhao, *Aligned silver nanorod arrays produce high sensitivity surface-enhanced Raman spectroscopy substrates*. Applied Physics Letters, 2005. **87**(3):031908.
25. Driskell, J.D., Y. Zhu, C.D. Kirkwood, Y. Zhao, R.A. Dluhy, and R.A. Tripp, *Rapid and sensitive detection of rotavirus molecular signatures using surface enhanced Raman spectroscopy*. Plos One, 2010. **5**(4):e10222.
26. Abell, J.L., J.D. Driskell, R.A. Dluhy, R.A. Tripp, and Y.P. Zhao, *Fabrication and characterization of a multiwell array SERS chip with biological applications*. Biosensors and Bioelectronics, 2009. **24**(12):3663-3670.
27. Chu, H.Y., Y.J. Liu, Y.W. Huang, and Y.P. Zhao, *A high sensitive fiber SERS probe based on silver nanorod arrays*. Optics Express, 2007. **15**(19):12230-12239.
28. D. Driskell, J., S. Shanmukh, Y. Liu, S. B. Chaney, X.J. Tang, Y.P. Zhao, and R. A. Dluhy, *The use of aligned silver nanorod arrays prepared by oblique angle deposition as surface enhanced Raman scattering substrates*. The Journal of Physical Chemistry C, 2008. **112**(4):895.
29. Liu, Y.J., H.Y. Chu, and Y.P. Zhao, *Silver nanorod array substrates fabricated by oblique angle deposition: morphological, optical, and sers characterizations*. The Journal of Physical Chemistry C, 2010. **114**(18):8176-8183.

30. Zhao, Y.P., S.B. Chaney, S. Shanmukh, and R.A. Dluhy, *Polarized surface enhanced Raman and absorbance spectra of aligned silver nanorod arrays*. The Journal of Physical Chemistry B, 2006. **110**(7):3153-3157.
31. Abell, J., J. Garren, and Y. Zhao, *Dynamic rastering surface-enhanced Raman scattering (SERS) measurements on silver nanorod substrates*. Applied Spectroscopy, 2011. **65**(7):734-740.
32. Negri, P., N.E. Marotta, L.A. Bottomley, and R.A. Dluhy, *Removal of surface contamination and self-assembled monolayers (SAMs) from silver (Ag) nanorod substrates by plasma cleaning with argon*. Applied Spectroscopy, 2011. **65**(1):66-74.
33. Sherma, J. and B. Fried, *Handbook of Thin-Layer Chromatography*. 2nd ed. 1996, Easton, PA: Marcel Dekker, Inc.
34. Du, X.B., H.Y. Chu, Y.W. Huang, and Y.P. Zhao, *Qualitative and quantitative determination of melamine by surface-enhanced Raman spectroscopy using silver nanorod array substrates*. Applied Spectroscopy, 2010. **64**(7):781-785.
35. Zhou, Q., Y.P. He, J. Abell, Z.J. Zhang, and Y. Zhao, *Surface-enhanced Raman scattering from helical silver nanorod arrays*. Chemical Communications, 2011. **47**(15):4466-4468.
36. Zhou, Q., X. Zhang, Y. Huang, Z. Li, Y. Zhao, and Z. Zhang, *Enhanced surface-enhanced Raman scattering performance by folding silver nanorods*. Applied Physics Letters, 2012. **100**(11):113101-113103.
37. Song, C., J.L. Abell, Y. He, S. Hunyadi Murph, Y. Cui, and Y. Zhao, *Gold-modified silver nanorod arrays: growth dynamics and improved SERS properties*. Journal of Materials Chemistry, 2012. **22**(3):1150-1159.

38. Song, C., J. Chen, J.L. Abell, Y. Cui, and Y. Zhao, *Ag-SiO₂ Core-Shell Nanorod Arrays: Morphological, Optical, SERS, and Wetting Properties*. *Langmuir*, 2011. **28**(2):1488-1495.

Figures

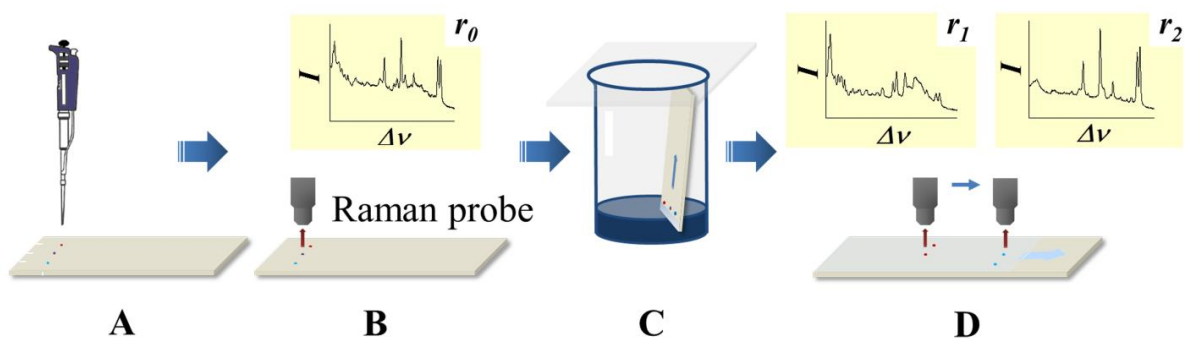


Figure 3.1 Schematic representation of the ULTC-SERS process. A Loading samples on substrate; B Acquiring SERS signal; C UTLC development; D Acquiring SERS spectra along development direction.

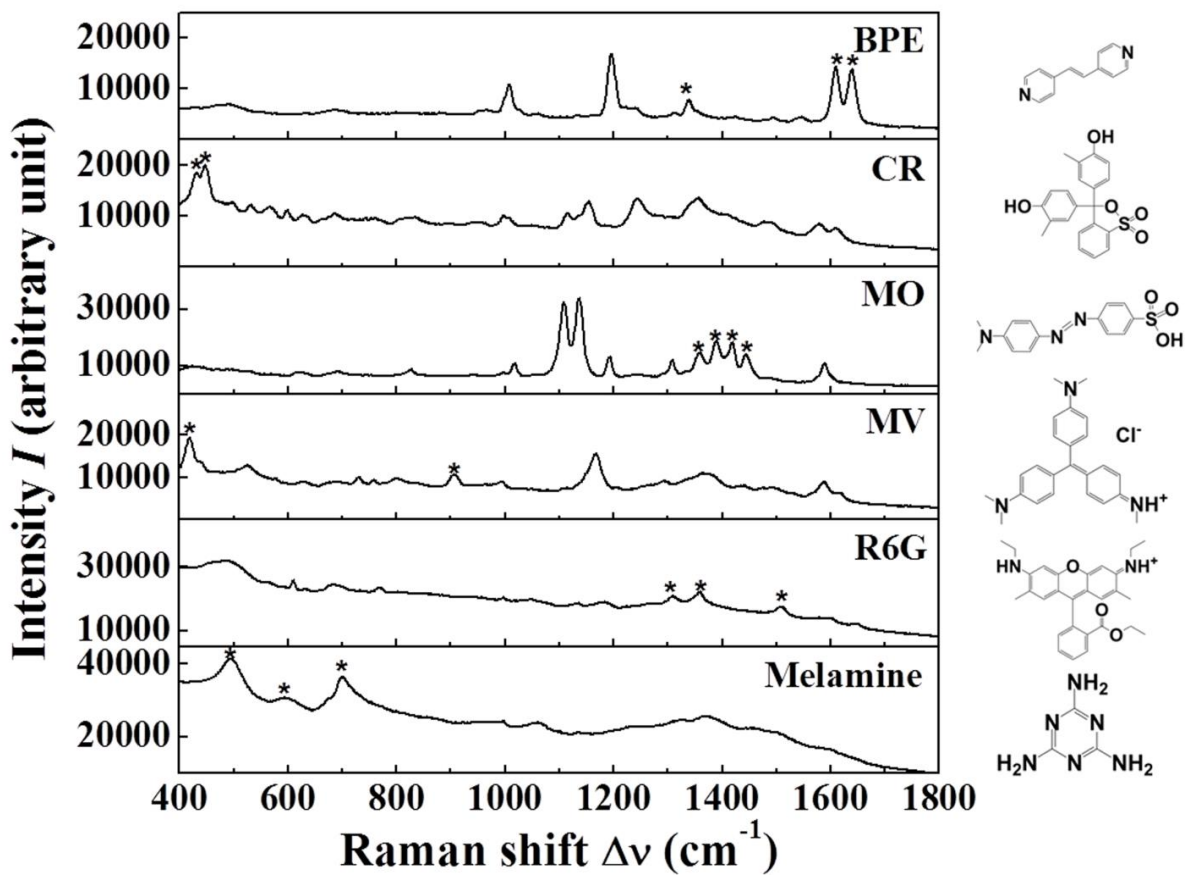


Figure 3.2 SERS spectra of the analytes used in the four- and two-component mixtures. Asterisks indicate signature peaks used for chromatogram generation.

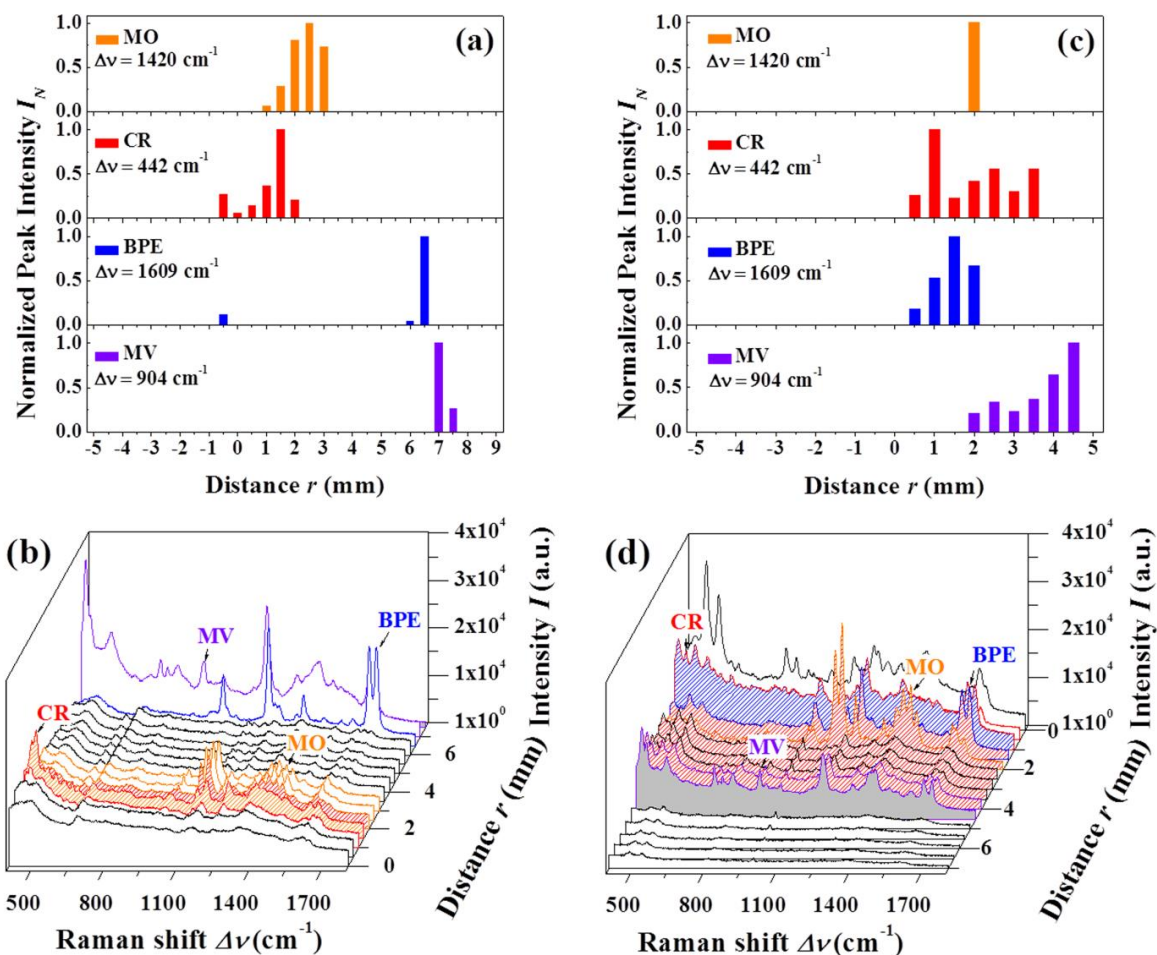


Figure 3.3 Separation of MO, CR, BPE, and MV with UTLC-SERS in methanol (a and b) and acetonitrile (c and d). Chromatograms (a and c) show the normalized intensity of the signature peaks as a function of position along ULTC-SERS plate after development, in which 0 on the x-axis indicates the sample origin. In the corresponding SERS spectra (b and d), orange, red, blue, and violet curves represent MO, CR, BPE, and MV spectra at locations with the highest signature peak intensity; walls filled with colored slashes indicate the presence of mixtures of corresponding components; walls filled with solid grey color indicate the solvent front.

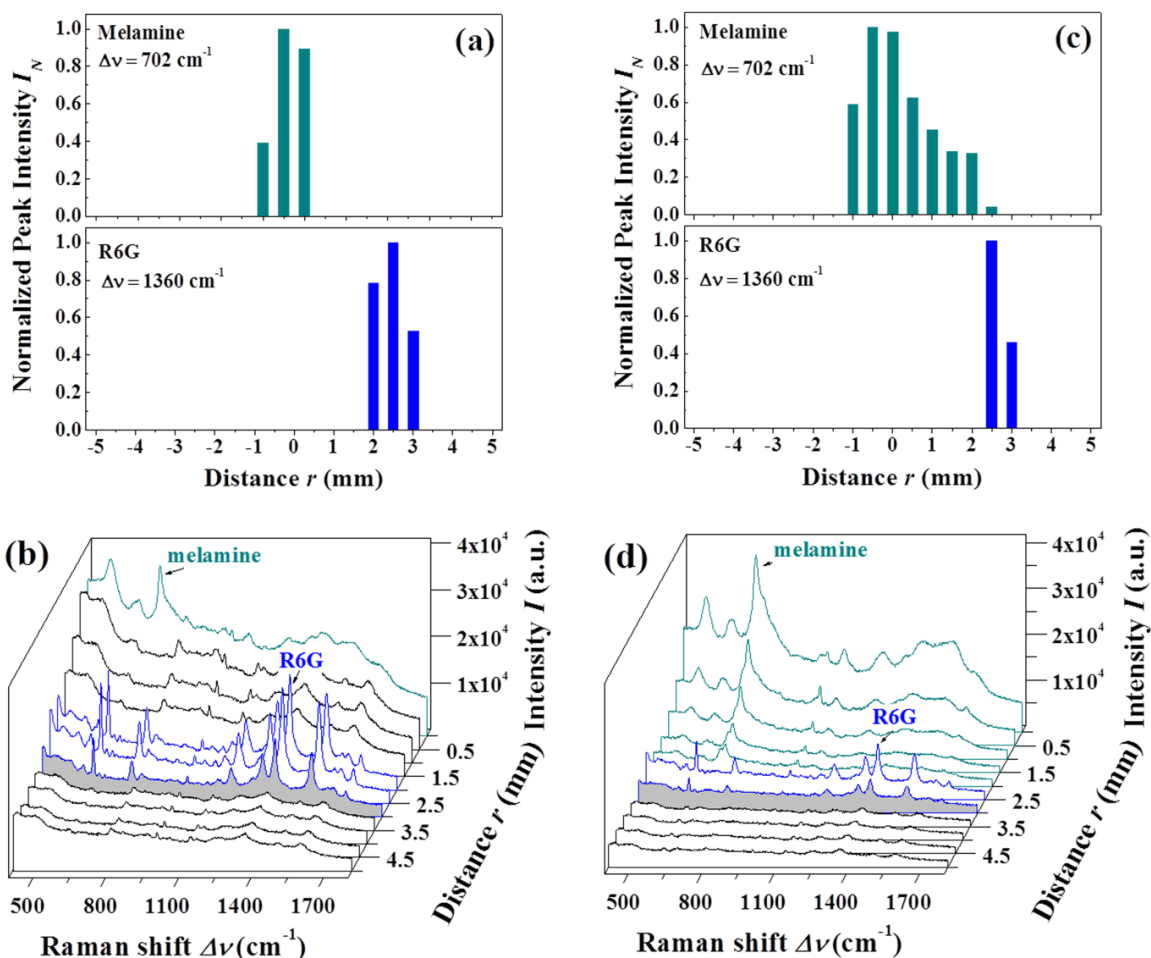


Figure 3.4 Separation of melamine and Rhodamine 6G (R6G): (a) and (b) equimolar mixture of melamine and R6G (1:1); (c) and (d) 100:1 mixture of melamine and R6G. In the chromatograms (a and c), 0 indicates the sample origin, whereas cyan and blue bars indicate the normalized peak intensity of melamine (702 cm^{-1}) and R6G (1360 cm^{-1}), respectively. In the corresponding SERS spectra, cyan and blue curves represent melamine and R6G spectra at locations with the highest signature peak intensity; walls filled with grey color indicate the solvent migration front.

CHAPTER 4
CHARACTERIZATION OF POLYCYCLIC AROMATIC HYDROCARBONS USING
RAMAN AND SURFACE ENHANCED RAMAN SPECTROSCOPY²

² Jing Chen, Yao-wen Huang, and Yiping Zhao. To be submitted to *Journal of Raman Spectroscopy*.

Abstract

Polycyclic aromatic hydrocarbons (PAHs) are ubiquitous atmospheric pollutants and food contaminants, which exhibit potent carcinogenicity, mutagenicity, and teratogenicity. Traditional PAH detection techniques based on liquid chromatography and gas chromatography faces challenges in routine inspection, due to complicated sample preparation and low throughput. Surface enhanced Raman spectroscopy (SERS) can be potentially used as an alternative technique in PAH analysis. However, there is limited information on the intrinsic Raman and SERS fingerprints of PAHs. In this study we have acquired the Raman and SERS spectra of seven PAH compounds, and compared their experimental spectra with theoretical Raman spectra using density function theory (DFT). The vibrational modes corresponding to the Raman peaks have also been assigned using DFT. Such information could be useful for developing SERS assays for simple and rapid PAH identification.

Introduction

Polycyclic aromatic hydrocarbons (PAHs) are a group of compounds with fused aromatic rings but do not contain heteroatoms or substitution groups. PAHs are formed during the incomplete combustion of fossil fuels and other carbon-containing fuels such as wood and charcoal at high temperatures (500 – 700 °C), though formation can also occur at lower temperatures (100 - 150 °C) over a period on the geological time scale [1]. PAHs can most frequently be found in soil and sediments for their lipophilic nature, but are also considered widespread organic pollutants in the atmosphere. Human exposure to PAHs is mainly through inhalation of polluted air and ingestion of contaminated food, particularly those prepared at high temperatures (e.g., smoked foods) and seafood during oil spills. Once entering the human body,

PAHs could act as carcinogens or carcinogenic synergists. Some PAHs also bind to genetic materials and exhibit mutagenic and teratogenic effects [2].

Traditionally, detection of PAHs has mostly been relying on chromatography techniques. The current gold standards for PAH identification are liquid chromatography using fluorescence detectors (LC/FLD) or gas chromatography coupled with mass spectrometry (GC/MS) [1, 3]. The detection limits could typically reach sub parts per billion (ppb) levels. However, lengthy and laborious sample preparation is often required in GC and LC, especially with detection from high fat content matrices [3]. More recently, alternative techniques have been proposed for PAH identification, including a capillary zone electrophoresis method [4], and optical and spectroscopic methods such as surface enhanced Raman spectroscopy (SERS) [5-8].

SERS takes advantage of the enhanced electromagnetic field near nanostructured metal surfaces (*i.e.*, SERS substrates) to enhance the Raman scattering signal of target analytes, thereby providing molecular fingerprints even at trace amounts [9-11]. In the literature, the spectra of several PAH compounds (*e.g.*, naphthene, anthracene, fluorene, pyrene, phenanthrene, tetracene, and chrysene) have been documented early in the 1970s and 1980s using conventional Raman, Fourier transform Raman, coherent anti-Stokes Raman, and resonance Raman techniques [12, 13]. However, direct SERS detection of PAHs is limited by the poor adsorption of PAHs onto the SERS active substrates. As a result, a significant portion of research effort has been directed to functionalizing the SERS substrates for improved PAH adsorption [14-20]. During substrate surface modification, the intrinsic SERS signatures of PAHs were largely neglected. On the other hand, the molecular vibrational modes associated with the PAH peaks have not been well characterized in previous studies.

In order to reveal the inherent PAH Raman and SERS fingerprints and provided theoretical basis for future PAH analysis, we have obtained the Raman and SERS spectra of seven PAH compounds, and compared the experimental data with the theoretical Raman spectra predicted by density function theory. The detailed band assignments have been provided, and the SERS detection limits have also been determined on silver nanorod array (AgNR) substrates.

Materials and Methods

Materials

The PAHs used in this study (Table 4.1) were all obtained from Sigma Aldrich (St. Louis, MO). Methanol was purchased from J. T. Baker (Phillipsburg NJ). Silver (99.999%) and titanium (99.995%) were obtained from Kurt L. Lesker (Clairton, PA).

Density function theory (DFT) calculation

The theoretical Raman spectra of seven PAH compounds were calculated using the Gaussian 03W DFT package. The DFT calculations were based on Becke's three-parameter exchange function (B3) [21] with the dynamic correlation function of Lee, Yang, and Parr (LYP) [22]. The molecular geometries of the antibiotics were optimized using the hybrid B3 (exchange) and the LYP (correlation) function (B3LYP) in conjunction with a modest 6-311g** basis set.

Fabrication of AgNR substrates

SERS-active silver nanorod (AgNR) array substrates were fabricated using oblique angle deposition (OAD) in a custom-built electron beam evaporator as described previously [23, 24]. Briefly, glass slides were cleaned with Piranha solution (80% sulfuric acid, 20% hydrogen peroxide), rinsed with deionized (DI) water, dried with nitrogen, and loaded into the deposition chamber above the source material. Under high vacuum ($<10^{-6}$ Torr) conditions, 20 nm of

titanium and 200 nm of silver were deposited onto the glass slides at a normal incidence angle at a deposition rate of 0.2 nm/s and 0.3 nm/s, respectively. Then the substrate surface normal was rotated to 86 ° with respect to the incident vapor direction, and silver continued to be deposited at a rate of 0.3 nm/s. The last OAD step yielded a film of aligned nanorods ~ 900 nm in length, ~ 100 nm in rod diameter, with a tilting angle of approximately 73 ° with respect to the substrate normal [23, 25]. To remove the organic contaminants accumulated during fabrication and storage, before the SERS measurements, the as-deposited AgNR substrates were cleaned for 2 min in a custom built inductively-coupled RF plasma chamber, which operated at 30 W under a constant flow of ultra-pure argon with a chamber pressure ~ 600 mTorr [26].

Bulk Raman spectra

The Raman spectra of five PAHs (ACP, BaA, BaP, F, and P) were collected directly from the powder using a portable Raman analyzer, Enwave ProRaman 785A2 (Enwave Optronics, Irvine, CA) equipped with a 785 nm diode laser at a power of 60 mW and a spectral acquisition time of 10 s.

SERS spectra

For the SERS measurements, 0.1 µL aliquots of PAHs at 200 µg/mL in methanol were applied to the AgNR substrates and dried under ambient conditions, and spectra were collected through a 10 × objective lens at an excitation power of 60 mW and a collection time of 10 s.

Limits of detection (LODs)

A series of PAH dilutions were prepared in methanol, with the final concentration ranging from 50 ng/mL to 1000 ng/mL. After the dilutions were applied to the AgNRs and dried, SERS spectra were acquired at 60 mW, 10 s using a 10 x objective lens. At least three spectra were collected from randomly selected locations on the same substrate, and substrates fabricated

from two independent batches were used to account for batch-to-batch variations. The lower LOD was determined using the 3σ method [27], in which the intensities of characteristic SERS peaks was compared with a threshold value determined by $3\times$ standard deviation of the spectral intensity at a featureless spectral region ($1750\text{-}1800\text{ cm}^{-1}$).

Results and Discussion

DFT-calculated Raman spectra of PAHs

The DFT-calculated Raman spectra of seven PAH compounds between 300 and 1800 cm^{-1} are shown in Figure 4.1, with the corresponding 3-D molecular structures and vibrational mode assignments listed in Appendix B. According to the DFT prediction, an abundance of Raman peaks appear near $1200 - 1600\text{ cm}^{-1}$. Several distinct peaks are also found at lower wavenumbers ($300 - 1000\text{ cm}^{-1}$) with lower intensities. The peaks in the low-wavenumber region can mainly be attributed to the C-C bending modes, while those appearing at the mid-wavenumber regions tend to result from the C-H bending modes. Because of the fused aromatic ring structure, all the carbon atoms in the PAH molecules are coplanar (see Fig. B.1-B.7 in Appendix B); hence it is not surprising that the majority of these bending modes are restrained within this plane. Nevertheless, out-of-plane C-C and C-H bending which contribute to very intense Raman peaks can also be identified.

It is worth noting that the vibrational mode assignments only convey the most dominant oscillations, but in most cases, the predicted peaks are rather a result of the collective vibrations of multiple or all of the atoms and bonds within the molecule. Influenced by other oscillations within the same molecule, peaks of similar vibrational modes are often observed at different

wavenumbers for different compounds. This leads to a unique Raman fingerprint for each PAH compound as shown in Figure 4.1.

In addition, DFT can also estimate the magnitude of the predicted vibrational modes, as expressed by their Raman activity (Fig. 4.1). Obviously, the C-H bending modes tend to contribute to more intense Raman peaks near the mid-wavenumber range, due to the higher polarizability of the C-H bending modes compared with the C-C bending modes. Consequently, the PAHs with a larger number of C-H moieties, such as BaP, BaA, and ANT, tend to have higher predicted Raman activity compared to small PAHs with fewer C-H groups (*e.g.*, ACP and ACY). Furthermore, PAHs with more complex and asymmetric structures, such as BaP and BaA, tend to yield more Raman peaks that are closely packed within a short spectral range, while fewer and more resolved peaks are found in simpler and more symmetric molecules like ANT.

Bulk Raman spectra of selected PAHs

The bulk Raman spectra were also obtained from five PAHs which were supplied in the powder form (ACP, BaA, BaP, F, and P). As shown in Fig. 4.2, sharp and well-resolved peaks can be identified in the spectra of ACP, F, and P. The Raman spectrum of P obtained in this study is consistent with those acquired in previous reports [13] with minor differences in relative peak intensities, which is likely to be caused by the use of a different excitation wavelength. Overall, despite the structural similarities, each PAH displays its distinct Raman peaks. As discussed in the previous section, the peak shifts are mainly caused by influence of other vibrational modes within the conjugated ring system.

Since non-resonance Raman signals are generally very weak, and fluorescence has a longer excited state lifetime compared to Raman scattering, Raman signals can be easily overwhelmed by fluorescence signals, causing an inability to identify Raman peaks from pronounced

fluorescence backgrounds [28]. Among the tested PAHs, BaP and BaA have the lowest fluorescence excitation energies [29], making their Raman signal more susceptible to fluorescence interference. Hence less resolved peaks with much lower intensities are found in the BaA and BaP spectra due to the strong fluorescent background, which also agrees with the literature findings [30].

Some differences between the experimentally acquired Raman spectra and the DFT-calculated Raman spectra are quite obvious. The observed discrepancies are threefold: emergence and absence of peaks, shifts in peak position, and changes in Raman signal intensity. In general, fewer peaks are observed in the experimental spectra compared with the DFT Raman spectra, as indicated in Appendix C, Tables B.1 - B.7 (Note: For brevity of the tables, Raman peaks with low predicted intensities are not listed.). This is because the DFT algorithm has an inherent tendency to over-estimate the vibrational modes [31]. The probabilities for the vibrational modes are not all equal, and some predicted oscillations only contribute negligibly to the overall Raman scattering. Thus the signal of these weak vibrational modes is difficult to be picked up by current Raman techniques. On the other hand, adjacent peaks tend to merge into single peaks in the experimental spectra because of the limited spectral resolution provided by the instrument. Absence of certain peaks in the experimental spectra is rare but also observed. A reasonable explanation is that since DFT estimation only presents the vibrational modes for the “optimized” structure (*i.e.*, the molecular configuration that results in the lowest overall energy state), the vibrational modes that are not in the favored configuration tend to be underestimated or ignored. Moreover, DFT has a limitation in its ability to optimize molecular configurations, and the results are also dependent on the input parameters and functions used. Therefore, the optimization results do not necessarily represent the true configuration in which the molecules

exist in most abundance. Shifts in peak position are another commonly observed phenomenon with DFT calculation due to the abovementioned reasons. Finally, the largest discrepancy between the theoretical and experimental data is the signal intensity. In previous studies it is reported that DFT tends to overestimate certain vibrational modes while underestimate others [31]. For example, the experimental spectra do not agree with the DFT prediction that peak intensities near the 1200 - 1600 cm^{-1} region are higher than other spectral regions; instead, an even distribution of peak intensities across the entire scanned region is observed.

SERS spectra of selected PAHs

The obtained SERS spectra are compiled in Figure 4.3. Although SERS peaks are identified in all PAH spectra, those of ACP and ACY are strikingly similar to the negative control (methanol on blank substrates) peaks. Distinguishable peaks are observed in the control spectra even after Ar^+ plasma cleaning, indicating that a small portion of organic residues still persisted on the substrate surface. As methanol is applied to the substrate and then evaporates, the nanorods undergo slight deformation in response to the surface tension of the evaporating solvent, which leads to decreased distance between the rod tips [32]. This so-called “nanobundling” effect is known to facilitate the formation of SERS hot spots, so that the Raman signal of the molecules near the hot spots can be dramatically enhanced. In the methanol control sample, though no PAH is to remain on the substrate surface after solvent evaporation, the surface contaminant residues can still produce pronounced SERS signal that interferes with target detection. For molecules with large Raman cross-sections (*e.g.*, Raman reporters) and high adsorption rates, signal from the target can often outcompete this interference so no or only weak contamination peaks are observed in the SERS spectra. For most analytes, signals from both the target and contaminant residues can be found in the spectra. A typical example is the 690 cm^{-1}

contamination peak found in all the SERS spectra in Figure 4.3, regardless of the presence of distinct PAH peaks. The interference is particularly detrimental to the detection of molecules with relatively small Raman cross-sections, as in the cases of ACP and ACY. As indicated in Figure 4.1, the DFT-calculated spectra of ACP and ACY show weak Raman activities compared to other PAHs. This is in concert with the observation on the SERS spectra of ACP and ACY, in which no obvious PAH signal could be identified, as they are most susceptible to the interference from contamination.

Distinct target peaks can be found in the SERS spectra of all other PAHs. Tables B.1-B.7 in Appendix B provide more detailed information on the observed peaks and corresponding vibrational modes. The spectra are all normalized to remove the fluorescence baseline in BaA and BaP so that the PAH spectra may be compared. Each PAH exhibits its characteristic features in the SERS spectrum. Some peaks are shared by two or more PAHs, indicative of similar vibrational modes. For instance, the $\sim 1406\text{ cm}^{-1}$ peak found in both ANT and P is attributed to C-H and C-C in-plane bending modes (Appendix Tables B.3 and B.7). Although the compositions of all PAHs are very similar (all consisting of only carbon and hydrogen atoms at similar ratios), the fingerprint region ($300 - 1600\text{ cm}^{-1}$) contributed mostly by C-C stretching and bending vibrations can still provide invaluable information in differentiating the PAHs. Using the SERS spectra acquired on the AgNRs, differentiation can be achieved by identifying characteristic peaks (except ACP and ACY) without the aid of multivariate statistical analyses.

Overall, the SERS spectra of ANT, BaP, P, and F agree well with previous reports. Still, some obvious discrepancies can be observed. For example, the 1419 and 1634 cm^{-1} peaks of BaP reported by Bao *et al* [6] have shifted to 1428 and 1619 cm^{-1} , respectively. The 415 , 742 , and 1611 cm^{-1} of F are found at 429 , 729 , and 1600 cm^{-1} in this study, and the previously reported

1401 cm^{-1} peak of F and 492 cm^{-1} peak of ANT cannot be identified in our experiments. However, such disagreements are expected, considering the different types of SERS substrates and detection formats used. Because SERS substrates are involved, the inter-study discrepancies of the SERS data can be much greater than those found in the bulk Raman spectra.

A glimpse at the SERS spectra of BaA, BaP, F, and P suggests that spectral deviation from their bulk Raman spectra are a common phenomenon. Not surprisingly, the SERS spectra exhibit more peaks compared to the bulk Raman spectra. This is because the weak vibrational modes that cannot be detected using Raman spectroscopy may be revealed owing to the signal enhancement provided by SERS. Meanwhile, the interaction between the PAH molecule and the silver substrate can also introduce new vibrational modes, or alter the molecular configuration which leads to changes in the detected SERS signal. Interaction between silver and the analyte molecule can also impact the SERS spectra in the form of peak shifting, and if a vibrational mode is repressed due to adsorption to silver, the corresponding Raman peak can also disappear in the SERS spectra [33]. As discussed before, it is also possible for the interfering contamination peaks to emerge in the PAH spectra, if the peaks do not already exist in the spectra.

Consistent with the DFT calculation, the SERS peak intensities (particularly those of BaP and BaA) appear to be higher in the spectral region between 1000 and 1600 cm^{-1} . This suggests that the higher wavenumber modes might exert greater impact on the spectra. However, this phenomenon is confounded by the fact that the Raman instrument used in this study is reported to be ultra-sensitive at this spectral range.

Overall, the SERS and bulk Raman spectra of PAHs show high resemblance despite some anticipated discrepancies. The majority of the observed PAH SERS peaks can be assigned to one or more vibrational modes based on DFT calculation [33].

Limits of detection (LODs) of PAHs in methanol solution

Concentration-dependent PAH spectra and corresponding characteristic peak intensities are shown in Appendix B Figures B.8 through B.14. In general, at low PAH concentrations, peaks from surface contaminants dominate the SERS spectra, completely masking signal from the PAHs. As the concentration increases to above a certain threshold (*i.e.*, the LOD), weak PAH peaks begin to emerge. The LODs for ACP, ACY, ANT, BaA, BaP, F, and P are determined to be > 1000, > 1000, 50, 100, 50, 100, and 10 $\mu\text{g/mL}$, respectively. The LODs for ACP and ACY are above the highest available concentration due to their small scattering cross-sections. For other PAHs, the LODs are also high, which is consistent with previous literature findings where low sensitivity is reported when PAHs were directly detected on SERS-active metal surfaces. The low detection sensitivity has been widely attributed to the low affinity of PAHs to metallic surfaces. Low LODs are only achieved on chemically functionalized substrates, or on substrates with ultra-high enhancement factors enabled by specific geometries. Surface functionalization enhances the detection sensitivity either by improving the adsorption rate of PAHs or by providing interparticle junctions that act as SERS hot spots. Hexanethiol [34], decanethiol [16], calix[4]arene [19], cyclodextrin derivatives [15], per-6-deoxy-(6-thio)- β -cyclodextrin (CD-SH) [35], humic acids [17, 20] have been reported, with the LODs ranging from 10^{-5} to 10^{-6} $\mu\text{g/mL}$. Novel SERS substrates with ultra-high enhancement factors, such as Au on TiO_2 nanotube arrays [36] and AuNPs on alginate gel [6], have been proposed in PAH detection as well, and LODs could reach as low as 0.365 nM for BaP (equivalent to 9.2×10^{-5} $\mu\text{g/mL}$). However, in these

studies, the SERS substrates were often soaked in the PAH solution for a certain period of time (e.g., 1 h) to allow the PAHs to partition to the substrate surface. This strategy is unfortunately highly impractical in our UTLC-SERS scheme, as in chromatographic development allows little, if any time for the partitioning process.

In addition to the lack of surface modification, the LODs may also be limited by the extremely small sample volume (0.1 μL) used in this study. The vast majority of reported low LODs methods involve sampling as much as 10 mL of PAH solution. This “fishing for target” strategy helps attract and concentrate the analyte molecules to the sensing surface, thereby increasing the apparent LOD. In the UTLC-SERS approach, however, the sample spots are restricted to less than 1 mm in diameter in order to achieve meaningful UTLC separation. Therefore, sample volumes greater than 0.1 μL are undesirable. This requirement inevitably reduces the total mass of PAHs deposited onto the substrate, which can compromise the ultimate LOD. In fact, the LOD of a detection method is a result of multiple factors, including the area on the substrate which liquid samples spread into, the area of the incident laser spot, and the true mass sensitivity of the sensing platform. The true mass sensitivity of the SERS platform can be expressed as the lowest amount of PAHs that could be detected, *i.e.*, lowest detectable mass (LDM) of the analytes, as calculated by

$$\text{LDM} = \frac{CVA}{A_0}$$

where C is the concentration of the PAH, V is the volume of sample solution ($V = 0.1 \mu\text{L}$), A is the area of the Raman laser spot ($A = 0.0143 \text{ mm}^2$), and A_0 is the area of the circular spot which the sample has spread into ($A_0 = 12.6 \text{ mm}^2$). From a microscopic perspective, the LDMs for ANT, BaA, BaP, F, and P are $\sim 5.7 \times 10^{-12}$, 1.1×10^{-11} , 5.7×10^{-12} , 1.1×10^{-11} , and 1.1×10^{-12} g, respectively, demonstrating a high inherent sensitivity of the sensing platform. However, other

factors, including the small sampling volume and poor adsorption rates of PAHs, still hinder the overall sensitivity of the detection method.

In the cases of BaP and P, the peak intensities undergo a decrease when the concentration increases to $> 500 \mu\text{g/mL}$ (Fig. B.12 and B.14). Based on the AgNR geometry, the actual surface area of the $0.1 \mu\text{L}$ sample spot is approximately $6.1 \times 10^{13} \text{ nm}^2$, and the number of molecules within the spot is $2.4 \times 10^{15} - 3 \times 10^{15}$. Therefore, the average surface coverage of the BaP or P molecules is between 39 and 49 molecules / nm^2 , which is very close to what is sufficient to form a monolayer if a uniform coverage is assumed. Hence, the surface will be packed by BaP and P at $\sim 500 \mu\text{g/mL}$. Since previous studies have reported a reduction in SERS intensity due to adsorbate excited state quenching [37], it is not surprising that the peak intensities of BaP and P have experienced a decline at $1000 \mu\text{g/mL}$. Interestingly, such signal reduction is not observed in other PAHs at the similar concentrations. This is mainly because the varying adsorption rates and Raman cross-sections among the PAHs can lead to different thresholds for this signal saturation effect.

Conclusions

In this study, we have characterized seven PAH compounds with their SERS and/or Raman spectra, and compared the experimentally acquired spectra with those predicted by DFT. DFT calculation facilitated the spectral band assignment, and also provided insights into the observed differences in SERS intensity. Characteristic SERS peaks were identified for each PAH compound except ACP and ACY, whose signal intensities were below the detection threshold. Although the inherent sensitivity of the SERS platform was high, the determined LODs of PAHs were relatively high as a result of poor molecular adsorption rates and small sample volume.

Future work will be directed to SERS substrate improvement and developing sample preparation protocols to improve the LODs of PAHs from real samples.

Acknowledgements

This work was supported by National Science Foundation under contract number CBET-1064228 and UGA College of Agricultural and Environmental Sciences Experimental Station. The authors thank Dr. Xibo Li for setting up DFT calculations.

References

1. Plaza-Bolanos, P., A.G. Frenich, and J.L.M. Vidal, *Polycyclic aromatic hydrocarbons in food and beverages. Analytical methods and trends*. Journal of Chromatography A, 2010. **1217**(41):6303-6326.
2. Scientific Committee on Food, European Commission, *Opinion of the scientific committee on food on the risks to human health of polycyclic aromatic hydrocarbons in food*, 2002, European Commission (EC): Brussel.
3. Moret, S. and L.S. Conte, *Polycyclic aromatic hydrocarbons in edible fats and oils: occurrence and analytical methods*. Journal of Chromatography A, 2000. **882**(1-2):245-253.
4. Ferey, L., N. Delaunay, D.N. Rutledge, C.B.Y. Cordella, H. This, A. Huertas, Y. Raoul, and P. Gareil, *Optimizing separation conditions of 19 polycyclic aromatic hydrocarbons by cyclodextrin-modified capillary electrophoresis and applications to edible oils*. Talanta, 2014. **119**:572-581.
5. AOAC, *Polycyclic aromatic hydrocarbons and benzo[a]pyrene in food. Spectrophotometric method.*, 2005.
6. Bao, L., P.T. Sheng, J. Li, S.Y. Wu, Q.Y. Cai, and S.Z. Yao, *Surface enhanced Raman spectroscopic detection of polycyclic aromatic hydrocarbons (PAHs) using a gold nanoparticles-modified alginate gel network*. Analyst, 2012. **137**(17):4010-4015.
7. Schmidt, H., N.B. Ha, J. Pfannkuche, H. Amann, H.D. Kronfeldt, and G. Kowalewska, *Detection of PAHs in seawater using surface-enhanced Raman scattering (SERS)*. Marine Pollution Bulletin, 2004. **49**(3):229-234.

8. Stewart, S.D. and P.M. Fredericks, *Fourier-Transform Surface-Enhanced Raman-Scattering for the Detection and Identification of Polyaromatic Hydrocarbons*. Journal of Raman Spectroscopy, 1995. **26**(8-9):629-635.
9. Fleischmann, M., P.J. Hendra, and A.J. McQuillan, *Raman spectra of pyridine adsorbed at a silver electrode*. Chemical Physics Letters, 1974. **26**(2):163-166.
10. Kneipp, K., H. Kneipp, S. Abdali, R.W. Berg, and H. Bohr, *Single molecule Raman detection of enkephalin on silver colloidal particles*. Spectroscopy: An International Journal, 2004. **18**(3):433-440.
11. Nie, S.M. and S.R. Emery, *Probing single molecules and single nanoparticles by surface-enhanced Raman scattering*. Science, 1997. **275**(5303):1102-1106.
12. Asher, S.A., *Ultraviolet resonance Raman spectrometry for detection and speciation of trace polycyclic aromatic hydrocarbons*. Analytical Chemistry, 1984. **56**(4):720-724.
13. Maddams, W. and I. Royaud, *The characterization of polycyclic aromatic hydrocarbons by Raman spectroscopy*. Spectrochimica Acta Part A: Molecular Spectroscopy, 1990. **46**(2):309-314.
14. Xie, Y.F., X. Wang, X.X. Han, W. Song, W.D. Ruan, J.Q. Liu, B. Zhao, and Y. Ozaki, *Selective SERS detection of each polycyclic aromatic hydrocarbon (PAH) in a mixture of five kinds of PAHs*. Journal of Raman Spectroscopy, 2011. **42**(5):945-950.
15. Xie, Y.F., X. Wang, X.X. Han, X.X. Xue, W. Ji, Z.H. Qi, J.Q. Liu, B. Zhao, and Y. Ozaki, *Sensing of polycyclic aromatic hydrocarbons with cyclodextrin inclusion complexes on silver nanoparticles by surface-enhanced Raman scattering*. Analyst, 2010. **135**(6):1389-1394.

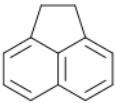
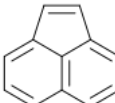
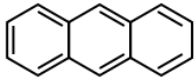
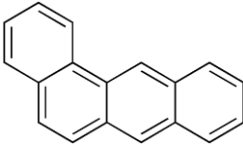
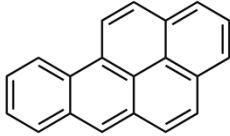
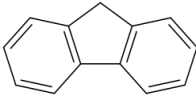
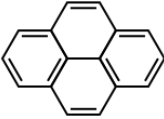
16. Jones, C.L., K.C. Bantz, and C.L. Haynes, *Partition layer-modified substrates for reversible surface-enhanced Raman scattering detection of polycyclic aromatic hydrocarbons*. Analytical and Bioanalytical Chemistry, 2009. **394**(1):303-311.
17. Qu, L.L., Y.T. Li, D.W. Li, J.Q. Xue, J.S. Fossey, and Y.T. Long, *Humic acids-based one-step fabrication of SERS substrates for detection of polycyclic aromatic hydrocarbons*. Analyst, 2013. **138**(5):1523-1528.
18. Guerrini, L., J.V. Garcia-Ramos, C. Domingo, and S. Sanchez-Cortes, *Building highly selective hot spots in Ag nanoparticles using bifunctional viologens: application to the SERS detection of PAHs*. The Journal of Physical Chemistry C, 2008. **112**(20):7527-7530.
19. Guerrini, L., J.V. Garcia-Ramos, C. Domingo, and S. Sanchez-Cortes, *Nanosensors based on viologen functionalized silver nanoparticles: few molecules surface. Enhanced Raman spectroscopy detection of polycyclic aromatic hydrocarbons in interparticle hot spots*. Analytical Chemistry, 2009. **81**(4):1418-1425.
20. Leyton, P., I. Cordova, P.A. Lizama-Vergara, J.S. Gomez-Jeria, A.E. Aliaga, M.M. Campos-Vallette, E. Clavijo, J.V. Garcia-Ramos, and S. Sanchez-Cortes, *Humic acids as molecular assemblers in the surface-enhanced Raman scattering detection of polycyclic aromatic hydrocarbons*. Vibrational Spectroscopy, 2008. **46**(2):77-81.
21. Becke, A.D., *Density-functional thermochemistry. III. The role of exact exchange*. Journal of Chemical Physics, 1993. **98**(7):5648.
22. Lee, C., W. Yang, and R.G. Parr, *Development of the colle-salvetti correlation-energy formula into a functional of the electron density*. Physical Review. B, Condensed Matter, 1988. **37**(2):785-789.

23. Liu, Y.J., H.Y. Chu, and Y.P. Zhao, *Silver nanorod array substrates fabricated by oblique angle deposition: morphological, optical, and sers characterizations*. The Journal of Physical Chemistry C, 2010. **114**(18):8176-8183.
24. Fu, J.X., A. Collins, and Y.P. Zhao, *Optical properties and biosensor application of ultrathin silver films prepared by oblique angle deposition*. The Journal of Physical Chemistry C, 2008. **112**(43):16784-16791.
25. D. Driskell, J., S. Shanmukh, Y. Liu, S. B. Chaney, X.J. Tang, Y.P. Zhao, and R. A. Dluhy, *The use of aligned silver nanorod arrays prepared by oblique angle deposition as surface enhanced Raman scattering substrates*. The Journal of Physical Chemistry C, 2008. **112**(4):895.
26. Negri, P., N.E. Marotta, L.A. Bottomley, and R.A. Dluhy, *Removal of surface contamination and self-assembled monolayers (SAMs) from silver (Ag) nanorod substrates by plasma cleaning with argon*. Applied Spectroscopy, 2011. **65**(1):66-74.
27. Knighton, W.B. and E.P. Grimsrud, *Linearization of electron capture detector response to strongly responding compounds*. Analytical Chemistry, 1983. **55**(4):713-718.
28. Matousek, P., M. Towrie, and A. Parker, *Fluorescence background suppression in Raman spectroscopy using combined Kerr gated and shifted excitation Raman difference techniques*. Journal of Raman Spectroscopy, 2002. **33**(4):238-242.
29. Romanovskaya, G.I. and N.A. Lebedeva, *Fluorescence determination of polyaromatic hydrocarbons against a background of self-fluorescence of natural, drinking, and waste-waters*. Journal of Analytical Chemistry, 1993. **48**(12):1400-1405.

30. Colangeli, L., V. Mennella, G. Baratta, E. Bussoletti, and G. Strazzulla, *Raman and infrared spectra of polycyclic aromatic hydrocarbon molecules of possible astrophysical interest*. The Astrophysical Journal, 1992. **396**:369-377.
31. Wu, X.M., S.M. Gao, J.S. Wang, H.Y. Wang, Y.W. Huang, and Y.P. Zhao, *The surface-enhanced Raman spectra of aflatoxins: spectral analysis, density functional theory calculation, detection and differentiation*. Analyst, 2012. **137**(18):4226-4234.
32. Abell, J.L., J.D. Driskell, and Y.P. Zhao, *Controllable and reversible hot spot formation on silver nanorod arrays*. Chemical Communications, 2014. **50**(1):106-108.
33. Le Ru, E. and P. Etchegoin, *Principles of surface-enhanced raman spectroscopy and related plasmonic effects*. 2008: Elsevier.
34. Jiang, X., Y. Lai, M. Yang, H. Yang, W. Jiang, and J. Zhan, *Silver nanoparticle aggregates on copper foil for reliable quantitative SERS analysis of polycyclic aromatic hydrocarbons with a portable raman spectrometer*. Analyst, 2012. **137**(17):3995-4000.
35. Wang, Z.Y., H. Wu, C.L. Wang, S.H. Xu, and Y.P. Cui, *Gold aggregates- and quantum dots- embedded nanospheres: Switchable dual-mode image probes for living cells*. Journal of Materials Chemistry, 2011. **21**(12):4307-4313.
36. Sheng, P.T., S.Y. Wu, L. Bao, X. Wang, Z. Chen, and Q.Y. Cai, *Surface enhanced Raman scattering detecting polycyclic aromatic hydrocarbons with gold nanoparticle-modified TiO₂ nanotube arrays*. New Journal of Chemistry, 2012. **36**(12):2501-2505.
37. Zeman, E., K. Carron, G. Schatz, and R. Van Duyne, *A surface enhanced resonance Raman study of cobalt phthalocyanine on rough Ag films: Theory and experiment*. The Journal of Chemical Physics, 1987. **87**(7):4189-4200.

Tables

Table 4.1 PAH compounds used in this study and their corresponding SERS limits of detection (LODs) and lowest detectable mass (LDMs)

Chemical Name	Abbreviation	Molecular structure	LOD ($\mu\text{g/mL}$)	LDM (g)
acenaphthene	ACP		> 1000	$> 1.1 \times 10^{-10}$
acenaphthylene	ACY		> 1000	$> 1.1 \times 10^{-10}$
anthracene	ANT		50	5.7×10^{-12}
benz(a)anthracene	BaA		100	1.1×10^{-11}
benzo(a)pyrene	BaP		50	5.7×10^{-12}
fluorene	F		100	1.1×10^{-11}
pyrene	P		10	1.1×10^{-12}

Figures

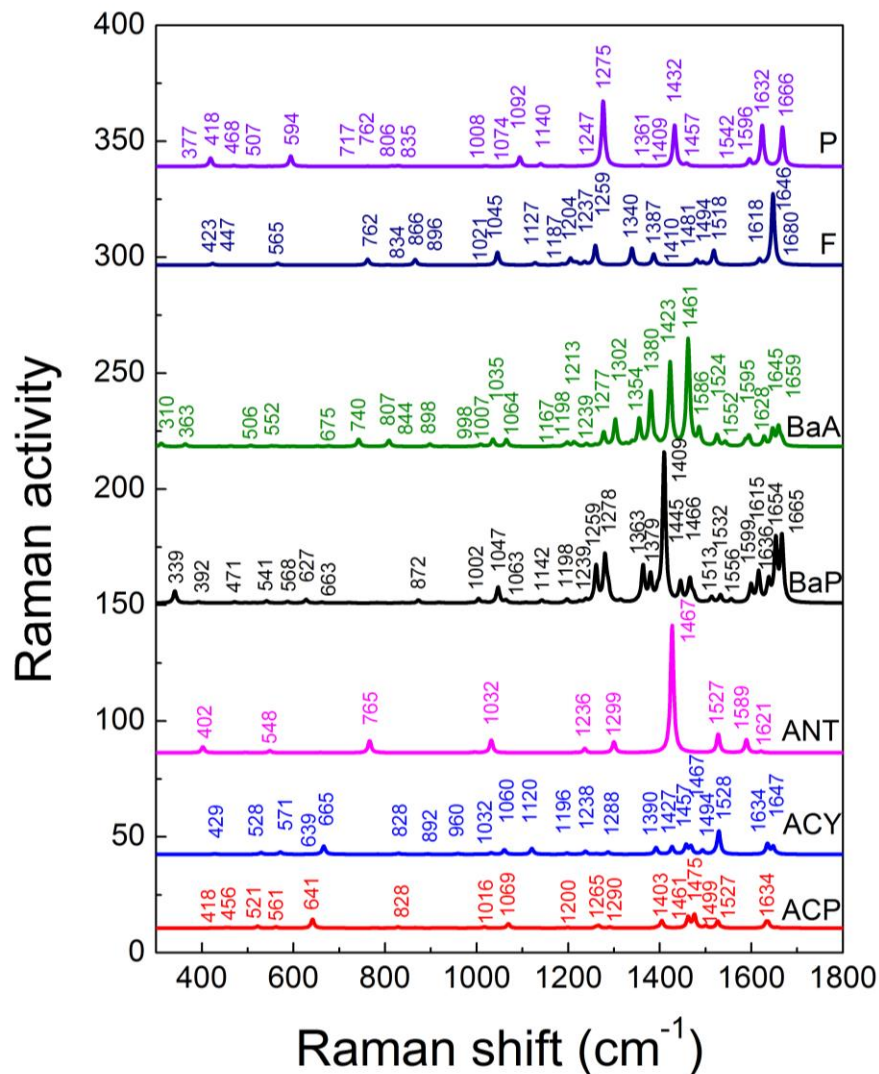


Figure 4.1 DFT-calculated Raman spectra of seven PAH compounds. The spectra were calculated using Gaussian 03W DFT package based on Becke's three-parameter exchange function (B3) with the dynamic correlation function of Lee, Yang, and Parr (LYP). The spectra were vertically offset for clarity.

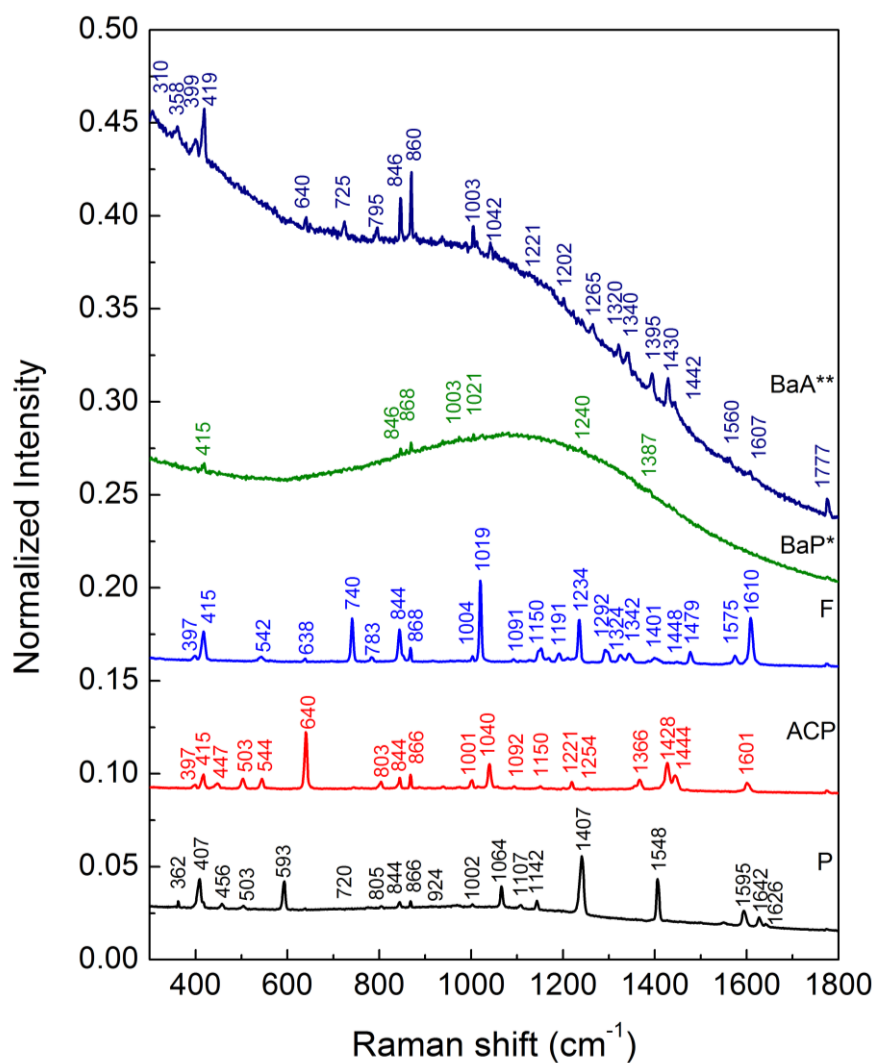


Figure 4.2 Bulk Raman spectra of BaA, BaP, F, ACP, and P after vector normalization. Asterisks indicate that the intensity of BaA and BaP was multiplied by 10 and 5 times, respectively, and the spectra were vertically offset for clarity.

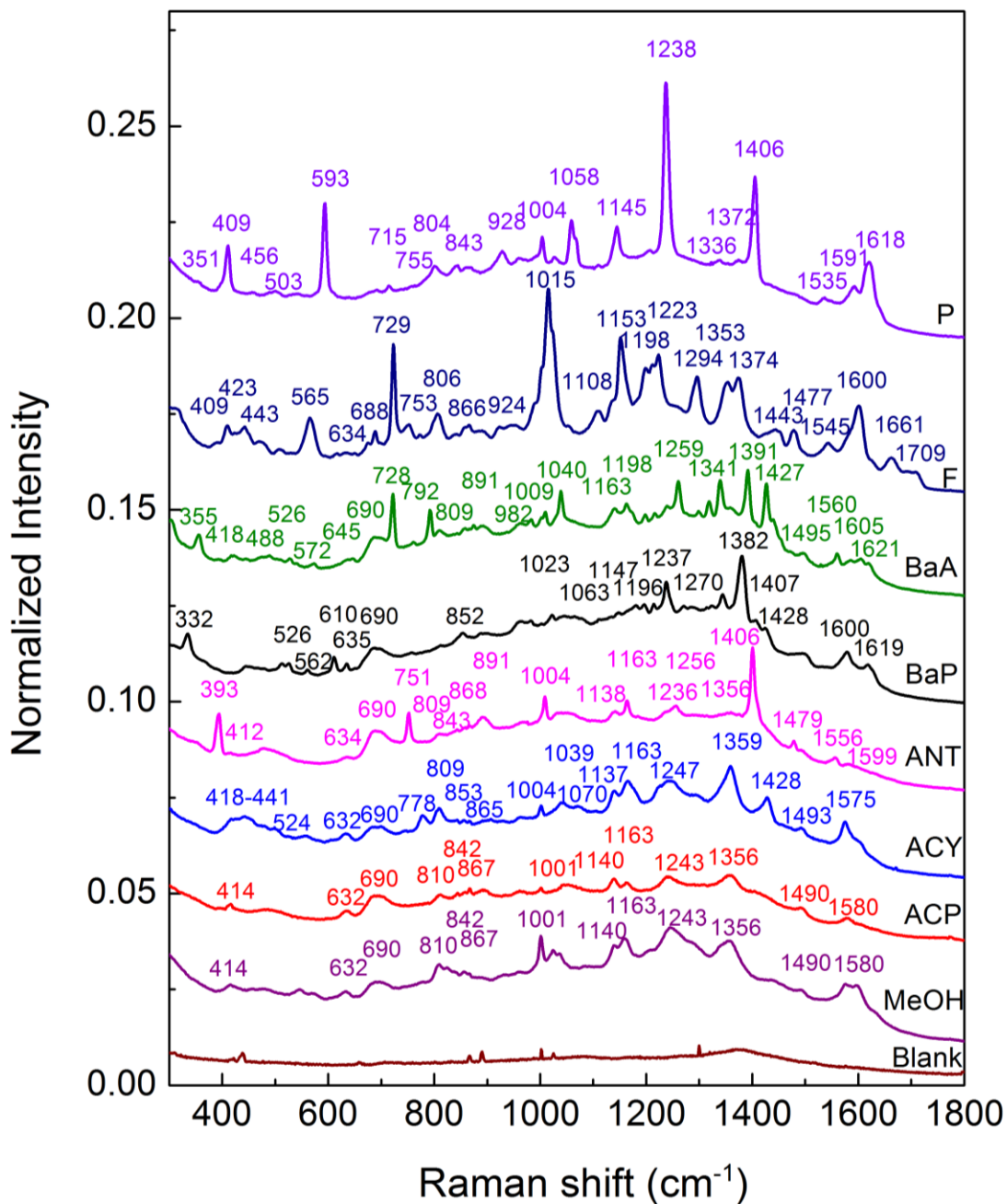


Figure 4.3 SERS spectra of seven PAH compounds on the AgNR substrates and the solvent (methanol) control. The SERS spectra were collected at 60 mW, 10 s through a 100 × objective lens. The spectra have been normalized to the vector lengths and vertically offset for clarity.

CHAPTER 5
TOWARDS ULTRA-THIN LAYER CHROMATOGRAPHY AND SURFACE ENHANCED
RAMAN SPECTROSCOPY DETECTION OF POLYCYCLIC AROMATIC
HYDROCARBONS³

³ Jing Chen, Yao-wen Huang, and Yiping Zhao. To be submitted to *Sensors and Actuators B*.

Abstract

Detection of mixture samples using surface enhanced Raman scattering (SERS) could be improved after an on-chip ultra-thin layer chromatography (UTLC) process. In this study we have modified the SERS-active silver nanorod (AgNR) substrates with thiols, and optimized the mobile phase solvents for UTLC-SERS detection of three carcinogenic contaminants, benz(a)anthracene (BaA), benzo(a)pyrene (BaP), and pyrene (P). Thiol modification changed the polarity of the AgNR substrates and negatively impacted the SERS intensity of detection targets. However, partial loss of SERS intensity was compensated for by improved UTLC retention. A mobile phase system consisting of methanol: water at 95:5 (v/v) was found to be most effective for separating BaP from BaA and P, which improved the differentiation of the latter two based on their SERS fingerprints.

Introduction

Polycyclic aromatic hydrocarbons (PAHs) are a large group of compounds with a significant impact on public health due to their carcinogenic, mutagenic, and teratogenic potentials [1]. PAHs are commonly found in the sediments but are also ubiquitous atmospheric pollutants. In addition, contaminated foods, such as food cooked at high temperatures (e.g., smoked and grilled foods), are also identified as major dietary source of PAHs. Rapid and effective detection of PAHs from such matrices therefore become highly desirable in the routine inspection of these foods. Traditionally, PAHs are detected using liquid (LC) or gas chromatography (GC) techniques coupled with fluorescence detection or mass spectrometry (MS) [2, 3]. Despite high accuracy and sensitivity, sophisticated sample preparation and low

throughput have limited the application of LC or GC based techniques in routine screening of PAHs from food samples.

Surface enhanced Raman spectroscopy (SERS) is a rapid, non-destructive, and sensitive technique, which could potentially be used as an alternative to LC/GC methods. SERS utilizes the enhanced electromagnetic field near nanostructured noble metal surfaces to amplify the Raman scattering signal by factors up to 10^{15} times [4]. The unique SERS spectra could be used as molecular fingerprints for ultra-sensitive detection of a variety of analytes, including chemical contaminants, toxins, and bacterial and viral pathogens. However, when applied to real sample detection, SERS is challenged by the interference from components which co-exist in the food matrix. In order to improve the specificity, SERS can be performed in conjunction with target recognition elements such as antibodies [5, 6], but such an extrinsic detection format relies on the availability and specificity of antibodies. On the other hand, the intrinsic molecular information is also lost when Raman reporter molecules are used. Label-free intrinsic SERS is highly desirable for its simplicity and lower cost. Unfortunately, it is also most susceptible to interference from non-target components. Post-spectroscopic analysis using chemometrics is commonly used to facilitate spectral differentiation [7-9]. However, chemometrics methods heavily rely on statistic models built upon reference libraries, and these libraries often prove ineffective to support analysis in real world samples.

Recently, we have demonstrated that by incorporating a simple ultra-thin layer chromatography (UTLC) separation directly on the SERS-active silver nanorod (AgNR) substrates prior to SERS measurements could significantly improve the selectivity of SERS detection [10]. The mixture components equilibrated at different locations on the SERS substrate due to their interaction with the silver surface and the mobile phase solvents, where their

individual SERS spectra could be detected by the Raman probe. In addition, UTLC also demonstrated the potential as a preparative procedure for cleaning up the matrix residue and reveal the spectra of weakly adsorbing targets. However, the stationary phase in a chromatographic system must be chemically inert, *i.e.*, chemical reactions between the stationary phase material and the test sample should be avoided, because these reactions may alter the local chromatographic conditions by generating new species, gas, precipitation, or heat. Moreover, the time required to reach a chemical equilibrium is often longer than that required for an adsorption/desorption equilibrium. This temporal factor can easily disturb the chromatographic equilibriums. Because UTLC on bare AgNRs utilizes silver as the stationary phase, the chemical reactivity of silver may complicate the chromatographic separation. On the other hand, the affinity between silver and test analytes may result from an unknown mechanism that is different from conventional adsorption chromatography, in which the polarity of stationary phase plays a key role. These all add to uncertainties in the silver-based UTLC.

A possible way of circumventing these complications is to modify the substrate surface with chemically bonded phases, which can act as the stationary phase and block the contact between silver and the analytes. In fact, surface modification to the SERS-active substrates has been extensively explored previously, among which thiol modification remains a mainstream for its simplicity and the strong bonding between thiols and the metal surface [11-14]. On the other hand, chemically bonded phases are one of the most popular stationary phases in chromatography, particularly in reverse phase chromatography. Instead of interacting directly with the sorbent material, the analytes interact with the extended groups of the bonded phase, which can be tuned to the requirements of different applications. Thiol modification of the silver

surface can therefore be utilized not only to resolve the chemical activity of silver, but also to adjust the polarity of the stationary phase.

On the other hand, the mobile phase solvent is also an important factor which directly affects the UTLC outcomes. It is also the most effective means to change analyte retention. Effective separation of different PAHs relies on careful selection of mobile phase solvents.

In this study, we have modified the AgNR substrate surface with thiol molecules, which serve as chemically bonded stationary phases in UTLC-SERS. The changes in surface properties, SERS properties, as well as chromatographic properties after modification have also been evaluated. The composition of mobile phase solvents was also adjusted for the ULTC-SERS detection of three model PAH compounds, in order to built a foundation for their detection in real food samples.

Materials and Methods

Materials

PAHs (benz(a)anthracene, benzo(a)pyrene, and pyrene) and thiols (2-mercaptoethanol, 1-propanethiol, 6-mercapto-1-hexanol, and 1-octanethiol) were purchased from Sigma Aldrich (St. Louis, MO). Silver (99.999%) and titanium (99.995%) were obtained from Kurt L. Lesker (Clairton, PA).

Preparation of AgNR substrates

The AgNR substrates were fabricated using oblique angle deposition (OAD) in a custom-built electron beam evaporator [15, 16]. Briefly, 1×1 inch² glass slides were cleaned with Piranha solution (80% sulfuric acid, 20% hydrogen peroxide), rinsed with deionized (DI) water, and dried with compressed nitrogen before loading into the deposition chamber. Under ultra-low

chamber pressure ($<10^{-6}$ Torr), 20 nm titanium and 200 nm silver films were deposited onto the glass slides at normal angle at a rate of 0.2 nm/s and 0.3 nm/s, respectively. Then the substrate surface normal was rotated to 86° with respect to the incident vapor direction, and a final layer of AgNRs were deposited at a rate of 0.3 nm/s. The AgNRs were ~ 900 nm in length, ~ 100 nm in rod diameter, with a tilting angle of approximately 73° with respect to the substrate normal [15, 17]. Before each experiment, the as-deposited AgNR substrates were cleaned for 2 min in a custom built inductively-coupled RF plasma chamber, which operated at 30 W under a constant flow (chamber pressure maintained at ~ 600 mTorr) of ultra-pure argon to remove any organic contaminants accumulated during fabrication and storage [18].

Thiol functionalization of AgNRs

To prepare thiol solutions for modification, polar thiols (ME and MH) were dispersed and serially diluted in DI water, and nonpolar thiols (PT and OCT) were diluted in hexanes. The AgNR substrates were soaked in a sealed glass petri-dish containing 5 mL of thiol solution for 30 min at room temperature. After 30 min, MH and ME modified substrates were removed from the petri-dish, rinsed gently with DI water for 10 s, and blow-dried with nitrogen. PT and OCT modified substrates were rinsed with hexanes without blow-drying. The modified substrates were immediately used for contact angle measurements, SERS measurements, or UTLC development.

Contact angle measurements

Water contact angle measurements were conducted using an OCA Contact Angle Tool (Data Physics, San Jose, CA). For each measurement, 2 μL of DI water were dropped onto the substrate surface through a needle syringe that was automatically controlled by a step motor. A camera and a light source were placed on opposite sides of the sample droplet. After the snapshot of the water contour was captured by the camera, the left and right contact angles were measured

using a built-in program. Because the AgNR substrate is an anisotropic surface, different contact angle values may be obtained depending on the camera's viewing angle relative to the nanorod tilting direction. For consistent comparison, the left and right contact angles obtained parallel and perpendicularly to the AgNR orientation were measured.

UTLC process

A cocktail of BaA, BaP, and P each at 200 $\mu\text{g}/\text{mL}$ was prepared in methanol. 0.1 μL of this cocktail solution, as well as individual PAH solutions at 200 $\mu\text{g}/\text{mL}$ were applied onto the AgNR substrate and dried under ambient conditions. Then the substrate was placed in a 35 mL beaker containing ~ 3.5 mL of mobile phase solvents, such that the sample spots were ~ 1 mm above the liquid meniscus. The beaker was pre-saturated with the mobile phase vapor for at least 10 min prior to UTLC and covered with a watch glass during UTLC. After 5 min, the substrate was taken out of the beaker and dried, and the solvent front was immediately marked by scratching the substrate with tweezer tips.

SERS measurements

All SERS measurements were performed using a portable Raman analyzer, Enwave ProRamanL 785A2 (Enwave Optronics, Irvine, CA) equipped with a 785 nm diode laser and a $10\times$ objective lens at a power of 60 mW and a spectral acquisition time of 10 s. For intensity comparison, 0.1 μL of PAH at 200 $\mu\text{g}/\text{mL}$ were applied to the substrates, dried, and the SERS spectra were directly collected from the sample spots. For the substrates which had been subject to UTLC separation, SERS spectra were collected in 0.5 mm steps along the UTLC development direction, from the center of the original sample spots to ~ 2 mm beyond the identified solvent front.

Optimization of mobile phase solvents

Methanol and water were mixed at 50:50, 70:30, 90:10, and 95:5 (v/v) and used for developing the UTLC plate on unmodified AgNR substrates.

Data analysis

The SERS spectra were fitted to the characteristic PAH peaks using a mixed Gaussian/Lorentzian function using the GRAMS/AI Spectroscopy package (Thermo Scientific, Waltham, MA). For each sample component, the peak intensities along the development direction were divided by the highest peak intensity found in that component to generate a series of normalized peak intensities. The normalized intensities were plotted against the developing distance to visualize the UTLC separation. The retention factors (R_f s) were calculated using the following equation:

$$R_f = \frac{L_{solute}}{L_{solvent}}$$

where L_{solute} is the distance travelled by the individual PAH (mm), and $L_{solvent}$ is the total distance travelled by the mobile phase solvent (mm).

Results and Discussion

Surface properties of modified substrates

The surface hydrophobicity, indicated by water contact angle, is expected to change after thiol modification [19]. Depending on the degree of contamination, the unmodified AgNR substrates usually have a water contact angle ranging from 25 ° to 45 ° (data not shown). After plasma cleaning, the contact angles of AgNRs reduced to 6.7 ° to 25 ° (Fig. 5.1), suggesting the formation of a more hydrophilic surface owing to the removal of organic contaminants. It is also

evident that the nanostructure arrangement has altered the wetting properties of silver, which is known to be hydrophobic [20]. As expected, the contact angles vary depending on the viewing angles, consistent with previous findings on anisotropic silver nanostructures [21].

When the substrates were modified with polar thiols, ME and MH, the contact angles further decreased to $< 10^\circ$ and $< 5^\circ$, respectively (Fig. 5.1a-b). The fluctuations in contact angle at low ME or MH concentrations (100 nM - 10 μ M) were likely a result of the variation in thiol configuration on the AgNR surface. When modified with non-polar thiols, the AgNR arrays instantly became hydrophobic, as the water contact angles increased to 115° - 135° (Fig. 5.1c-d). As the concentration of PT or OCT increased, the contact angles remained relatively stable, especially on the OCT modified substrates. This implies that dense monolayers of non-polar thiols could readily form at concentrations as low as 100 nM. Indeed, when PT was diluted further to an extremely low concentration, 1 nM, the water contact angles were almost identical to, if not greater than those observed at higher concentrations (Fig. 5.1c). This demonstrates a greater tendency for non-polar thiols to attach to the silver surface and form dense monolayers compared to polar thiols.

Effect of surface modification on the SERS signal

The purpose of thiol modification was to make the AgNR substrates more suitable for UTLC separation. Unfortunately, inserting an additional layer of thiol molecules between the SERS-active surface and the target PAHs could potentially increase the sensing distance and decrease PAH signal intensity. In the meantime, thiol reagents could also invoke their own SERS peaks, which could interfere with the identification of PAHs. In order to evaluate the potential influence of thiol modification on the SERS detection of target PAHs, the intensity was compared on the thiol modified substrates. As shown in Figure 5.2, the SERS spectra of blank substrates were

minimally affected by exposure to ME or MH at concentrations below 100 μM (Fig. 5.2a-b). Only peaks from surface contaminants could be identified at these concentrations. However, when the thiol concentration increased to 100 μM , prominent ME and MH signals began to dominate the SERS spectra, featuring a strong peak at 634 cm^{-1} in the ME spectra, which was attributed to C-S stretching in the gauche isomer [22], and a series of peaks between 1006 and 1083 in the MH spectra. At lower thiol concentrations, some weak thiol bands could be observed at 634, 1610 cm^{-1} , *etc.* in the ME spectra, and 874 and 1006 cm^{-1} in the MH spectra, indicating some thiol molecules were immobilized on the substrate, but the degree of immobilization was marginal compared to that at 100 μM .

After ME or MH modification, new peaks were introduced to the PAH spectra (Appendix Fig. C.1-C.2). As expected, compared to those found on unmodified AgNR substrates (indicated by black dashed curves in Fig. C.1-C.2), the PAH peak intensities were significantly lower. Interestingly, the SERS intensity of PAHs did not display a simple negative correlation with ME concentration (Fig. 5.3). The PAH peaks on 100 nM and 1 μM ME modified substrates could barely be identified. Instead, the spectra were dominated by surface contaminant peaks (Appendix Fig. C.1-C.2). Previous studies have demonstrated a tendency of the nanorods to bundle in response to the surface tension during evaporation of solvents, forming the so-called SERS hot spots [23]. However, when molecules are fixed on the AgNR surface and expose hydrophilic tails such as $-\text{COOH}$ and $-\text{OH}$ to the surrounding, the formed nanorod clusters may be “de-bundled” once polar solvents rewet the surface [24]. Therefore, at low ME or MH concentrations, the surface contaminant residues could not be replaced by the thiols; meanwhile, few hydroxyl groups were anchored onto the AgNRs to facilitate the debundling of nanorods during PAH addition. This means the SERS hot spots were inaccessible to incoming PAH

molecules, since new hot spots could not form on already bundled AgNRs. When the thiol concentration increased to above 10 μM , the ME molecules were sufficient to displace some of the contaminant residues on the silver surface. ME or MH immobilization reduced signals from contamination, and provided hydroxyl groups necessary for the subsequent debundling process. The deposited PAH molecules could then approach individual nanorods and be enclosed into the newly formed nanobundles during methanol evaporation.

As suggested by the contact angle measurements, non-polar thiols PT and OCT more readily attached to the AgNRs compared to ME and MH. The SERS spectra of blank substrates after PT modification display multiple PT peaks throughout the spectral region between 300 and 1700 cm^{-1} , and the signal intensity exhibited a steady increase with increasing PT concentration (Fig. 5.2c). Extremely weak to no signal from the PAHs were retrieved on the PT modified AgNRs (Appendix Fig. C.3). This was mainly caused by the spectral interference from the PT peaks, which tended to overlap or merge with the adjacent PAH bands. Likewise, in the spectra of the OCT modified substrates, pronounced OCT peaks dominated the entire spectral region at low concentrations (100 nM - 10 μM). The background intensity declined as its concentration exceeded 100 μM (Fig. 5.2d), due to adsorbate excited state quenching [25]. Naturally, the dense coverage of a long-chain modification agent on the AgNRs had a negative impact on target detection. As Appendix Figures C.4 indicates, the peaks of BaA, BaP, and P could barely be detected on any of the OCT modified substrates, except for the weak BaP peaks near 527, 1345, and 1381 cm^{-1} and P peaks near 593, 1063, 1238, and 1407 cm^{-1} on 100 nM - 10 μM OCT modified substrates (Fig. C.4c-d). The PAH characteristic bands also showed peak intensities close to the detection threshold (Fig. 5.3d). In addition to weak signal intensity, some of these peaks were also confounded by the adjacent OCT peaks. Like PT, OCT exerted a strong

interference to PAH detection for its wide distribution of SERS peaks, especially at the PAH fingerprint regions.

In current LC analysis of PAHs, reverse phase chromatography is considered most effective in separating multiple PAHs within the same sample. In this study, non-polar modification using PT and OCT has resulted in superhydrophobic substrates, whose SERS spectra also confirmed successful attachment of the alkyl chains to the silver surface. Unfortunately, non-polar thiol modification has proven undesirable for post chromatographic SERS detection owing to their strong spectral interferences.

UTLC on thiol modified substrates

Following surface property and SERS intensity evaluations, UTLC separation of selected PAHs were performed on the thiol modified substrates. Before UTLC, PAH SERS signal could be detected on 10 and 100 μM ME modified substrates, which is consistent with the results shown in Appendix Figure C.1. The separation of BaA, BaP, and P on 10 μM ME modified substrates (Fig. 5.4a) indicates that though the PAH bands were poorly resolved (*i.e.*, bands were overlapping), some degree of separation could be detected. Specifically, the BaP component in the mixture migrated a shorter distance compared to BaA, whereas P consistently traveled the longest distance among all. On 100 μM ME modified substrates, the P band became broader, spanning a longer distance along the development direction (Fig. 5.4b). At the same time, the PAH bands became less resolved, with the BaA and BaP bands almost completely overlapping with each other. The absolute signal intensities were also weaker due to greater ME interference (data not shown). No SERS signal was recovered after UTLC on low concentrations of ME/MH, or PT/OCT modified substrates. Hence, based on the evaluation of substrate surface properties,

SERS signal intensity, and UTLC retention, nonpolar thiols (particularly ME at 10 μM) demonstrated the greatest potential for UTLC-SERS detection of BaA, BaP, and P.

Optimization of mobile phase solvents

The ideal mobile phase solvents must be chemically inert, evaporate completely after UTLC, and readily wet the AgNR substrates in order to provide satisfactory UTLC migration. Common lab solvents, including methanol, acetonitrile, hexanes, dichloromethane, chloroform, toluene, acetone, isopropanol, and 18 M Ω ultra-pure water were tested for their migration distance on the AgNRs and possible impact on the SERS spectral background (see Appendix C for details). Four representative solvents with varying polarities, methanol, acetonitrile, hexanes, and dichloromethane, were selected as candidate mobile phase solvents and used to separate BaA, BaP, and P. According to Appendix Figure C.6, methanol yielded the longest solvent migration distance, whereas solvent migration with acetonitrile, hexanes, and dichloromethane was not satisfactory. After methanol was added to these solvents, significant improvements in the migration distance were observed (Appendix Fig. C.7). However, there PAH bands still tended to overlap to a large extent.

In the literature, the majority of HPLC methods included water in the mobile phase system for PAH analysis [2, 3]. Water is added to the organic solvent (usually acetonitrile) to adjust its elution strength on PAHs. In this study, we have also attempted to add water in the mobile phase as a modifier to adjust the elution strength. The percentage of water in the mobile phase was decreased from 50% to 5% (v/v), and water was ultimately replaced completely by methanol. Although a whole spectrum of percentages between these two solvents were intended, we found it impossible to use a water percentage above 50%, since the substrates were either too poorly wetted (*e.g.*, at 100% water content), or the UTLC development processes were frequently

disrupted because of the mobile phase's irregular routes caused by excess water. At high percentages of water, the mobile phase tended to bypass the sample spots in the ascending process, due to strong repulsion between non-polar PAHs and highly polar water molecules. As a consequence, lateral migration, in which the mobile phase migrated horizontally instead of vertically, greatly undermined the UTLC outcome. Moreover, because it took a considerably longer time for water to evaporate, the excess unevaporated water was found to form small droplets and flow back towards the sample origin due to gravity. Unavoidably, this undesired backflow of water caused serious cross-contamination and led to failure of UTLC.

As shown in Fig. 5.5a, initially, all three PAH compounds were restrained within their original locations and little migration was identified using a mobile phase of methanol: water 1:1 (v/v). As the percentage of water decreases to 30% (v/v), P began to migrate along with the solvents to very close to the front (Fig. 5.5b). In the meantime, BaA also started to migrate with the solvent, but to a lesser extent compared with P. BaP, on the other hand, remained unaffected and was still confined near the sample origin. When the percentage of water continued to decrease to 10% (v/v), a dramatic change in the PAH retention occurred (Fig. 5.5c). While P remained at the frontier of elution and BaA followed immediately behind, the BaP molecules were also eluted to the solvent front. The retention of BaP was still stronger compared with the other two PAHs, and obvious tailing was observed in the BaP bands. A further decrease in the water content to 5% resulted in less severe tailing of the BaP band, which also exhibited apparently lower retention factor than BaA and BaP (Fig. 5.5d). Finally, in a methanol-only environment, all PAHs yields narrow bands at the solvent front (Appendix Fig. C.6a).

The R_f s of three PAHs were plotted against the water content in Figure 5.6a. As the water content increased from 0 to 50%, the R_f values experienced a steady decline (with a spike at 10%

of water). Of course, the R_f values could only be used to depict a general trend of the retention behaviors. The chromatographic band width could also play an important role in the calculated R_f s, as broader bands often interfered with the determination of band centers. The band widths of BaA, BaP, and P were plotted as a function of water content in the mobile phase (Fig. 5.6b). Relatively narrow bands $\sim 1 - 1.5$ mm in diameter were commonly found using mobile phases composed of either high (up to 50%) or low (0% - 5%) percentages of water, and the bands reached maximum widths when the mobile phase consisted of 10% - 30% of water.

Overall, on unmodified AgNR substrates, it was difficult to completely separate the tested PAH compounds within a distance of 7-10 mm, regardless of the mobile phase solvents used. However, some degree of separation between BaP and the other two PAHs was achieved using methanol: water 95:5 (v/v). Though BaA and P consistently migrated to similar distances, their SERS fingerprints, especially those near 593 and 724 cm^{-1} , were useful in differentiating these two compounds. Since the BaP bands were mostly separable from the other two PAHs, the fluorescence background which accompanies BaP also shifted away from BaA and P. This way, signal from BaA and P was no longer overwhelmed by this fluorescence background, making spectral differentiation more reliable.

According to the results from unmodified AgNR substrates, a mobile phase consisting of methanol: water 95:5 (v/v) appeared to be most effective for separating BaA, BaP, and P. On the other hand, SERS signal analysis indicated that $10\text{ }\mu\text{M}$ ME modified substrates was most suited for UTLC-SERS detection of selected PAHs. Hence the UTLC retention of PAHs on $10\text{ }\mu\text{M}$ ME modified AgNR substrates were also investigated using methanol: water 95:5 (v/v) as the mobile phase. The normalized intensities of the BaA, BaP, and P peaks were plotted against the development distance in Fig. 5.7. In the mixture, P remained the most readily eluted component,

migrating to the solvent front. The BaA band, partially overlapping with the P band, showed a slightly stronger retention. Finally, the BaP molecules were most reluctant to migrate among the three PAHs, but the BaP band still overlapped with the BaA band and to a lesser extent with the P band. Comparing with the retention when methanol was used as the only mobile phase solvent on ME modified substrates (Fig. 5.4a), it is clear that the addition of water has caused a higher retention of the PAHs, as indicated by the broadening of the chromatographic bands. On the other hand, the modified mobile phase also achieved slightly better separation between BaA and P.

Conclusions

In this study, we have modified the SERS-active AgNR substrates with functional thiol groups, and optimized the mobile phase solvents for UTLC-SERS detection of three PAH compounds, BaA, BaP, and P. Thiol modification has altered the surface polarity of the as-deposit AgNR substrates. Although the SERS signal intensity of the targets was negatively affected, decent PAH signal could still be recovered on ME modified AgNRs. After thiol modification, the UTLC retention behaviors were also slightly changed. A mobile phase system consisting of methanol: water at 95:5 (v/v) was found to be most effective for separating BaP from the other two PAHs. The successful separation of BaP has reduced its fluorescence interference on differentiation of BaA and P based on the SERS fingerprints. Future work will be focused on further improving the UTLC solvent migration distance to allow for higher separation efficiency.

Acknowledgements

This work was supported by National Science Foundation under contract number CBET-1064228 and UGA College of Agricultural and Environmental Sciences Experimental Station.

References

1. Scientific Committee on Food, European Commission, *Opinion of the scientific committee on food on the risks to human health of polycyclic aromatic hydrocarbons in food*, 2002, European Commission (EC): Brussel.
2. Moret, S. and L.S. Conte, *Polycyclic aromatic hydrocarbons in edible fats and oils: occurrence and analytical methods*. Journal of Chromatography A, 2000. **882**(1-2):245-253.
3. Plaza-Bolanos, P., A.G. Frenich, and J.L.M. Vidal, *Polycyclic aromatic hydrocarbons in food and beverages. Analytical methods and trends*. Journal of Chromatography A, 2010. **1217**(41):6303-6326.
4. Nie, S.M. and S.R. Emery, *Probing single molecules and single nanoparticles by surface-enhanced Raman scattering*. Science, 1997. **275**(5303):1102-1106.
5. Wang, Y.L., S. Ravindranath, and J. Irudayaraj, *Separation and detection of multiple pathogens in a food matrix by magnetic SERS nanoprobos*. Analytical and Bioanalytical Chemistry, 2011. **399**(3):1271-1278.
6. Bizzarri, M., A. Rita, and M. Cannistraro, *SERS detection of thrombin by protein recognition using functionalized gold nanoparticles*. Nanomedicine: Nanotechnology, Biology and Medicine, 2007. **3**(4):306-310.
7. Abell, J.L., J. Lee, Q. Zhao, H. Szu, and Y. Zhao, *Differentiating intrinsic SERS spectra from a mixture by sampling induced composition gradient and independent component analysis*. Analyst, 2012. **137**(1):73-76.
8. Hennigan, S.L., J.D. Driskell, R.A. Dluhy, Y.P. Zhao, R.A. Tripp, K.B. Waites, and D.C. Krause, *Detection of mycoplasma pneumoniae in simulated and true clinical throat swab*

- specimens by nanorod array-surface-enhanced Raman spectroscopy*. Plos One, 2010. **5**(10):e13633.
9. Patel, I.S., W.R. Premasiri, D.T. Moir, and L.D. Ziegler, *Barcoding bacterial cells: A SERS based methodology for pathogen identification*. Journal of Raman Spectroscopy, 2008. **39**(11):1660-1672.
 10. Cheung, W., I.T. Shadi, Y. Xu, and R. Goodacre, *Quantitative analysis of the banned food dye Sudan-1 using surface enhanced Raman scattering with multivariate chemometrics*. The Journal of Physical Chemistry C, 2010. **114**(16):7285-7290.
 11. Sandroff, C.J. and D.R. Herschbach, *Surface-enhanced Raman study of organic sulfides adsorbed on silver: facile cleavage of sulfur-sulfur and carbon-sulfur bonds*. The Journal of Physical Chemistry, 1982. **86**(17):3277-3279.
 12. Abell, J.L., J.M. Garren, J.D. Driskell, R.A. Tripp, and Y. Zhao, *Label-free detection of micro-RNA hybridization using surface-enhanced Raman spectroscopy and least-squares analysis*. Journal of the American Chemical Society, 2012. **134**(31):12889-12892.
 13. Sanles-Sobrido, M., L. Rodriguez-Lorenzo, S. Lorenzo-Abalde, A. Gonzalez-Fernandez, M.A. Correa-Duarte, R.A. Alvarez-Puebla, and L.M. Liz-Marzan, *Label-free SERS detection of relevant bioanalytes on silver-coated carbon nanotubes: The case of cocaine*. Nanoscale, 2009. **1**(1):153-158.
 14. Negri, P., G. Chen, A. Kage, A. Nitsche, D. Naumann, B. Xu, and R.A. Dluhy, *Direct optical detection of viral nucleoprotein binding to an anti-influenza aptamer*. Analytical chemistry, 2012. **84**(13):5501-5508.

15. Liu, Y.J., H.Y. Chu, and Y.P. Zhao, *Silver nanorod array substrates fabricated by oblique angle deposition: morphological, optical, and sers characterizations*. The Journal of Physical Chemistry C, 2010. **114**(18):8176-8183.
16. Fu, J.X., A. Collins, and Y.P. Zhao, *Optical properties and biosensor application of ultrathin silver films prepared by oblique angle deposition*. The Journal of Physical Chemistry C, 2008. **112**(43):16784-16791.
17. D. Driskell, J., S. Shanmukh, Y. Liu, S. B. Chaney, X.J. Tang, Y.P. Zhao, and R. A. Dluhy, *The use of aligned silver nanorod arrays prepared by oblique angle deposition as surface enhanced Raman scattering substrates*. The Journal of Physical Chemistry C, 2008. **112**(4):895.
18. Negri, P., N.E. Marotta, L.A. Bottomley, and R.A. Dluhy, *Removal of surface contamination and self-assembled monolayers (SAMs) from silver (Ag) nanorod substrates by plasma cleaning with argon*. Applied Spectroscopy, 2011. **65**(1):66-74.
19. Kwok, D. and A. Neumann, *Contact angle measurement and contact angle interpretation*. Advances in Colloid and Interface Science, 1999. **81**(3):167-249.
20. Reinfelder, J.R. and S.I. Chang, *Speciation and microalgal bioavailability of inorganic silver*. Environmental Science & Technology, 1999. **33**(11):1860-1863.
21. Song, C., J. Chen, J.L. Abell, Y. Cui, and Y. Zhao, *Ag-SiO₂ core-shell nanorod arrays: Morphological, optical, SERS, and wetting properties*. Langmuir, 2011. **28**(2):1488-1495.
22. Tarabara, V.V., I.R. Nabiev, and A.V. Feofanov, *Surface-enhanced Raman scattering (SERS) study of mercaptoethanol monolayer assemblies on silver citrate hydrosol*.

- Preparation and characterization of modified hydrosol as a SERS-active substrate.* Langmuir, 1998. **14**(5):1092-1098.
23. Fan, J.-G., D. Dyer, G. Zhang, and Y.-P. Zhao, *Nanocarpet effect: pattern formation during the wetting of vertically aligned nanorod arrays.* Nano Letters, 2004. **4**(11):2133-2138.
24. Abell, J.L., J.D. Driskell, and Y.P. Zhao, *Controllable and reversible hot spot formation on silver nanorod arrays.* Chemical Communications, 2014. **50**(1):106-108.
25. Zeman, E., K. Carron, G. Schatz, and R. Van Duyne, *A surface enhanced resonance Raman study of cobalt phthalocyanine on rough Ag films: Theory and experiment.* The Journal of Chemical Physics, 1987. **87**(7):4189-4200.

Figures

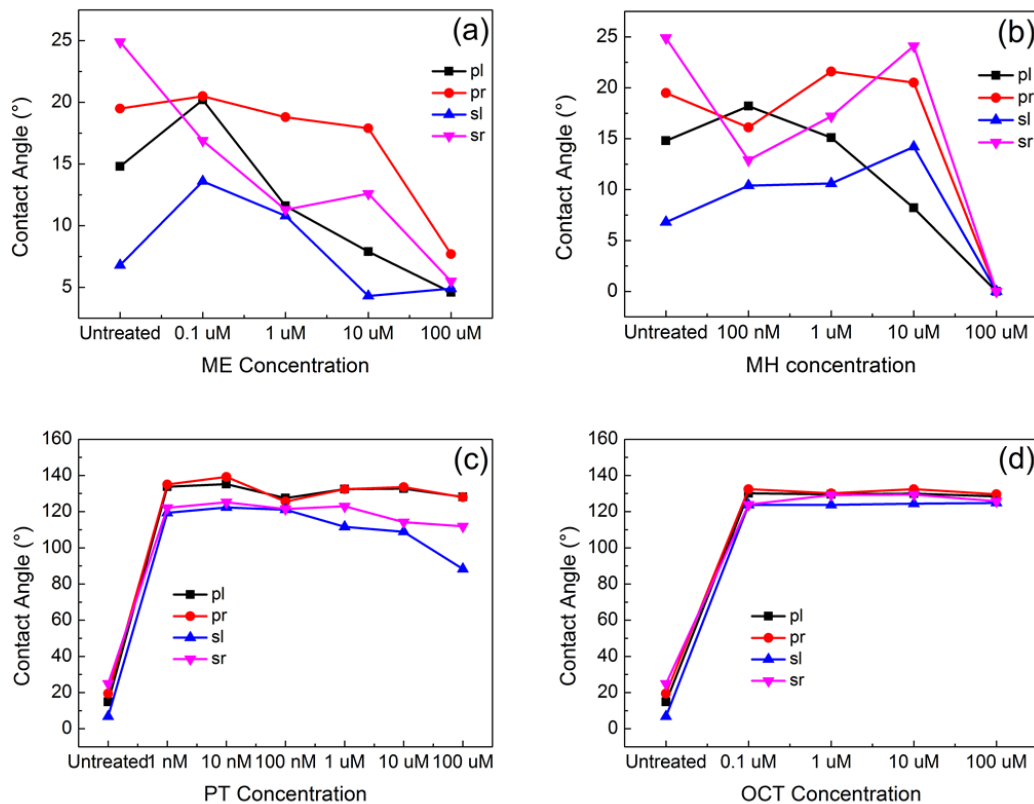


Figure 5.1 Water contact angle on (a) ME (b) MH (c) PT and (d) OCT modified AgNR substrates. The contact angles are expressed as the left (l) and right (r) angles measured on substrates with the AgNRs oriented parallel (p) or perpendicularly (s) to the viewing angle.

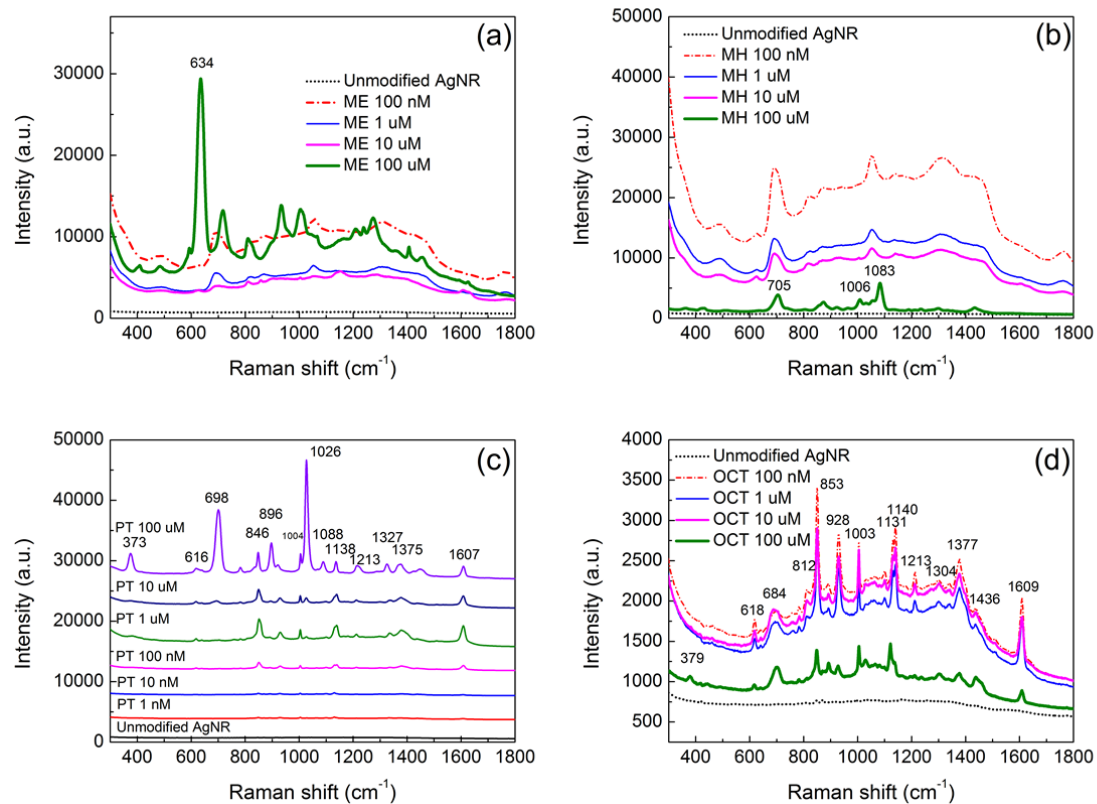


Figure 5.2 SERS spectra of blank substrates after thiol modification (a) ME modified substrates (b) MH modified substrates (c) PT modified substrates (d) OCT modified substrates. All spectra were collected at 60 mW, 10 s. Spectra were vertically offset for clarity in (c).

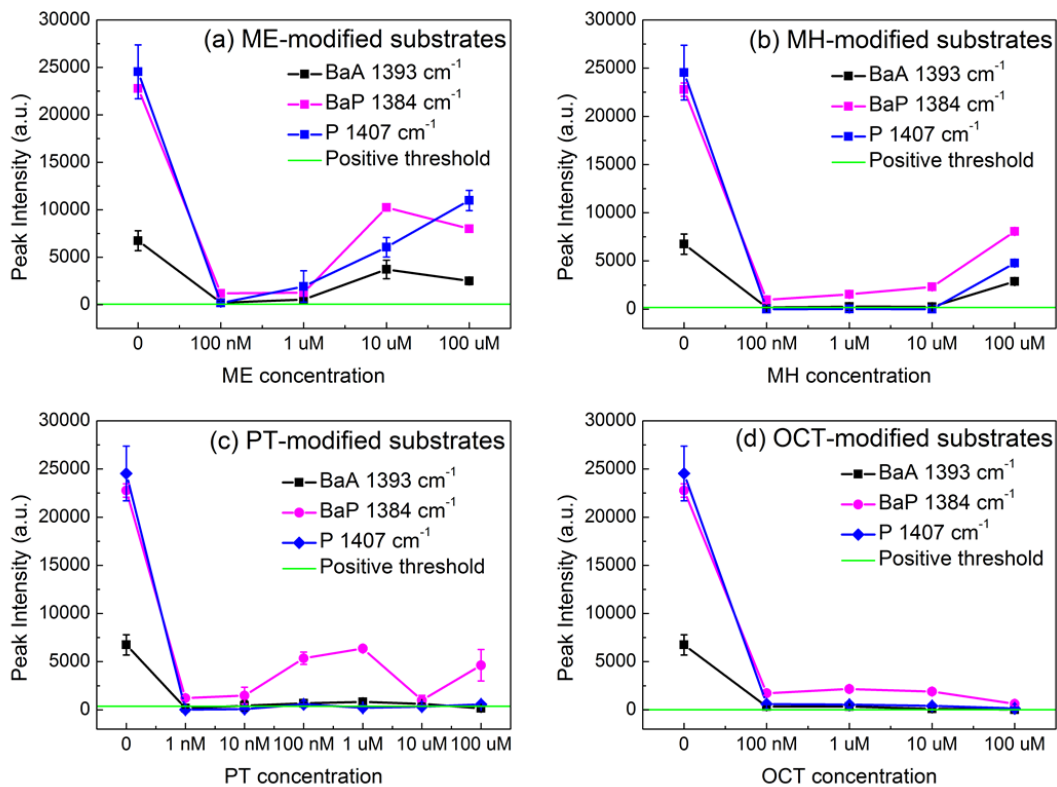


Figure 5.3 SERS intensity of 200 $\mu\text{g/mL}$ BaA, BaP, and P on (a) ME (b) MH (c) PT and (d) OCT modified substrates. The positive threshold was three times of the standard deviation in the spectral intensity at a smooth region ($1750\text{-}1800\text{ cm}^{-1}$).

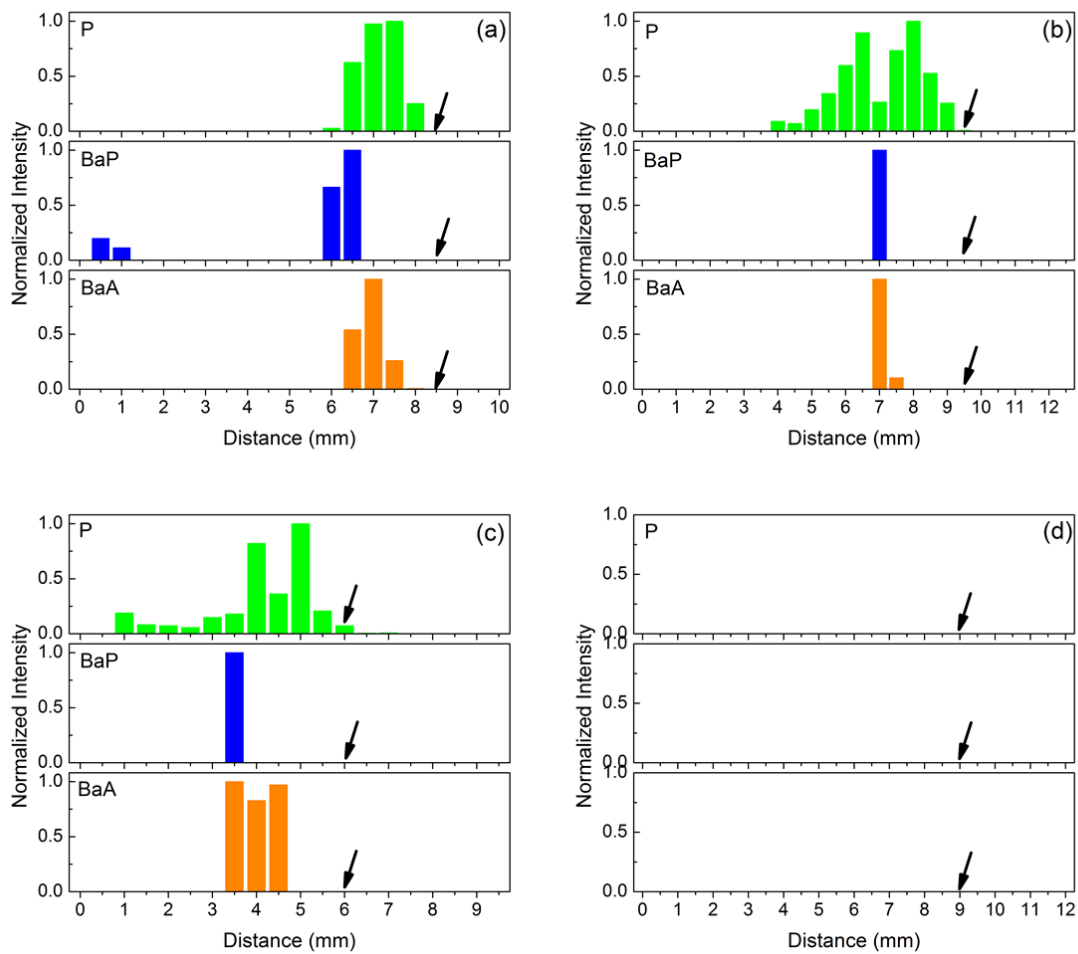


Figure 5.4 UTLC separation of BaA, BaP, and P on (a) 10 μM ME (b) 100 μM ME (c) 10 μM MH and (d) 100 μM MH modified AgNR substrates. UTLC was conducted using methanol as the mobile phase solvent. Black arrows indicate solvent front location.

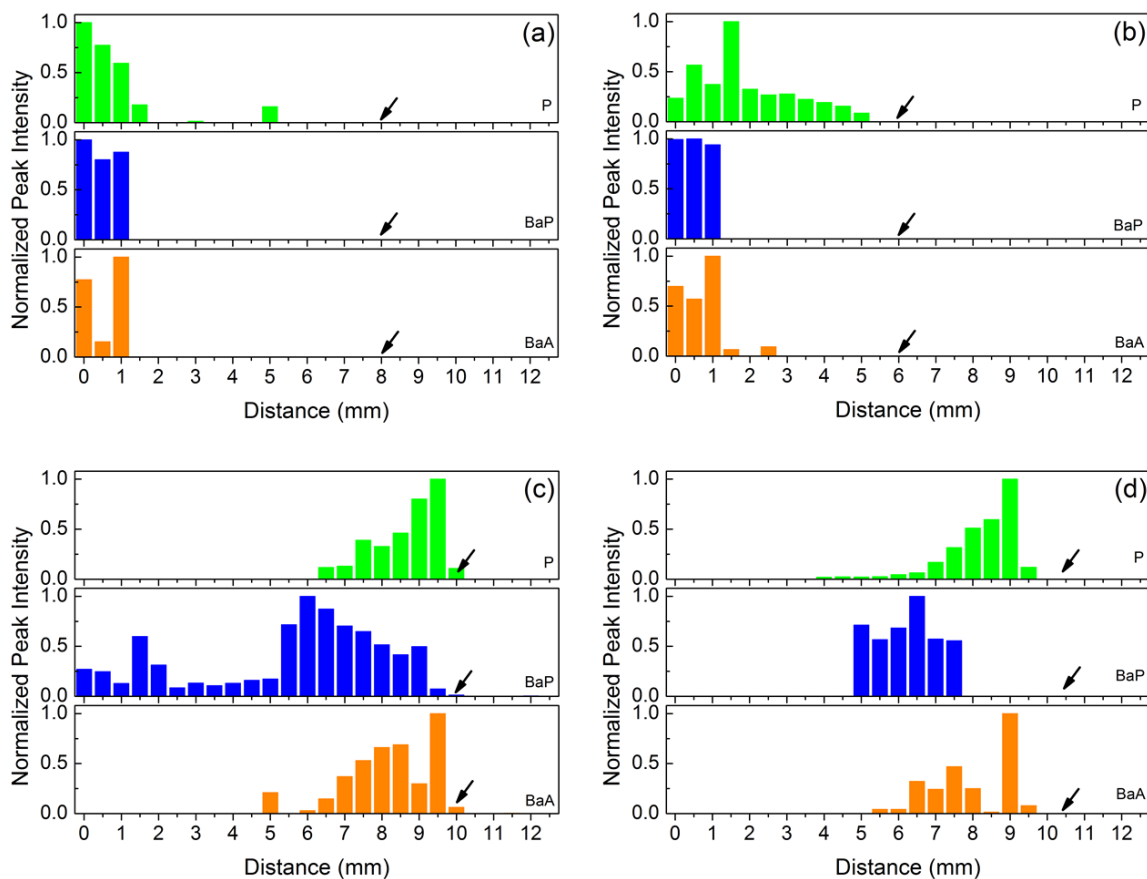


Figure 5.5 UTLC separation of BaA, BaP, and P on unmodified AgNR substrates using methanol and water mixed at different ratios. (a) methanol: water 50:50 (v/v) (b) methanol: water 70:30 (v/v) (c) methanol: water 90:10 (v/v) and (d) methanol: water 95:5 (v/v). Black arrows indicate the solvent front measured for each sample spot.

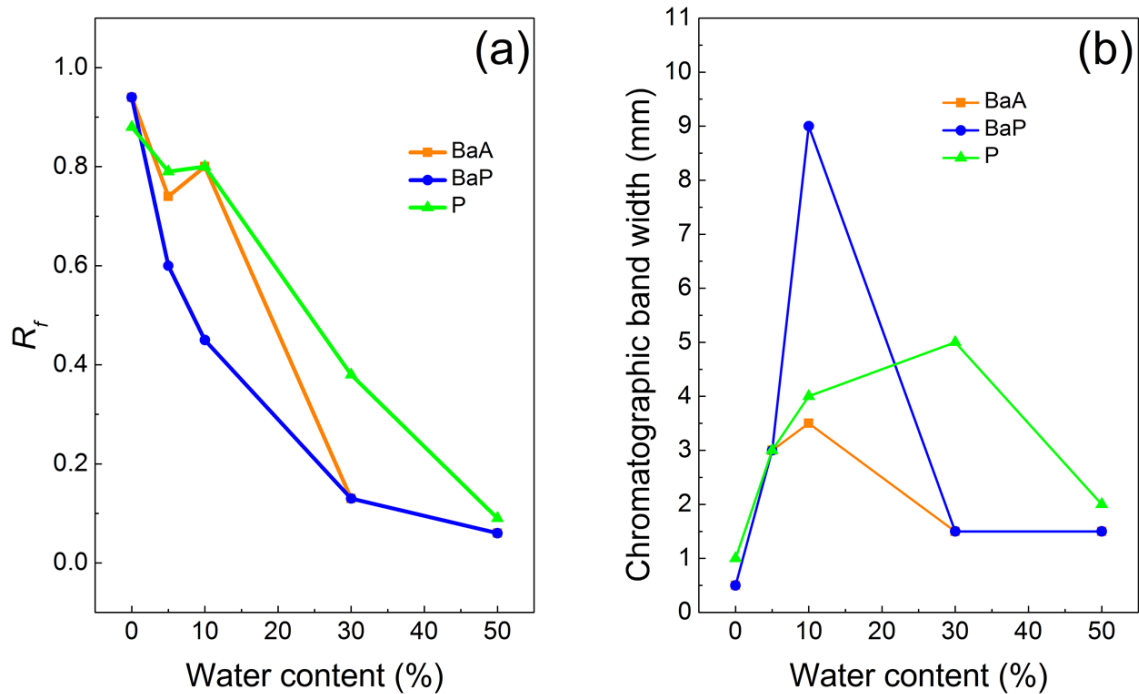


Figure 5.6 (a) R_f values and (b) chromatographic band widths of BaA, BaP, and P developed by mixtures of methanol and water on unmodified AgNR substrates

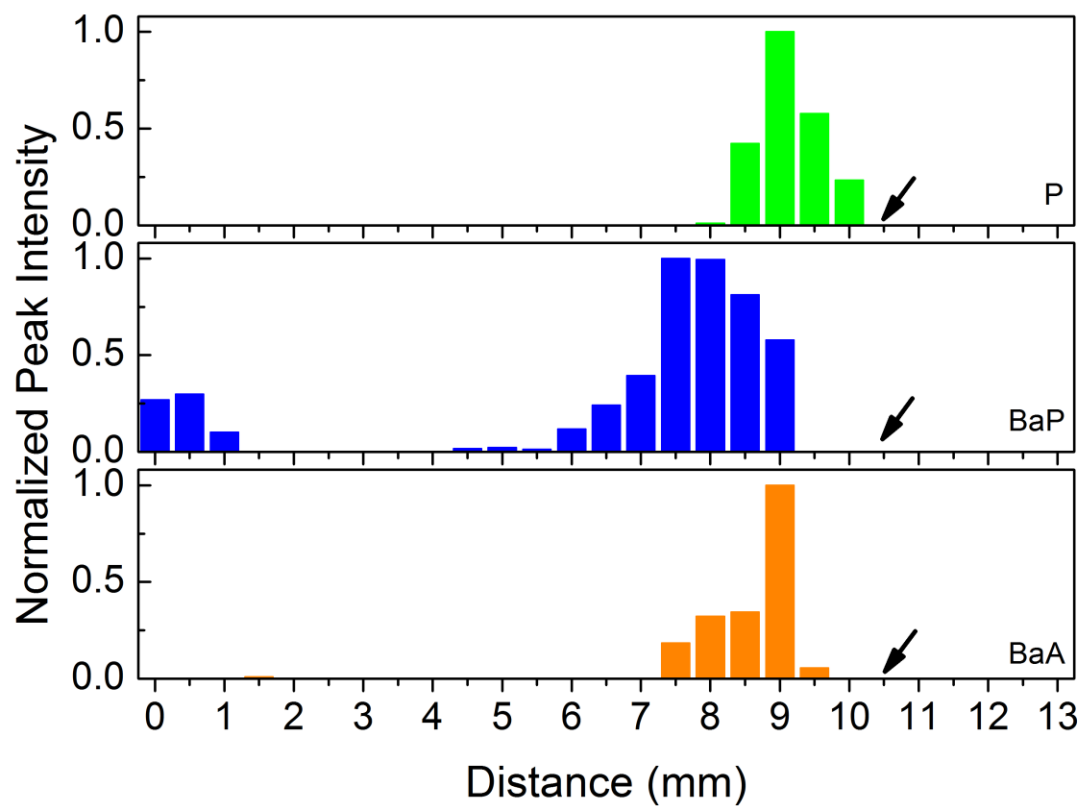


Figure 5.7 UTLC separation of BaA, BaP, and P on 10 μ M ME modified AgNR substrates using methanol: water 95:5 (v/v). Black arrows indicate the solvent front measured for each sample spot.

CHAPTER 6

DETECTION OF POLYCYCLIC AROMATIC HYDROCARBONS FROM COOKING OIL USING ULTRA-THIN LAYER CHROMATOGRAPHY AND SURFACE ENHANCED RAMAN SPECTROSCOPY⁴

⁴ Jing Chen, Yao-wen Huang, and Yiping Zhao. To be submitted to *Sensors and Actuators B*.

Abstract

In this work, we have demonstrated the use of on-chip ultra-thin layer chromatography (UTLC) and surface enhanced Raman spectroscopy (SERS) in the detection of hazardous food contaminants, polycyclic aromatic hydrocarbons (PAHs) from cooking oil samples. After a simple acetonitrile extraction step, the organic phase was directly applied to the SERS-active silver nanorod (AgNR) substrate without further cleanup, and subject to UTLC separation on the AgNR surface. The spectral interference from co-extracted oil residues was mitigated by UTLC, and the SERS detection limits were found to be equivalent or lower than those found in PAH standard solutions. In this study, the interference from the oil matrix was also quantitatively assessed, and the PAH extraction procedure was optimized for UTLC-SERS. UTLC-SERS provides a simple but effective means for post-extraction sample cleanup directly on the sensing surface.

Introduction

Polycyclic aromatic hydrocarbons (PAHs) are ubiquitous atmospheric pollutants consisting of fused aromatic rings. These compounds are formed during incomplete combustion of fuels, and are commonly found in soil and sediments. However, a significant amount of PAHs are also found in contaminated foods, particularly food cooked at high temperatures, such as barbecued and smoked foods. During an oil spill, seafood products could also be contaminated by PAHs [1, 2]. Due to their lipophilic properties, PAHs tend to accumulate in food with high fat contents, such as edible oil. The PAHs in oil products are usually formed when the oil-bearing seeds are dried in direct contact with the combustion products of the heat source [3]. However, significant levels of PAHs are also commonly identified in repeatedly used cooking oil, such as

deep fryer oil and recycled cooking oil, as such environments promote the formation of free radicals and the pyrolysis process necessary for PAH formation. Once ingested from contaminated food, PAHs could act as carcinogens or as carcinogenic synergists and lead to cancer. In addition, these compounds have also demonstrated mutagenic and teratogenic properties, which are linked to adverse birth outcomes and deficiencies in the newborn [4, 5].

Current gold standards for PAH detection from food are based on liquid chromatography (LC) or gas chromatography (GC), which are coupled to fluorescence detection or mass spectrometry (MS) [2]. The LC and GC based techniques are highly accurate and sensitive, and have been developed to analyze PAHs in different matrices. However, the low throughput of column chromatography has largely limited their usefulness in routine inspection of PAHs. On the other hand, sample preparation remains a demanding task in GC and LC, which also diminishes the overall rapidity of the assay. Traditionally, sample preparation for PAHs involves of an extraction step (*e.g.*, liquid-liquid partition or saponification) followed by one or more purification procedures (*e.g.*, column chromatography or solid-phase extraction (SPE)) and a final solvent evaporation step [6]. In the past decade, new methods centering acetonitrile extraction/ partitioning and dispersive SPE cleanup have been introduced, which have considerably reduced the complexity and duration of sample preparation for the analyses of pesticide residues and other organic pollutants including PAHs [7-11]. The cleanup step is critical in sample preparation, especially for fatty food matrices, since lipids and lipophilic components (mainly triglycerides) have similar dispersive properties to PAHs. The co-extracted lipids are likely to create major complications for chromatographic separation. For this reason, rapid sample preparation methods are limited to detection in non-fatty to moderately fatty

matrices such as vegetables and seafood. Removal of triglyceride residues from the extract while retaining PAHs remains a major challenge in LC and GC based analyses.

As an alternative to LC and GC, surface enhanced Raman spectroscopy (SERS) is an ultra-sensitive tool for rapid, non-destructive molecular identification based on the characteristic Raman vibrational fingerprints. SERS has been exploited in the detection of a wide variety of chemical and biological targets, and have demonstrated the potential of single molecule detection. However, the application of SERS in real world samples is hindered by the spectral interferences from co-existing components and the food matrix. Recently, we have demonstrated the potential of direct coupling of SERS and ultra-thin layer chromatography (UTLC) for improved selectivity of mixture samples. The UTLC-SERS strategy proved a potential for separating different components in mixtures on the SERS-active substrates. Furthermore, it also served to recover signal from weakly adsorbing targets from massive matrix interferences, which could be useful for food analysis. In a series of studies, we have modified the SERS substrates and optimized the mobile phase solvents for the UTLC-SERS separation of PAHs in standard solutions.

In this study, we have continued to explore the potential application of the UTLC-SERS technique in PAH detection from edible oils. The interference from oil matrix was first investigated, and after the conditions for PAH extraction were also probed. Finally, UTLC-SERS detection of representative PAH compounds was carried out.

Materials and Methods

Materials

Benz(a)anthracene (BaA), benzo(a)pyrene (BaP), and pyrene (P), 2-mercaptoethanol (ME), hexanes, and acetonitrile (99.8%) were purchased from Sigma Aldrich (St. Louis, MO). Methanol was purchased from J. T. Baker (Phillipsburg NJ). 18 M Ω water was prepared by a Milli-Q system (Millipore, Billerica, MA). Silver (99.999%) and titanium (99.995%) were obtained from Kurt L. Lesker (Clairton, PA). Vegetable oil, corn oil, olive/canola oil blend, and chili oil were from a local grocery store. An old oil sample was collected from a local household, which was used for repeatedly deep frying chicken and fish.

Fabrication of AgNR substrates

The AgNR substrates were fabricated using oblique angle deposition (OAD) in a custom-built electron beam evaporator [12, 13]. Briefly, 1×1 inch² glass slides were cleaned with 80% sulfuric acid and 20% hydrogen peroxide, rinsed with deionized (DI) water, dried with compressed nitrogen, and loaded into the evaporator chamber. Under vacuum conditions (<10⁻⁶ Torr), 20 nm of titanium and 200 nm of silver were deposited onto the glass slides at normal angle at a rate of 0.2 nm/s and 0.3 nm/s, respectively. The substrate surface normal was then rotated to 86° with respect to the incident vapor flux, and a final layer of 2000 nm AgNRs were deposited at a rate of 0.3 nm/s. The AgNRs were ~ 900 nm in length, ~ 100 nm in rod diameter, with a tilting angle of approximately 73° with respect to the substrate normal [12, 14]. Immediately before use, the as-deposited AgNR substrates were cleaned for 2 min in a custom built inductively-coupled RF plasma chamber, which operated at 30 W under a constant flow (chamber pressure maintained at ~ 600 mTorr) of ultra-pure argon to remove any organic contaminants accumulated during fabrication and storage [15].

Raman and SERS spectra of cooking oil products

The Raman spectra of vegetable, corn, olive/canola, chilli, and old oil samples were acquired using an Enwave ProRamanL 785A system (Enwave Optronics, Irvine, CA) equipped with a 785 nm diode laser at a power of 150 mW and a spectral acquisition time of 30 s. The oil samples were also diluted to 10^{-3} in hexanes, and 0.1 μL of each dilution was applied to the AgNR surface and dried for SERS measurements.

SERS measurements

Unless otherwise specified, all SERS measurements in this study were carried out through a $10\times$ objective lens at 60 mW and the spectral collection time was 5 s. For UTLC samples, SERS spectra were acquired in 0.5 mm steps along the UTLC development direction, from the center of the original sample spots to ~ 2 mm beyond the identified solvent front.

UTLC procedure

An aliquot of 0.1 μL of each sample was applied onto the AgNR substrate and dried under ambient conditions. Then the substrate was placed in a 35 mL beaker containing ~ 3.5 mL of mobile phase solvents, such that the sample spots were ~ 1 mm above the liquid meniscus. The beaker was pre-saturated with the mobile phase vapor for at least 10 min prior to UTLC and covered with a watch glass during UTLC. After 5 min, the substrate was taken out of the beaker and dried, and the solvent front was immediately marked by scratching the substrate with tweezer tips.

Extraction of PAHs from vegetable oil

Methanol, ethanol, isopropanol, and acetonitrile were selected as candidate solvents for extracting PAHs from oil. P was spiked in vegetable oil at 10 and 1 mg/mL. The spiked samples were mixed with the solvent, Vortexed for 1 min, and then settled at room temperature (RT) for

30 min to allow phase separation. The upper organic phase was then removed to a new tube, from which 0.1 μL was applied onto the AgNRs for SERS measurements without further treatment. The solvent resulting in the highest P intensity was selected in the final extraction protocol.

The sample: solvent ratio was optimized by using 200 – 1000 μL of solvent to extract 200 μL of oil sample spiked with 1 mg/mL P. To account for the dilution effect resulted from increased solvent volume, after extraction, the organic phase in all the samples was reduced to 100 μL through evaporation. In addition to direct SERS intensity comparison, the samples were also subject to UTLC with either methanol or a mixture of methanol and acetonitrile (1:1, v/v). The highest intensities along the development direction were compared.

Interference of oil to SERS detection of PAHs

The influence of co-extracted oil to the SERS detection of PAHs was assessed by spiking 100 ng/mL – 10 mg/mL P into oil-saturated acetonitrile. The saturated acetonitrile was prepared by mixing 30 mL neat acetonitrile with 10 mL vegetable oil and Vortexing for 1 min. The mixture was allowed to settle at RT for 30 min, and then the upper acetonitrile phase was removed to a new tube. 0.1 μL of P in neat and saturated acetonitrile was applied to unmodified AgNR substrates, dried, and the SERS spectra was collected. Then the saturated acetonitrile samples were subject to UTLC with methanol, followed by SERS spectral collection.

UTLC-SERS detection of PAHs from vegetable oil

Three PAHs, BaA, BaP, and P were mixed and spiked into fresh vegetable oil, resulting in a series of oil samples contaminated with 200 $\mu\text{g}/\text{mL}$ of each PAH. The samples were separated using a mixture of methanol and water (95:5 or 80:20, v/v) on ME modified AgNRs. The modified substrates were prepared by soaking AgNR substrates in 10 μM ME aqueous

solution for 30 min, rinsing with water, and then drying with nitrogen. As a comparison, UTLC was also carried out using methanol on ME modified substrates, or using a mixture of methanol and water on unmodified AgNR substrates.

Data analysis

The SERS spectra were fitted to the characteristic PAH peaks using a mixed Gaussian/Lorentzian function using the GRAMS/AI Spectroscopy package (Thermo Scientific, Waltham, MA). For each sample component, the peak intensities along the development direction were divided by the highest peak intensity found in that component to generate a series of normalized peak intensities to indicate chromatographic separation.

Results and Discussion

Raman and SERS Spectra of Cooking Oils

Raman and SERS signal of different oil products were first examined. The averaged Raman spectra are shown in Figure 6.1a. Weak to moderate peaks could be observed at 970, 1083, 1267, 1303, 1440, 1557, and 1657 cm^{-1} in the spectra of all sampled oil products, which have been assigned to the C-C skeletal modes, CH_2 twisting, and CH_2/CH_3 deformation, respectively. The 1557 and 1657 cm^{-1} peaks can be attributed to C=C stretching modes [16, 17]. Except the a pronounced fluorescence background in chili oil, all oil products demonstrated highly similar Raman spectra. Previously, Raman spectroscopy has been used to directly differentiate oil products with the assistance of chemometric analysis. However, it requires much higher power and spectral acquisition time; the differentiation power of chemometric analysis is also very limited at low adulteration levels [18, 19]. This is also consistent with the spectral resemblance

found in this study which demonstrated the limitation of Raman spectroscopy in oil inspection. More sensitive and specific techniques are required for identification of used oil.

Peaks at 960, 1083, and 1158 cm^{-1} found in the Raman spectra were also identified in the SERS spectra of oil, with minor shifts (Fig. 6.1b). Maximum SERS intensities were obtained when the oil samples were diluted to 10^{-2} . Further dilution tends to decrease the signal intensity again.

Interference of Oil to PAH Detection

The interference of co-extracted oil to PAH detection was quantitatively assessed using P as a model compound. Figure 6.2a plots the peak intensity before UTLC against the actual P concentration. After UTLC, the highest peak intensity along the development direction is also plotted against the actual P concentration in the same figure. In neat acetonitrile, P signal could be detected at as low as 500 ng/mL. The intensity experiences a drastic increase from ~ 41 a.u. at 500 ng/mL to ~ 8826 a.u. at 1000 $\mu\text{g/mL}$, after which the intensity slightly decreases to ~ 7116 a.u. at 10^4 $\mu\text{g/mL}$. In contrast, the signal intensity from P prepared in oil-saturated acetonitrile is considerably lower (approximately 1/70 - 1/30 of that in the neat solvent) at all detectable concentrations (orange curve in Fig. 6.2a). Below 10 $\mu\text{g/mL}$, the signal cannot be identified. This means the spectral interference of residual oil in the organic extract is not negligible. If the extract is used for direct SERS measurements without further cleanup, the presence of oil will severely hamper the detection limit (LOD becomes at least 20 times higher compared with that in neat solvent). After applying UTLC, the oil residues largely remain at the sample origin whereas the PAH was eluted to near the solvent front, where its SERS signal becomes more intense and identifiable at concentrations above 5 $\mu\text{g/mL}$ (blue curve in Fig. 6.2a). Still, the peak intensity after UTLC is significantly lower than that in neat acetonitrile, suggesting that the

signal quenching effect from oil residues is not completely overcome by UTLC. In the meantime, as the P molecules are eluted and scattered along a long distance, the SERS signal also becomes weaker due to a small number of molecules left at the solvent front.

The corresponding correlations between the logarithmic forms of the P signal intensities and the actual P concentration are plotted in Figures 6.2b-d. A strong linear relationship ($R^2 = 0.9858$) is suggested between 0.5 and 50 $\mu\text{g/mL}$ in the neat acetonitrile preparations. Similarly, the SERS intensity of P in oil-saturated acetonitrile is linearly correlated with the actual concentration within the range of 10 to 1000 $\mu\text{g/mL}$ ($R^2 = 0.9762$). After UTLC development, a weak linear relationship ($R^2 = 0.80417$) is also found in the oil-saturated acetonitrile group when P concentration is between 10 and 500 $\mu\text{g/mL}$. Using these prediction models, it may be possible to quantitatively or semi-quantitatively detect PAHs from oil extracts, if the unknown samples are run alongside the standards on the same substrate.

To provide a better understanding on the interfering effects, the concentration of oil residue in the organic extract was determined. The amount of oil residue per 2 mL saturated acetonitrile is determined to be 9.7 mg (*i.e.*, 4.85×10^{-3} g/mL). Thus the spectral interference observed in previous experiments is resulted from ~ 4.9 μg of oil residue within a ~ 1 mm (0.1 μL) sample spot. According to the results in Section 6.1, the SERS signal of oil also reaches its maximum intensity at similar concentrations. Thus it is not surprising that before UTLC the target PAH signal in the extract is severely impacted.

Extraction of PAHs from vegetable oils

Four common lab solvents, methanol, ethanol, isopropanol, and acetonitrile, which are immiscible with oil, were selected as candidate extraction solvents. Noticeably, extraction with

isopropanol resulted in a cloudy mixture in which the organic phase failed to effectively partition with the oil phase (data not shown). Therefore, it was excluded from the panel of candidate solvents.

At a high P concentration (10 mg/mL), weak but distinguishable P peaks at ~ 410 , 594, 1242, and 1407 cm^{-1} could be identified in its SERS spectra following extraction with methanol, ethanol, and acetonitrile (Fig. 6.3a). The corresponding peak intensities at 593 cm^{-1} show that extraction with methanol or acetonitrile provided relatively strong P signal (637 ± 75 and 530 ± 40 a.u., respectively). Ethanol extraction resulted in lower signal intensity, whereas in isopropanol extraction, the SERS signal of P was negligible (Fig. 6.3b). It is also worth noting that using previously established prediction model (Fig. 6.2c), P concentration in the acetonitrile extract was estimated to be ~ 778 $\mu\text{g/mL}$. Considering equal volume extraction, less than 1/10 of the initial P (10 mg/mL) has partitioned from the oil phase into the acetonitrile phase. At lower PAH concentrations, the extraction rate is expected to be lower, which again confirms the PAH's higher affinity to nonpolar oil matrix.

As expected, P spectra at a lower concentration (1 mg/mL) only exhibited peaks from the oil residues (Fig. 6.3c). Obviously, the initial P concentration in oil was too low to overcome the matrix effect. These extracts were then subject to UTLC with either methanol or methanol:acetonitrile 1:1 (v/v) as the mobile phase. The strongest peak intensity of each sample after UTLC was compared in Figure 6.3d. Clearly, the interference from oil co-extracts was eliminated from the ethanol extract after UTLC, making the P intensity comparable to that in the methanol extracts. Still, extraction with acetonitrile demonstrated higher overall P intensity. Considering that acetonitrile is widely preferred over methanol as an extraction solvent in

established HPLC methods, it was also selected for PAH extraction from oil samples for UTLC-SERS.

The effect of centrifugation was probed by comparing the SERS intensity of P after static settling and centrifugation. However, the results showed that although centrifuging could significantly speed up phase separation, its effect was not as significant (see Appendix D Fig. D.1 for details). Therefore, 30 min static settling was adopted in the final extraction protocol.

The optimal volume ratio between the oil sample and extraction solvent was determined. As shown in Figure 6.4, before applying UTLC, extraction with 200 μL of acetonitrile yielded the highest P intensities. As the solvent volume increased, P intensity first decreased and then slightly increased after acetonitrile exceeds 3 times the sample volume. Overall, the effect of solvent evaporation was not significant (compare light gray and black bars in Fig. 6.4). However, after solvent evaporation there was a slight but noticeable decreasing trend in the P intensity in response to increasing solvent volume, as indicated by the black bars in Fig. 6.4. This suggests that when the volume of acetonitrile exceeded 600 μL , though additional P molecules had partitioned into the organic phase because of the increased extraction solvent, more oil residues had also entered the organic phase so that the signal increase caused by the P partitioning equilibrium shift was cancelled out by stronger matrix interference.

A noticeable increase in the P intensity was observed at all five extraction ratios after UTLC as a result of mitigated matrix interference. In general, after UTLC, the extracts yielded stronger P signal after solvent evaporation, and the signal difference was greater in the large acetonitrile volume groups (800 and 1000 μL) (Groups c and d in Fig. 6.4). This confirms the speculation that interference from oil was the main cause for decreased P signal in these groups, and once the interference was eliminated or reduced, the target SERS signal could be remarkably

improved. Nevertheless, from Figure 6.4 it is clear that the benefit brought by solvent evaporation was not adequate to compensate for the lengthy process of evaporation. Since extraction using 600 μL of acetonitrile yielded the strongest P intensity after UTLC, 3:1 (v/v) was selected as the optimal extraction ratio between the extraction solvent and the oil sample.

PAH extraction protocol has been established as follows: a. Transfer 200 μL of oil sample to a 1.5 mL microcentrifuge tube, and pipette in 600 μL of acetonitrile; b. Vortex the sample at the maximum speed for a full minute, and set aside the tubes in darkness at RT for 30 min to allow the organic and oil phases to separate; c. Transfer the upper acetonitrile phase to a new tube and use 0.1 μL of this liquid directly for subsequent UTLC-SERS analysis.

Using such a protocol, the oil residues, which can negatively impact the SERS detection of PAHs, were left untreated. However, the UTLC process itself served as a cleanup procedure, which functionally resembled column chromatography used for post-extraction sample cleanup in HPLC and GC methods. In HPLC and GC, the presence of excess oil in the injected sample should be avoided for its potentially irreversible damage to the chromatographic column. Since the AgNR substrates are considered as a disposable UTLC plate, potential damages to the chromatographic plate need not be concerned. However, matrix effects to the UTLC development, *i.e.*, the impact of oil residues to the retention of PAHs and the detection sensitivity must be monitored.

UTLC-SERS detection of PAHs from vegetable oil

Figure 6.5a shows the SERS spectra before UTLC, which are dominated by the features of oil residues particularly within the spectral region between 1150 and 1600 cm^{-1} . The PAH signals were completely overwhelmed by the massive oil background. After UTLC development

with methanol: water 95:5 (v/v), the PAH molecules were released from the oil matrix and migrated to the solvent front, where characteristic PAH peaks could be identified in their SERS spectra at concentrations above 100 $\mu\text{g/mL}$. In the UTLC separation (Fig. 6.5 b-d) P was consistently eluted to immediately behind the solvent front, whereas the BaA and BaP components followed slightly behind. Their retention was consistent with that in the neat solvents, but the bands tended to overlap and the bands were also observed to be broader compared to developing in neat solvent (data not shown). Band elongation was most apparent at high PAH concentrations, which can span as long as 6.5 mm on the substrate. Band tailing at high sample concentrations are a common phenomenon in TLC, which is attributed to the accumulation of excess analyte molecules on the development pathway [20]. However, at concentrations close to the LODs, elongation was mainly due to the response diminishment effect induced by co-extracted oil residues. In this UTLC system, a third interaction between PAHs and matrix (oil) was introduced to the UTLC equilibrium in addition to the interactions between PAHs and the stationary and mobile phases. Since the PAHs had a higher affinity to lipids than to the relatively polar mobile phase, this interaction could cause a portion of the PAH molecules to be better retained on the substrate, leading to tailing of the chromatographic bands.

To improve the UTLC separation and potentially SERS detection, the mobile phase was adjusted to methanol: water 80:20 (v/v) (Fig. 6.6). All three PAH components could be detected at as low as 50 $\mu\text{g/mL}$ after the UTLC process. The band tailing effect was not aggravated by additional water; rather, at the highest concentration (1000 $\mu\text{g/mL}$), the band elongation effect was less severe compared with developing with methanol: water 95:5. Most likely, a high percentage of water in the mobile phase served to restrict the migration of co-extracted oil from the sample spot, thereby inhibiting the interaction between oil and PAHs and force the latter to

migrate further away. Consistent with developing in other mobile phases, P was eluted to the solvent front at all concentrations. The retention of BaA and BaP appeared to vary slightly at different concentrations: as the concentration increases, a wider gap was found between the BaP band and solvent front; on the contrary, the BaA component appeared more mobile, as evidenced by the closer distance between the BaA band and solvent front. Comparing with the UTLC development using the same mobile phase solvents on unmodified AgNRs and development using methanol on ME modified substrates, it is suggested that the separation of PAHs, however subtle, could be achieved through adjusting the mobile phase constitution, but the separation could only be achieved on chemically modified substrates (see Appendix D for detailed discussions).

Admittedly, an additional cleanup step to remove the co-extracted triglyceride after acetonitrile extraction might be a more effective approach to circumvent the complications introduced by the matrix. However, the UTLC treatment also provided effective cleanup directly on the sensing surface, with limit of detections equivalent to those found in neat solvents (data not shown). Furthermore, the three PAH compounds selected in this study have distinct SERS peaks which could be used for identification without UTLC. Therefore, qualitative detection was not deteriorated because of the overlapping of chromatographic bands. Still, as the number of target PAH compounds increases, identification based on the presence of unique SERS peaks will become less reliable. At this stage, R_f recognition can provide useful and complimentary information to SERS detection, but probing for more reliable and versatile UTLC systems will become inevitable.

Conclusions

In this work, we have applied the UTLC-SERS technique to the detection of three PAH compounds, BaA, BaP, and P from cooking oil samples. The interference of the oil matrix was investigated, and the PAH extraction procedure was optimized for UTLC-SERS. After a quick acetonitrile extraction step, the organic phase was directly used without further cleanup. Although the co-extracted oil residue posed significant interference to the detection of PAHs, UTLC on the SERS-active AgNR surface was able to eliminate the matrix effect, and the SERS detection limits were found to be equivalent or lower than those found in PAH standard solutions. Therefore, UTLC-SERS provides a simple but effective means for post-extraction sample cleanup directly on the sensing surface. The disposable AgNR chip also enables faster screening of PAHs with a higher throughput compared to conventional LC and GC methods.

Acknowledgements

This work was supported by National Science Foundation under contract number CBET-1064228 and UGA College of Agricultural and Environmental Sciences Experimental Station.

References

1. Speer, K., E. Steeg, P. Horstmann, T. Kuhn, and A. Montag, *Determination and distribution of polycyclic aromatic-hydrocarbons in native vegetable-oils, smoked fish products, mussels and oysters, and bream from the river elbe*. Journal of High Resolution Chromatography, 1990. **13**(2):104-111.
2. Plaza-Bolanos, P., A.G. Frenich, and J.L.M. Vidal, *Polycyclic aromatic hydrocarbons in food and beverages. Analytical methods and trends*. Journal of Chromatography A, 2010. **1217**(41):6303-6326.
3. Moret, S. and L.S. Conte, *Polycyclic aromatic hydrocarbons in edible fats and oils: occurrence and analytical methods*. Journal of Chromatography A, 2000. **882**(1-2):245-253.
4. Scientific Committee on Food, European Commission, *Opinion of the scientific committee on food on the risks to human health of polycyclic aromatic hydrocarbons in food*, 2002, European Commission (EC): Brussel.
5. Dejmek, J., I. Solanský, I. Benes, J. Lenček, and R.J. Srám, *The impact of polycyclic aromatic hydrocarbons and fine particles on pregnancy outcome*. Environmental Health Perspectives, 2000. **108**(12):1159.
6. Fromberg, A., A. Hojgard, and L. Duedahl-Olesen, *Analysis of polycyclic aromatic hydrocarbons in vegetable oils combining gel permeation chromatography with solid-phase extraction clean-up*. Food Additives and Contaminants, 2007. **24**(7):758-767.
7. Anastassiades, M., S.J. Lehotay, D. Stajnbaher, and F.J. Schenck, *Fast and easy multiresidue method employing acetonitrile extraction/partitioning and "dispersive solid-*

- phase extraction" for the determination of pesticide residues in produce. Journal of AOAC International, 2003. 86(2):412-431.*
8. Forsberg, N.D., G.R. Wilson, and K.A. Anderson, *Determination of parent and substituted polycyclic aromatic hydrocarbons in high-fat salmon using a modified QuEChERS extraction, dispersive SPE and GC-MS. Journal of Agricultural and Food Chemistry, 2011. 59(15):8108-16.*
 9. Gratz, S.R., L.A. Ciolino, A.S. Mohrhaus, B.M. Gamble, J.M. Gracie, D.S. Jackson, J.P. Roetting, 2nd, H.A. McCauley, D.T. Heitkemper, F.L. Fricke, W.J. Krol, T.L. Arsenault, J.C. White, M.M. Flottmeyer, and Y.S. Johnson, *Screening and determination of polycyclic aromatic hydrocarbons in seafoods using QuEChERS-based extraction and high-performance liquid chromatography with fluorescence detection. Journal of AOAC International, 2011. 94(5):1601-16.*
 10. Lehotay, S.J., A. de Kok, M. Hiemstra, and P. van Bodegraven, *Validation of a fast and easy method for the determination of residues from 229 pesticides in fruits and vegetables using gas and liquid chromatography and mass spectrometric detection. Journal of AOAC International, 2005. 88(2):595-614.*
 11. Luzardo, O.P., N. Ruiz-Suarez, M. Almeida-Gonzalez, L.A. Henriquez-Hernandez, M. Zumbado, and L.D. Boada, *Multi-residue method for the determination of 57 persistent organic pollutants in human milk and colostrum using a QuEChERS-based extraction procedure. Analytical and Bioanalytical Chemistry, 2013. 405(29):9523-9536.*
 12. Liu, Y.J., H.Y. Chu, and Y.P. Zhao, *Silver nanorod array substrates fabricated by oblique angle deposition: morphological, optical, and sers characterizations. The Journal of Physical Chemistry C, 2010. 114(18):8176-8183.*

13. Fu, J.X., A. Collins, and Y.P. Zhao, *Optical properties and biosensor application of ultrathin silver films prepared by oblique angle deposition*. The Journal of Physical Chemistry C, 2008. **112**(43):16784-16791.
14. D. Driskell, J., S. Shanmukh, Y. Liu, S. B. Chaney, X.J. Tang, Y.P. Zhao, and R. A. Dluhy, *The use of aligned silver nanorod arrays prepared by oblique angle deposition as surface enhanced Raman scattering substrates*. The Journal of Physical Chemistry C, 2008. **112**(4):895.
15. Negri, P., N.E. Marotta, L.A. Bottomley, and R.A. Dluhy, *Removal of surface contamination and self-assembled monolayers (SAMs) from silver (Ag) nanorod substrates by plasma cleaning with argon*. Applied Spectroscopy, 2011. **65**(1):66-74.
16. Bresson, S., M.E. Marssi, and B. Khelifa, *Raman spectroscopy investigation of various saturated monoacid triglycerides*. Chemistry and Physics of Lipids, 2005. **134**(2):119-129.
17. Ljusberg-Wahren, H. and K. Larsson, *A Raman spectroscopy study of mixed bile salt-monoglyceride micelles*. Chemistry and Physics of Lipids, 1981. **28**(1):25-32.
18. Baeten, V., M. Meurens, M. Morales, and R. Aparicio, *Detection of virgin olive oil adulteration by Fourier transform Raman spectroscopy*. Journal of Agricultural and Food Chemistry, 1996. **44**(8):2225-2230.
19. López-Déz, E.C., G. Bianchi, and R. Goodacre, *Rapid quantitative assessment of the adulteration of virgin olive oils with hazelnut oils using Raman spectroscopy and chemometrics*. Journal of Agricultural and Food Chemistry, 2003. **51**(21):6145-6150.
20. Sherma, J. and B. Fried, *Handbook Of Thin-Layer Chromatography*. Vol. 89. 2003: CRC press.

Figures

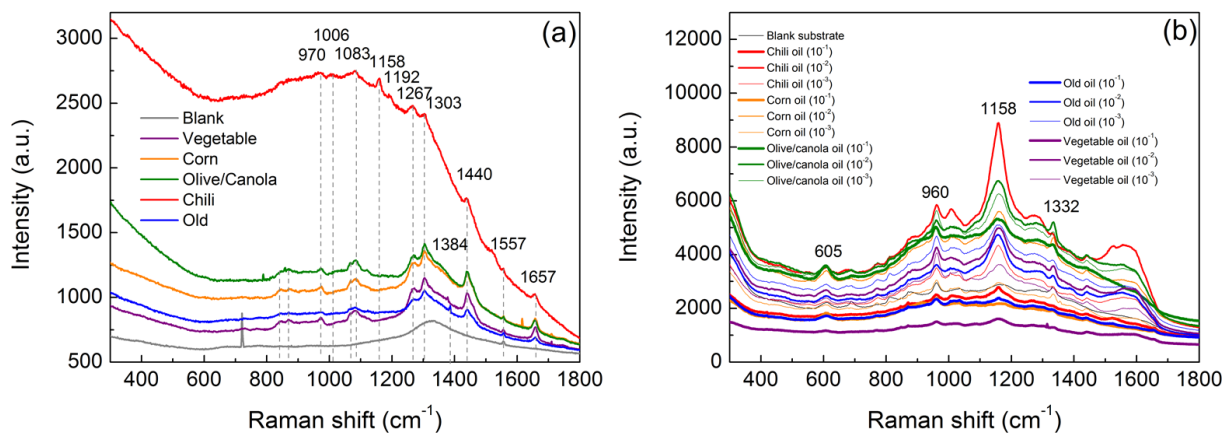


Figure 6.1 Averaged (a) Raman and (c) SERS spectra of edible oil products. The Raman spectra were collected at 150 mW for 30 s. SERS spectra were collected from 10⁻¹ to 10⁻³ dilution of oil at 60 mW for 10 s.

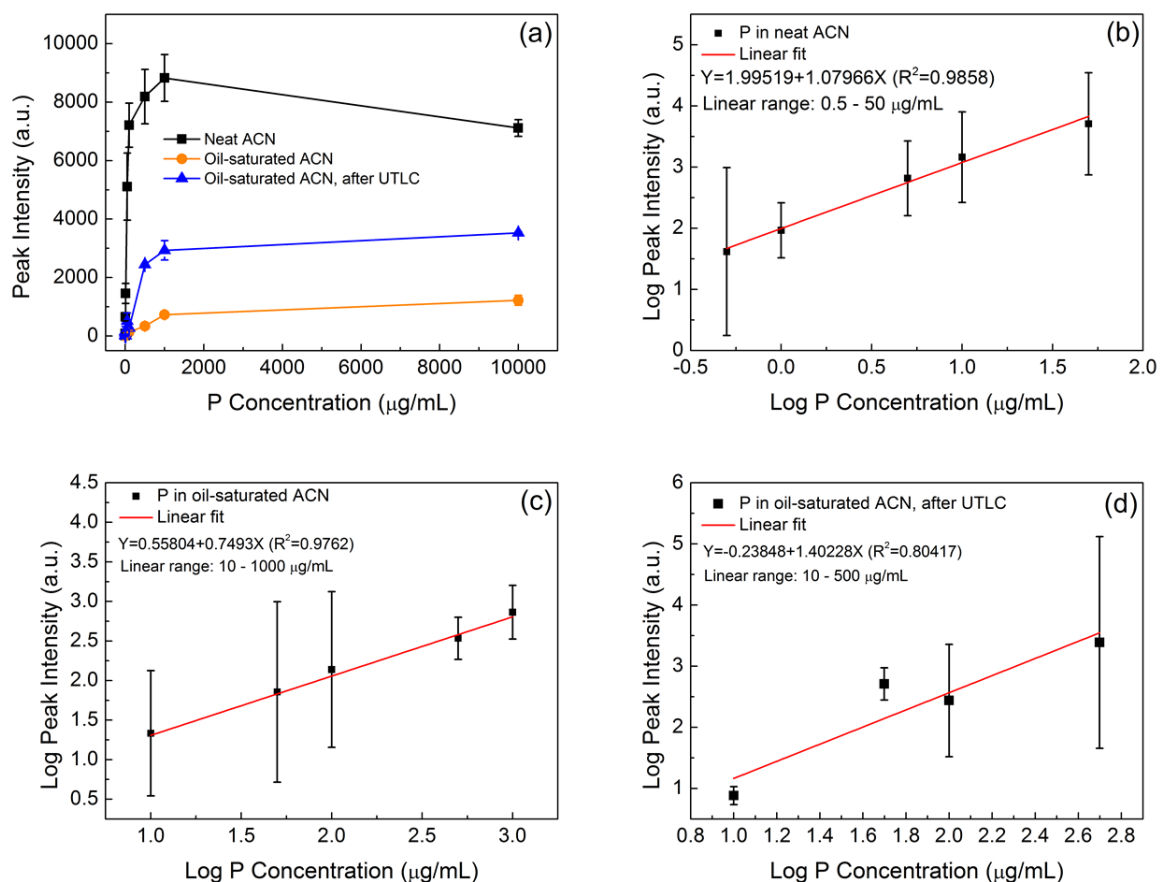


Figure 6.2 (a) SERS intensity of P dissolved in neat and oil-saturated acetonitrile (ACN) before and after UTLC in methanol (b)-(d) Correlation between the SERS peak intensity of P and actual P concentration in neat (b) and oil-saturated ACN before (c) and after (d) UTLC development in methanol.

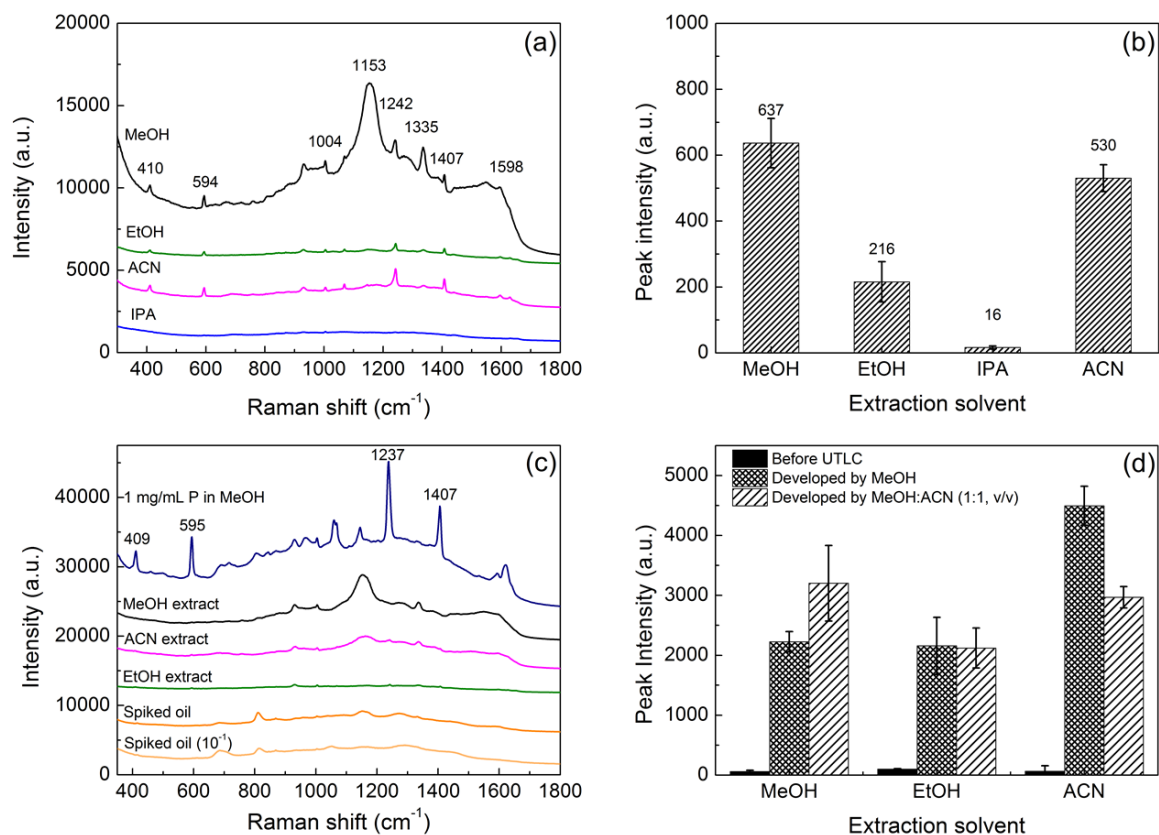


Figure 6.3 Effect of extraction solvents on the PAH extraction. (a) SERS spectra and (b) peak intensity at 594 cm⁻¹ of 10 mg/mL P in vegetable oil after extraction using methanol (MeOH), ethanol (EtOH), isopropanol (IPA), and acetonitrile (ACN) (c) SERS spectra and (d) peak intensity at 594 cm⁻¹ of 1 mg/mL P in vegetable oil using different solvents

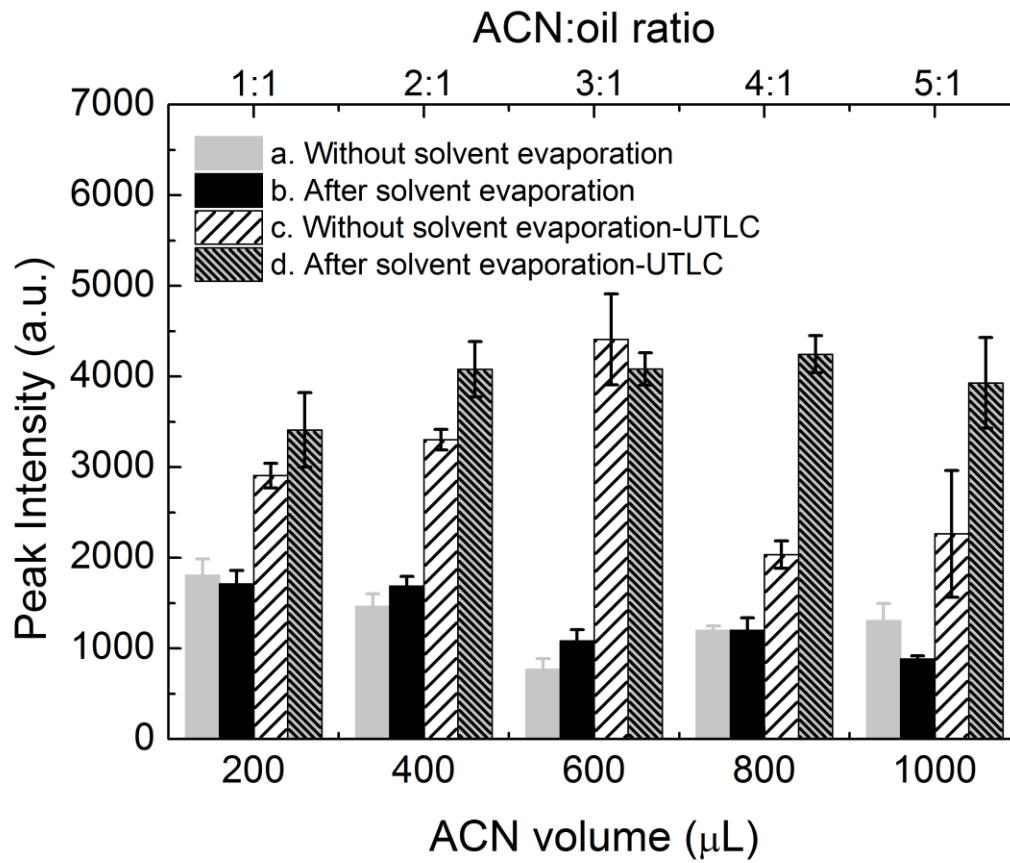


Figure 6.4 Effect of extraction solvent (ACN) volume and solvent evaporation on the SERS intensity of P

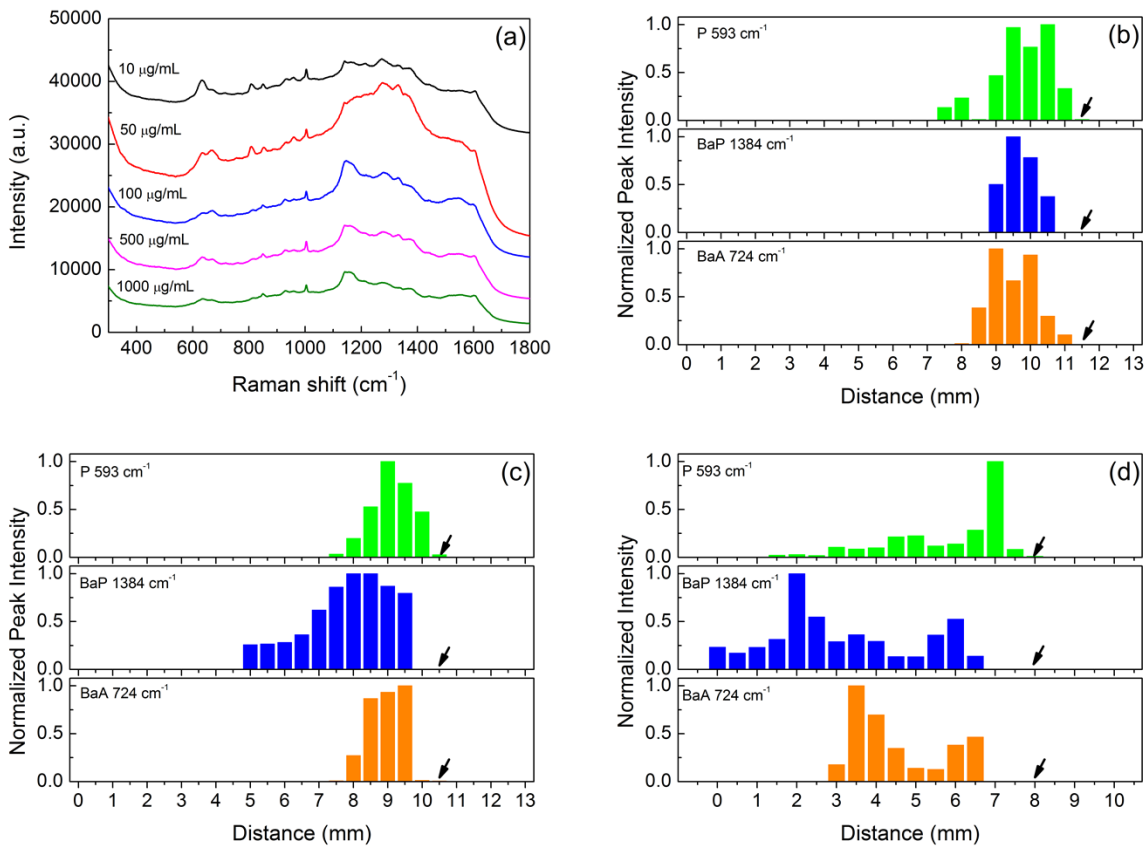


Figure 6.5 UTLC-SERS detection of PAHs using methanol: water (95:5, v/v) on 10 µM ME modified substrates. (a) SERS spectra of PAH extracts from vegetable oil before UTLC and UTLC separation of (b) 100 µg/mL (c) 500 µg/mL and (d) 1 mg/mL PAHs extracted from vegetable oil. Black arrows indicate the solvent front.

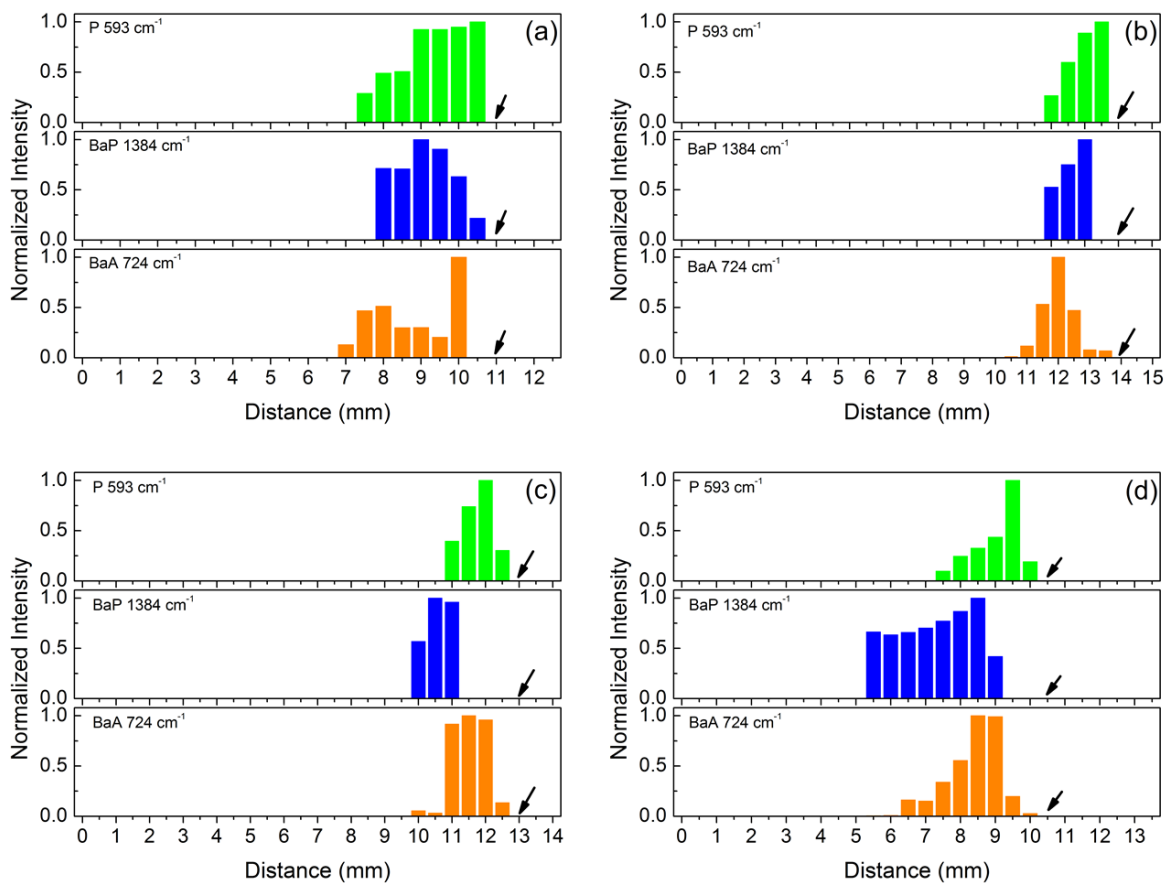


Figure 6.6 UTLC-SERS detection of PAH from oil extract using methanol: water 80:20 (v/v) on $10 \mu\text{M}$ ME modified substrates. (a) $50 \mu\text{g/mL}$ (b) $100 \mu\text{g/mL}$ (c) $500 \mu\text{g/mL}$ (d) 1 mg/mL . Black arrows indicate the solvent front.

CHAPTER 7

CONCLUSIONS AND FUTURE WORK

In this dissertation, a new analytical technique has been developed based on the principles of UTLC and SERS. This technique is based on the AgNR substrates fabricated by the oblique angle deposition process, which possesses nanoporous and SERS-enhancing properties essential for UTLC and SERS. The technique enables chromatographic separation directly on the sensing surface, and provides improved selectivity for SERS detection. A proof-of-principle study was carried out, in which a quaternary mixture consisting of dyes and Raman reporters were physically separated on the SERS-active AgNR substrate and detected individually after the 5-min UTLC process. Changing the mobile phase solvent led to different chromatographic retention among the tested analytes, which suggested that optimization of the chromatographic retention through mobile phases was feasible. Mixtures consisting of Rhodamine 6G and melamine at different concentration ratios demonstrated another advantage of the UTLC-SERS technique: target analytes which were present at low concentrations in complicated matrices could be liberated from the massive spectral background after chromatographic development, as the interfering matrix components were retained elsewhere on the SERS substrate.

The new UTLC-SERS technique was then applied to the detection of PAHs from edible oil samples. The Raman and SERS spectra of seven PAH compounds were first characterized and compared with the theoretical Raman spectra calculated by DFT. The spectra were consistent with minor discrepancies. DFT provided useful information on the vibrational modes

corresponding to the Raman or SERS peaks as well as insights on the Raman and SERS intensity. Three representative PAHs, BaA, BaP, and P, were selected as model compounds for the UTLC-SERS detection.

To overcome potential issues raised by the chemical reactivity of silver, surface of the AgNR substrates was modified with thiol compounds. Substrates were modified via self-assembling of thiol molecules on the SERS substrate either during soaking in dilutions or exposure to saturated thiol vapors, and the former approach were shown to be more suitable for detecting the selected PAHs. Modification with polar thiols rendered the AgNR substrates more hydrophilic, whereas nonpolar thiols increased the surface hydrophobicity. SERS intensity of testing targets on the modified substrates tended to decrease with increasing thiol concentration. However, the interference was negligible at low concentrations (100 nM - 10 μ M) on ME and MH modified substrates. On the contrary, PT and OCT modification at all concentrations could severely compromise the detection of PAHs. Hence 10 μ M ME modified substrates were selected for detection of PAHs in oils.

The mobile phase for PAH detection was selected from a panel of common organic lab solvents. These solvents exhibited different elution strengths in PAHs. Methanol proved to be the most promising base solvent due to its superior ability to wick the AgNRs (solvent front distance between 5 and 10 mm), in contrast to poor migration (< 5 mm) of other solvents. The elution strength of methanol could be adjusted using water at a percentage between 5% and 50%. The most effective mobile phase constitution was found to be methanol: water 95:5 (v/v), at which level the PAH bands appeared most resolved and narrow.

The SERS and Raman profiles of oil, as well as its interference to PAH detection was evaluated. The spectral interference from oil was most prominent in the 10^{-3} - 10^{-2} dilution,

which coincided with the concentration of oil residue in the PAH extract. The detection limits for BaA, BaP, and P in oil-saturated extraction solvent (acetonitrile) were determined to be 5 to 10 $\mu\text{g}/\text{mL}$. The extraction protocol of PAHs from vegetable oil was optimized. The UTLC retention of PAHs was affected by the presence of co-extracted oil residues. An adjusted ratio of methanol: water at 80:20 (v/v) was found to yield better UTLC outcome than methano: water 95:5 (v/v). The LODs after UTLC were found to be 50 $\mu\text{g}/\text{mL}$ for all three PAHs.

Apparently, neither of the chromatographic separation and detection limits is satisfactory comparing with the current HPLC or GC techniques. A major issue that hinders effective chromatographic separation is the poor solvent migration on the AgNR substrates, primarily because the thickness of the porous layer (2 μm) is too thin to provide adequate capillary action for sufficient solvent migration. Since the conventional UTLC plates utilize a 10-15 μm porous layer, it is also possible to improve solvent migration by increasing the nanorod length. However, the AgNRs are known to merge at the tips when their rod length exceeds 2-3 μm , which would hamper the SERS enhancement. Fortunately, it is also possible to incorporate an external driving force for solvent migration, such as a backpressure supplied by a liquid pump, or centrifugal force generated by rotating the substrate. Improved solvent migration can increase the number of separable components on the substrate, *e.g.*, the BaA, BaP, and P bands on the ME modified substrates might be completely separated over a longer developing distance. Moreover, solvent migration could also become more controllable using external forces, thereby resolving issues raised by uneven development.

Chemical modification of the AgNRs remains another strategy for improving chromatographic separation. However, due to its apparent negative impacts on SERS detection, the selection may be limited and the improvement may not be as significant as optimizing the

mobile phase solvents. In this dissertation, the mobile phase system is only crudely optimized due to the restriction of time and materials. In future research, more efficient mobile phase systems can be developed following rigid optimization strategies.

The LODs of PAHs in both neat organic solvents and in the oil extracts are clearly too high for practical applications. In the current gold standard for PAH detection, HPLC and GC, sample preparation plays an important role in concentrating the PAHs from the original 10-50 mL sample, whereas only 0.1 μL of the sample was used in the UTLC-SERS method without pre-concentration procedures. Increasing the depositing volume from 0.1 μL is not recommended, since the limited UTLC developing distance requires small sample spots and therefore low sample volumes to ensure meaningful separation. However, it is possible to utilize a larger portion of the extract and reduce into a smaller volume. In addition, the current extraction protocol still has relatively low extraction efficiency, and lacks a cleanup step after extraction. We have shown that the matrix effect can bring complications to the chromatographic development as well as deteriorating the detection sensitivity. Therefore, sample cleanup may be essential for establishing a more sensitive and reliable UTLC-SERS method for detecting PAHs from oil products.

APPENDIX A

ON-CHIP ULTRA-THIN LAYER CHROMATOGRAPHY AND SURFACE ENHANCED
RAMAN SPECTROSCOPY¹

Supplementary Information

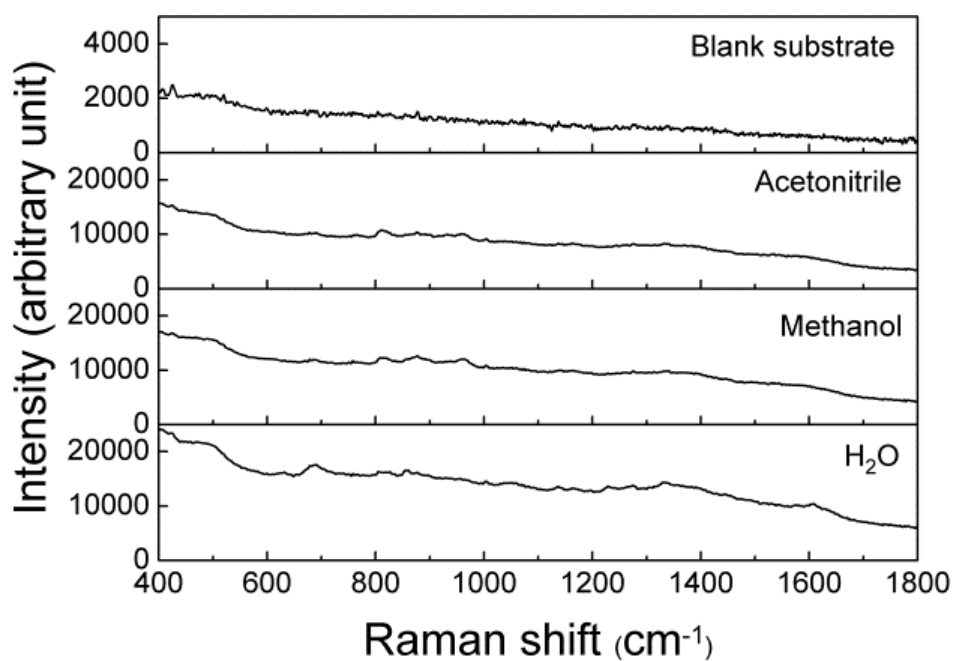


Figure A.1 SERS spectra of AgNR substrates pre-treated with mobile phase solvents

¹ Jing Chen, Justin Abell, Yao-wen Huang, and Yiping Zhao. 2012. *Lab on a Chip*. 12: 3096–3102 - Reproduced with permission of The Royal Society of Chemistry.

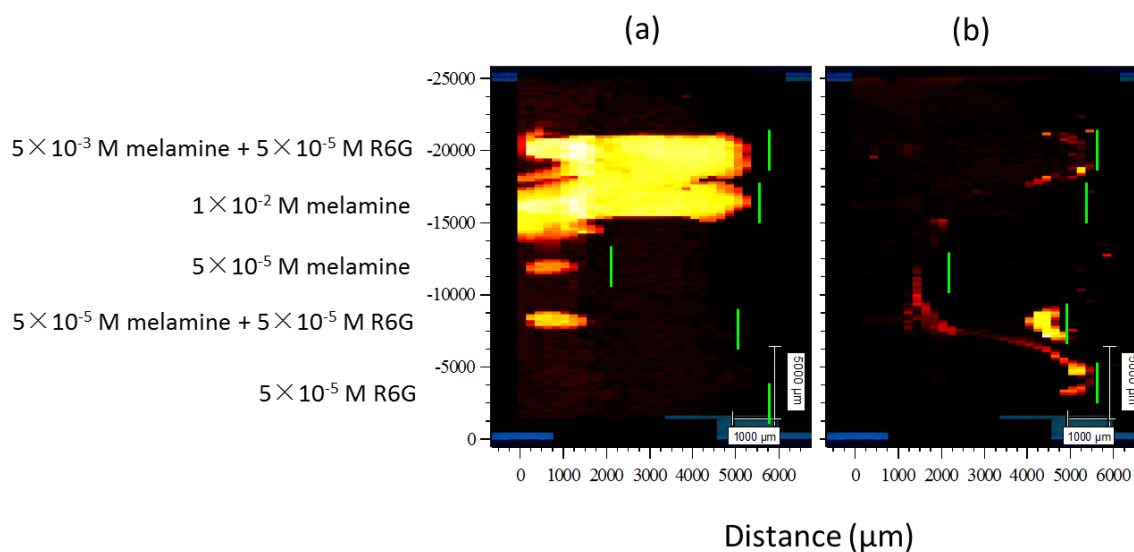


Figure A.2 Spatially-resolved SERS intensity map of (a) melamine (700 cm^{-1}) and (b) R6G (610 cm^{-1}). SERS spectra were acquired with a Renishaw inVia Raman Microscope with a step size of $200\text{ }\mu\text{m}$. The intensity of the melamine and R6G peaks are represented with a color scale in which black=zero intensity, red=low intensity, yellow=high intensity, and white=maximum intensity. Green lines represent the solvent front. In this case the solvent front is crooked due to uneven side edges of the substrate and disturbed solvent migration, causing the R6G molecules on the two side lanes to migrate towards the center lanes with the solvent front. At high concentrations, the melamine molecules tend to form a multilayer on the substrate, and the excess molecules are available for being carried by the mobile phase to the front. At a lower concentration, the melamine molecules are likely to form a single layer and remain near the sample origin.

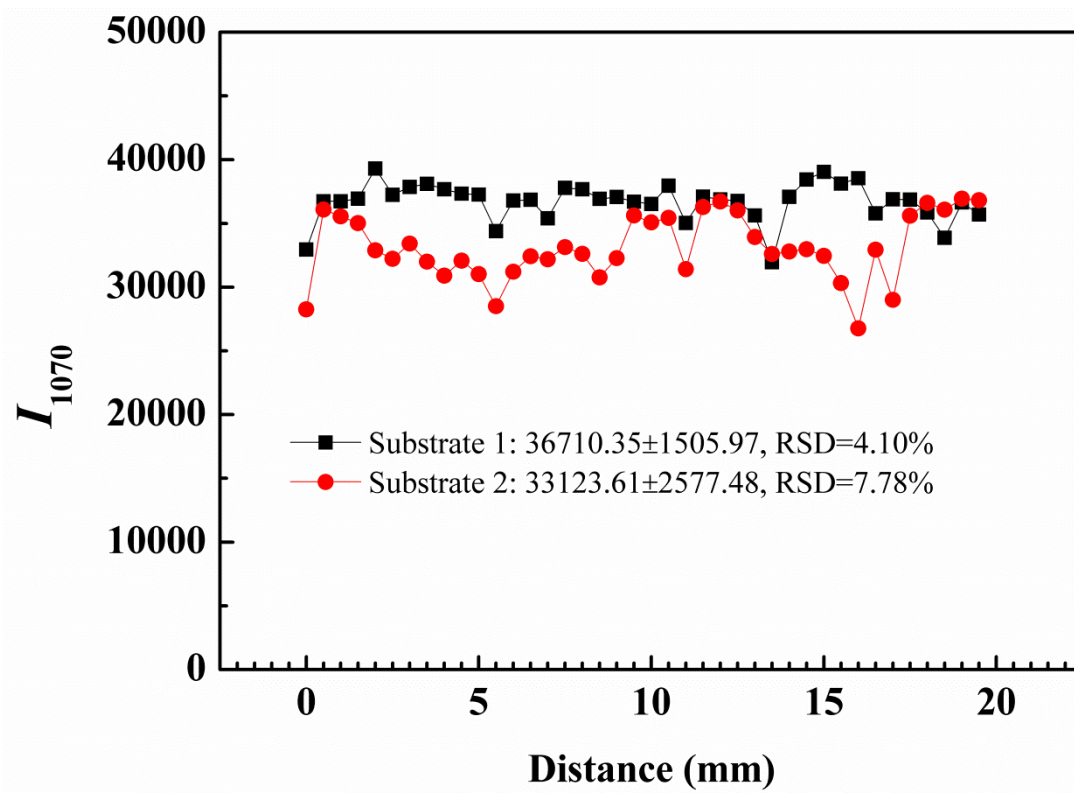


Figure A.3 Point-to-point fluctuation of the AgNR array substrates. Two 1 inch×1 inch substrates were soaked in 0.1 mM mercaptophenonol (MPh) for 30 min. The substrates were then gently rinsed with DI water to remove unadsorbed MPh molecules and dried with N₂. SERS spectra were collected along a straight line with a spatial interval of 0.5 mm from one edge of the substrates to the other. This is to simulate the process of spectra collection after the UTLC development. The spectra were then fitted to the 1070 cm⁻¹ peak of MPh, and the peak intensity I_{1070} is used to calculate the point-to-point relative standard deviations (RSDs) of the substrates. The results indicate that the AgNR arrays are highly reproducible SERS-active substrates with intra-substrate RSDs <8%.

APPENDIX B

CHARACTERIZATION OF POLYCYCLIC AROMATIC HYDROCARBONS USING
RAMAN AND SURFACE ENHANCED RAMAN SPECTROSCOPY²

Supplementary Information

Part I. DFT-calculated molecular structures of PAHs

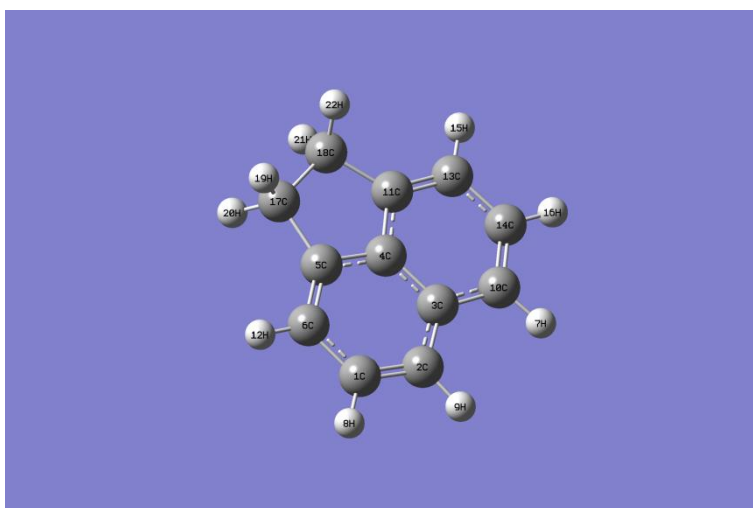


Figure B.1 DFT-calculated molecular structure of acenaphthene (ACP). Gray and silver spheres present carbon and hydrogen atoms, respectively.

² Jing Chen, Yao-wen Huang, and Yiping Zhao. To be submitted to *Journal of Raman Spectroscopy*.

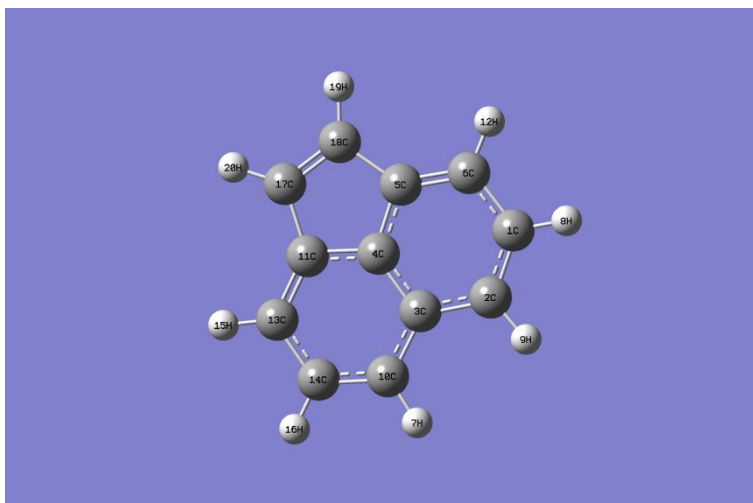


Figure B.2 DFT-calculated molecular structure of acenaphthylene (ACY). Gray and silver spheres present carbon and hydrogen atoms, respectively.

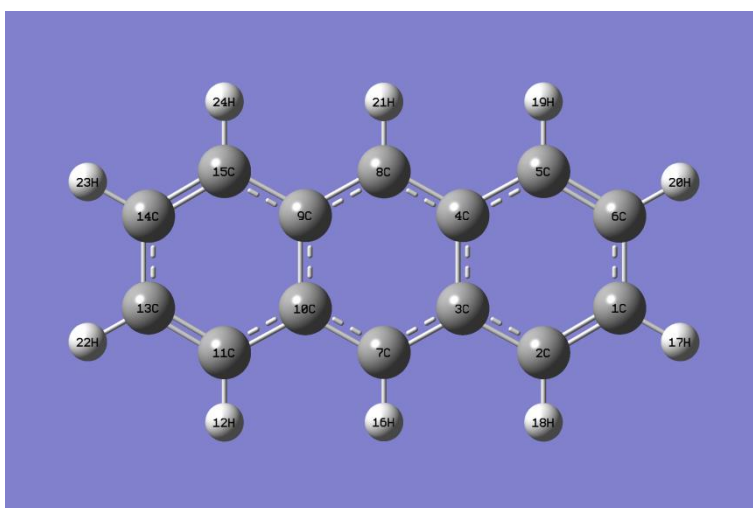


Figure B.3 DFT-calculated molecular structure of anthracene (ANT). Gray and silver spheres present carbon and hydrogen atoms, respectively.

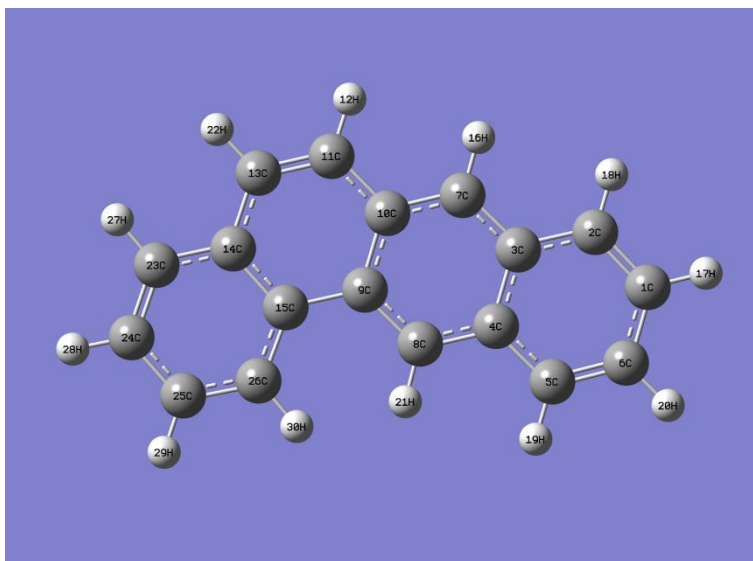


Figure B.4 DFT-calculated molecular structure of benz(a)anthracene (BaA). Gray and silver spheres present carbon and hydrogen atoms, respectively.

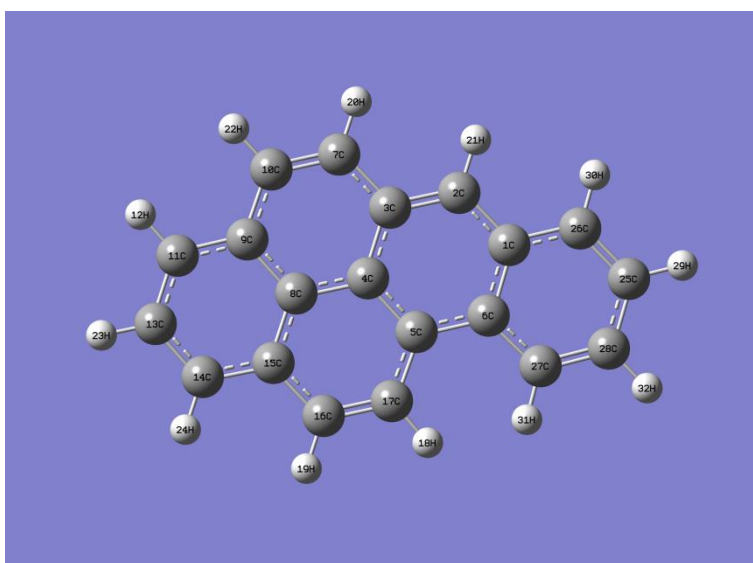


Figure B.5 DFT-calculated molecular structure of benzo(a)pyrene (BaP). Gray and silver spheres present carbon and hydrogen atoms, respectively.

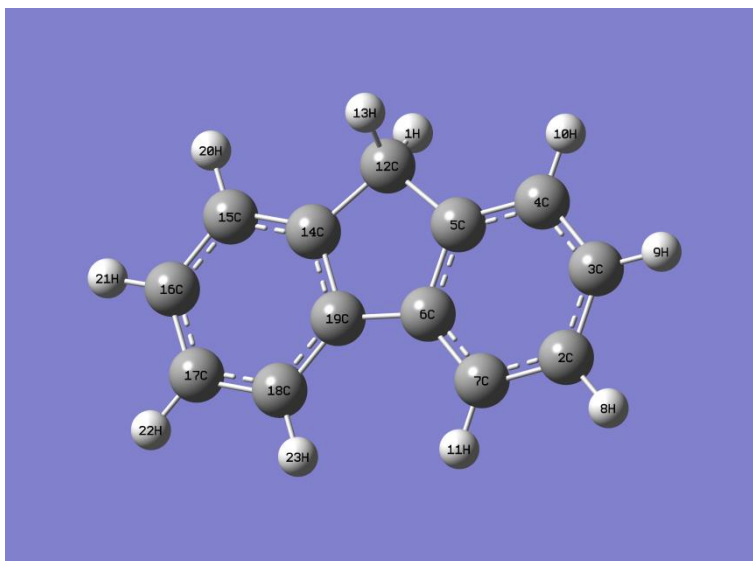


Figure B.6 DFT-calculated molecular structure of fluorene (F). Gray and silver spheres present carbon and hydrogen atoms, respectively.

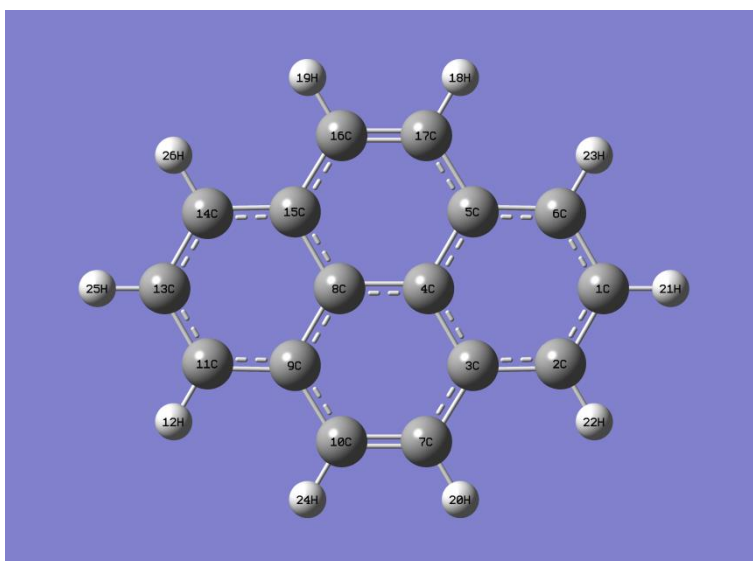


Figure B.7 DFT-calculated molecular structure of pyrene (P). Gray and silver spheres present carbon and hydrogen atoms, respectively.

Part II. Band assignments of PAH spectra

Table B.1 Band assignments for DFT-Raman, experimental Raman and SERS spectra of ACP

DFT-Raman	Experimental Raman	Experimental SERS	Vibrational Mode
--	397	--	--
--	415	414	--
429	--	--	C-H bending, C2-C3-C10 in-plane bending
458	--	--	C3-C4-C5-C11 in-plane bending, C-H bending
521	--	--	C2-C3-C10 in-plane bending, C10-C14-C13 bending, C6-C1-C2 bending
--	503	--	--
561	554	--	C-H bending, C11-C4-C5 in-plane bending
641	640	632	Ring breathing
--	803	--	--
828	844	842	C2-C1-C6-C5 in-plane bending, C10-C14-C13-C11 bending, C-H bending
--	866	--	--
1017	--	--	C-H bending, C-H wagging, C5-C17-C18-C11 asymmetric stretching
--	1040	--	--
1069	1150	--	C-H bending
1200	--	--	C-H twisting, C-H bending
--	1221	--	--
1265	1254	--	C-H wagging, C-H bending
1290	--	--	C-H bending, C-H wagging, C5-C17-C18-C11 asymmetric stretching
--	1366	--	--
1403	--	--	C3-C4 stretching, C-H bending, C-H wagging
--	1428	--	--
1461	1444	--	C5-C4-C11 symmetric stretching, C4-C3

			stretching, C-H bending
1475	--	--	C-H bending, C1-C2-C3 asymmetric stretching, C10-C14-C13 asymmetric stretching
1499	--	1490	C-H scissoring, C-H bending
1527	1533	--	C-H scissoring
--	--	--	--
--	1601	--	--
1634	--	--	C5-C4-C11-C3 asymmetric stretching, C-H bending, C3-C2-C10 bending, C1-C2 stretching, C10-C14 stretching,

Table B.2 Band assignments for DFT-Raman, experimental Raman and SERS spectra of ACY

DFT- Raman	Experimental SERS	Vibrational Mode
429	418-441	C-H bending, C2-C3-C10 bending
528	524	C3-C4 bending, C-H bending
571	558	C4-C11-C17 bending, C4-C5-C18 bending, C-H bending
665	--	Ring breathing
828	--	C-H bending, C11-C13-C14 bending, C5-C6-C1 bending
960	--	C-H bending
1032	1039	C-H bending, C5-C18 stretching, C11-C17 stretching,
1060	1070	C-H bending, C13-C14 stretching, C1-C6 stretching
1120	1137	C17-H bending, C18-H bending
1196	--	C1-H, C2-H, C10-H, C16-H bending
1238	1247	C6-H, C7-H, C13-H, C18-H bending
1288	1295	C2-H, C6-H, C10-H, C13-H bending
1390	--	C6-H, C13-H bending, C5-C4-C3-C11 symmetric stretching, C17- C18 stretching
1427	1428	C-H bending, C1-C2 stretching, C10-C14 stretching
1457	--	C2-H, C10-H bending, C5-C4-C3-C11 asymmetric stretching

1467	--	C1-H, C2-H, C10-H, C14-H bending
1494	1493	C6-H, C10-H bending, C5-C4-C11 asymmetric stretching
1528	--	C17-C18 stretching, C17-H, C18-H bending
1634	--	C5-C4-C11 bending, C5-C6, C13-C11 stretching, C6-H, C13-H bending
1647	--	C3-C4 stretching, C1-H, C2-H, C10-H, C14-H bending

Table B.3 Band assignments for DFT-Raman, experimental Raman and SERS spectra of ANT

DFT-Raman	Experimental SERS	Vibrational Mode
402	393	C-C in-plane bending, C-H bending
--	412	--
--	--	--
548	--	C7-H, C8-H bending
639	634	C-9-C15-C14 bending, C13-C11-C10 bending, C4-C5-C6 bending, C1-C2-C3 bending
757	751	C-H out-of-plane bending
--	809	--
--	843	--
863	868	C-H out-of-plane bending
882	891	C-H out-of-plane bending, ring twisting
1032	--	C13-C14, C1-C6 bending, C-H in-plane bending
1136	1138	C13-H, C14-H, C1-H, C7-H, C8-H, C6-H in-plane bending,
1236	1236	C11-H, C15-H, C7-H, C8-H, C2-H, C5-H in-plane bending
--	1256	--
1299	--	C3-C4-C8-C9-C10-C7 ring breathing; C2-H, C5-H, C11-H, C15-H in-plane bending
1348	1356	C-H bending, C10-C7-C3, C9-C8-C4 symmetric stretching
--	1406	--
1467	1479	--

1527	--	C1-C6, C13-C14 stretching, C-H bending
--	1556	--
1589	1599	C10-C9, C3-C4 stretching, C11-C13-C14-C15, C2-C1-C6-C5 asymmetric stretching, C-H bending
1621	--	C11-C13-C14-C15, C2-C1-C6-C5, C9-C8-C4, C10-C7-C3 asymmetric stretching, C7-H, C8-H bending

Table B.4 Band assignments for DFT-Raman, experimental Raman and SERS spectra of BaP

DFT-Raman	Experimental Raman	Experimental SERS	Vibrational Mode
341	--	332	Ring deformation, C-H in-plane bending
392	--	--	C-C in-plane bending
471	--	--	C-C in-plane bending, C-H in-plane bending
541	--	526	C-C in-plane bending, C-H bending
570	--	562	C-C out-of-plane bending, C-H out-of-plane bending
627	--	635	C-C in-plane bending, C-H in-plane bending
663	--	--	C26-C25-C28-C27 in-plane bending, C-H bending
--	846	852	--
872	868	--	C1-C6-C27 symmetric stretching, C-C in-plane bending, C-H bending
1002	1003	1001	C-H out-of-plane bending
--	1021	1023	--
1047	--	--	C28-C25-C26 symmetric stretching, C-C in-plane bending, C-H bending
1063	--	1063	C28-C25 stretching, C-C in plane bending, C11-H, C25-H, C26-H in-plane bending
1142	--	1147	C9-C10 stretching, C13-C14 stretching, C7, C16, C13, C14-H in-plane bending
1198	--	1196	Ring deformation, C2, C7, C26, C13, C14, C16-H in-plane bending

1239	1240	1237	C2, C-12, C17, C16, C25, C28-H in-plane bending
1259	--	1270	C14-C15 stretching, C14, C16, C27, C7, C2, C25, C11-H bending
1278	--	1286	C5-C27 stretching, ring deformation, C-H in-plane bending
1363	--	1344	Ring-deformation, C-H in-plane bending
1379	1387	1382	Ring deformation, in-plane C-C bending, C-H in- plane bending
1409	--	1407	Ring deformation, C-H in-plane bending
--	--	1428	--
1445	--	--	Ring deformation, C-H in-plane bending
1466	--	--	Ring deformation, C2, C14-H in-plane bending
--	--	1495	--
1513	--	--	C9-C10-C17 asymmetric stretching, C26-C1-C2 asymmetric stretching, C25, C26-H in-plane bending
1532	--	--	C13, C17-H in-plane bending, C-C in-plane bending
1556	--	--	C25-C28 stretching, C-H in-plane bending
1599	--	1600	Ring deformation, C-H in-plane bending
1615	--	1619	Ring deformation, C14-H in-plane bending
1636	--	--	Ring deformation, C11-H in-plane bending
1654	--	--	Ring deformation, C26, C27-H in-plane bending
1665	--	--	C7-C10 stretching, C7, C10-H in-plane bending

Table B.5 Band assignments for DFT-Raman, experimental Raman and SERS spectra of BaA

DFT- Raman	Experimental Raman	Experimental SERS	Vibrational Mode
310	310	305	C-C in-plane bending
--	--	335	--
363	358	--	C-C in-plane bending
406	399	395	C-C out-of-plane bending

437	419	418	C-C out-of-plane bending
486	--	488	C8, C7, C3, C4, C2, C5 out-of-plane bending
506	--	--	C-C in-plane bending
530	--	526	C-C out-of-plane bending
552	--	--	C-C in-plane bending
562	--	572	C-C out-of-plane bending
652	640	645	C1, C2, C3, C4, C5, C6 in-plane bending
675	--	--	C23, C26 in-plane bending, C-H bending
740	725	728	C9-C10 stretching, C7, C8 in-plane bending
--	795	792	--
807	--	809	C3, C4 stretching, C7, C8-H in-plane bending
837	846	843	C-H out-of-plane bending
874	860	856	C1, C2, C5, C6, C7, C8-H out-of-plane bending
898	--	891	C13, C11, C26, C8-H in-plane bending
998	--	982	C5, C6, C1, C2-H out-of-plane bending
1007	1003	1009	C23, C24, C25, C26, C11, C13-H out-of-plane bending
1035	1042	1040	C1, C2, C6, C5-H in-plane bending
1167	--	1163	C23, C24, C25, C26-H in-plane bending
1198	1202	1198	C7, C8, C1, C2, C5 in-plane bending
1213	1221	1216	C1, C5, C6, C23, C24, C25-H in-plane bending
1239	--	1240	C11, C5, C2 in-plane bending
1258	1265	1259	C13, C5-H in-plane bending
1277	--	--	C23, C26-H in-plane bending, C-C in-plane bending
1302	--	1299	C10-C11 stretching, C11, C2-H in-plane bending
1326	1320	1320	C7, C8-H in-plane bending
1354	1340	1341	Ring deformation, C13, C14-H in-plane bending
1380	1395	1391	C2, C8-H in-plane bending
1423	1430	1427	C1-C2-C3-C4-C5-C6 ring deformation, C8, C7-H in-plane bending
--	1442	1441	--

1461	--	1473	Ring deformation, C-H bending
1486	--	1495	C-C in-plane bending, C-H in-plane bending
1524	--	--	C1-C5 stretching, C-H in-plane bending
1552	1560	1560	C24-C25 stretching, C-H in-plane bending
1595	1607	1605	C24-C25, C14-C15, C9-C10, C3-C4, C1-C6 stretching
1628	--	1621	Ring deformation, C-H in-plane bending
1645	--	--	Ring deformation, C-H in-plane bending
1659	--	--	C11-C13 stretching, C-H in-plane bending
--	1777	--	Not found

Table B.6 Band assignments for DFT-Raman, experimental Raman and SERS spectra of F

DFT-Raman	Experimental Raman	Experimental SERS	Vibrational Mode
--	397	409	--
423	415	423	In-plane C-C bending
447	--	443	C-C out-of plane bending, C-H twisting, C-H out-of-plane bending
565	542	565	C-C in-plane bending
652	638	634	C-C in-plane bending, C-H in-plane bending
--	--	688	--
747	740	729	C-H out-of-plane bending, C-H twisting
762	--	753	C-C in-plane bending, C-H in-plane bending
767	783	773	C-H out-of plane bending, C-H wagging
806	--	806	C-H out-of plane bending, C-H wagging
834	844	841	C14-C12-C5 asymmetric stretching, C-C in-plane bending
866	868	866	C14-C12-C5 in-plane bending
896	--	890	C-H out-of-plane bending, C-H twisting
--	--	924	--

1021	1019	1015	C-C in-plane bending
1045	--	1054	C15, C18, C7, C4 in-plane bending
--	1091	1108	--
1127	1144	--	C-H in-plane bending
1187	1191	1198	C12-H13-H1 twisting
1204	1211	1210	C17, C2-H in-plane bending
1237	1234	1223	C12-H13-H1 wagging
1259	--	--	C4, C15-H in-plane bending
--	1292	1294	--
--	1324	--	--
1340	1342	1353	C6-C19 stretching, C7, C8-H in-plane bending
1387	1384	1374	Ring deformation, C-H in-plane bending
1410	1401	--	--
--	1448	1443	--
1481	1479	1477	C12-H13-H1 scissoring
1494	--	--	C12-H13-H1 scissoring
1518	--	--	C12-H13-H1 scissoring, C-H in-plane bending
1548	--	1545	--
1582	1575	--	--
1618	1610	1600	C2-C3 stretching, C-H in-plane bending
1646	--	1661	C4, C7, C15, C18-H in-plane bending
1680	--	--	--
1699	--	1709	--

Table B.7 Band assignments for the DFT-Raman, experimental Raman and SERS spectra of P

DFT-Raman	Experimental Raman	Experimental SERS	Vibrational Mode
365	362	351	C-H in-plane bending, C-C in-plane bending
418	408	409	C13, C1-H in-plane bending
468	456	456	C-C in-plane bending, C-H in-plane bending

507	503	503	C-H out-of-plane bending, C-C out-of-plane bending
594	593	593	Ring breathing
717	720	715	C-H out-of-plane bending, C-C out-of-plane bending
762	--	755	C-H in-plane bending, C-C in-plane bending
815	805	804	C11, C13, C1, C6-H out-of-plane bending
845	844	843	C10, C7, C16, C17-H out-of plane bending
871	866	863	C-H out-of-plane bending
927	924	928	C11, C14, C2, C6-H out-of-plane bending
1008	1002	1004	C1, C13-H out-of-plane bending
1074	1064	1058	--
1092	--	--	C11, C14, C2, C6-H in-plane bending
1140	1142	1145	C-H in-plane bending, C-C in-plane bending
1240	1242	1238	C11, C13, C14, C2, C1, C6-H in-plane bending
1275	--	--	C-C in-plane bending, C-H in-plane bending
--	--	1336	--
1361	--	1372	C-C in-plane bending, C-H in-plane bending
1409	1407	1406	C-C in-plane bending, C-H in-plane bending
1432	--	--	C4-C8 stretching, C-H in-plane bending
1457	--	--	C7, C10, C16, C17-H in-plane bending
1542	1548	1535	C1, C13-H in-plane bending
1596	1595	1591	C11, C14, C2, C6-H in-plane bending
1632	1626	1618	C14, C11, C2, C6-H in-plane bending
--	1642	--	--
1666	--	--	C16-C17, C4-C8, C7-C10 stretching, C-H in-plane bending

Part III. SERS limits of detection (LODs) for PAHs

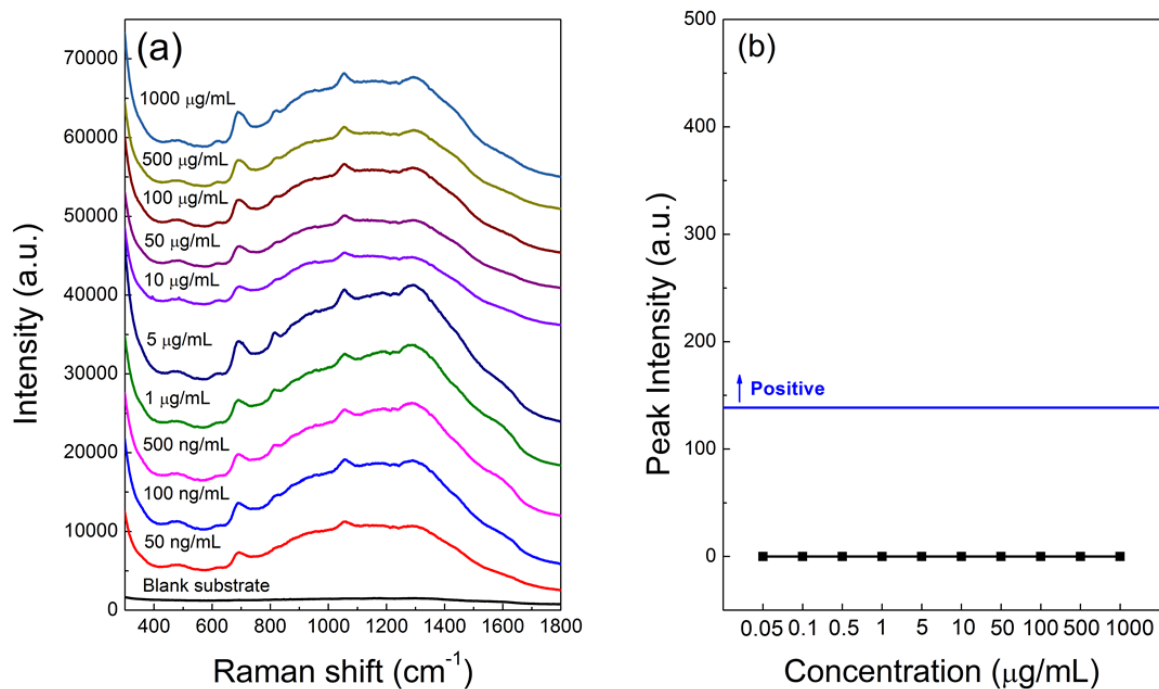


Figure B.8 (a) SERS spectra of ACP at different concentrations in methanol (b) Corresponding intensities at specific peaks. SERS spectra were acquired at 60 mW, 10s. The spectra were vertically offset for clarity.

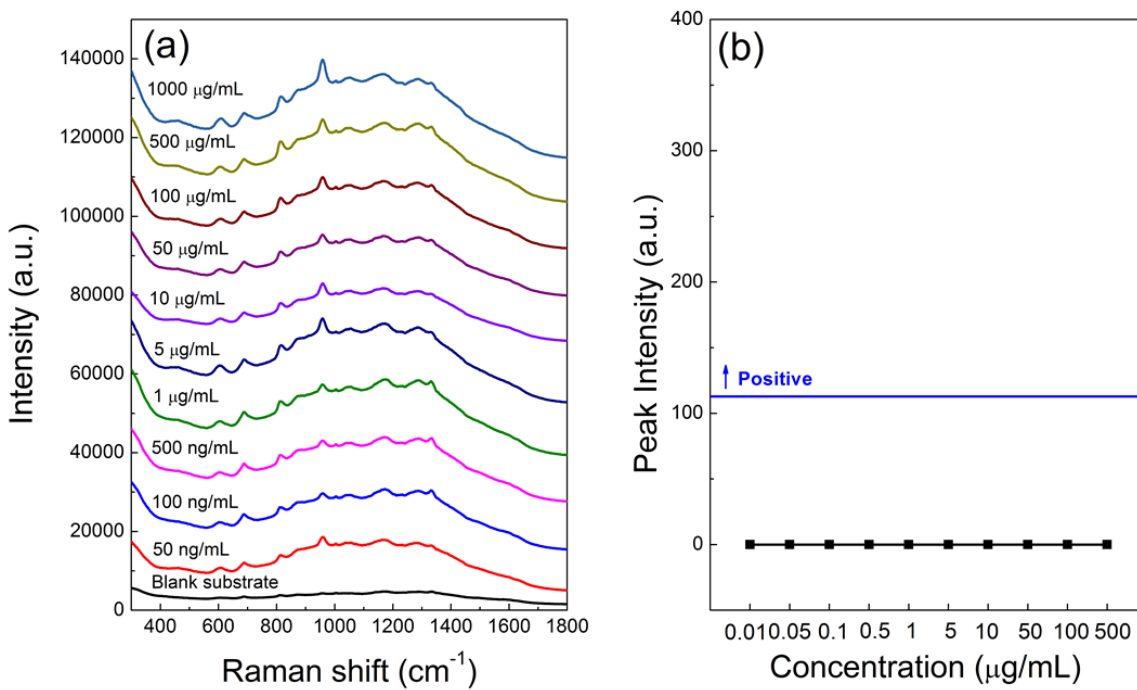


Figure B.9 (a) SERS spectra of ACY at different concentrations in methanol (b) Corresponding intensities at specific peaks. SERS spectra were acquired at 60 mW, 10s. The spectra were vertically offset for clarity.

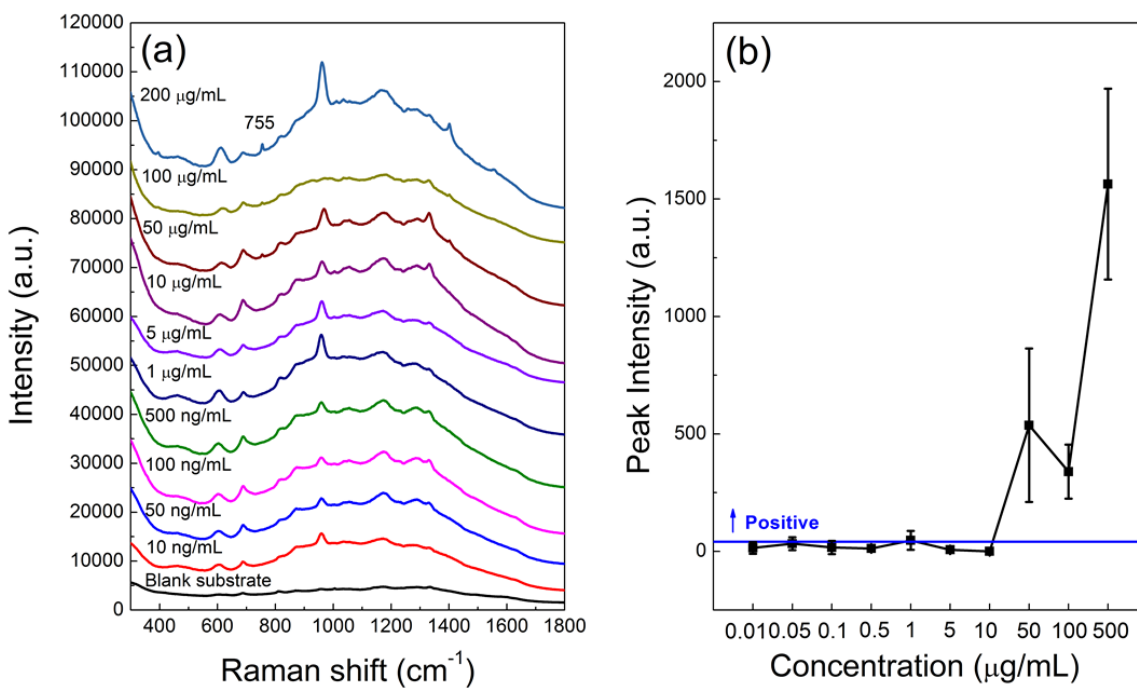


Figure B.10 (a) SERS spectra of ANT at different concentrations in methanol (b) Corresponding peak intensities at 755 cm^{-1} . SERS spectra were acquired at 60 mW, 10s. The spectra were vertically offset for clarity.

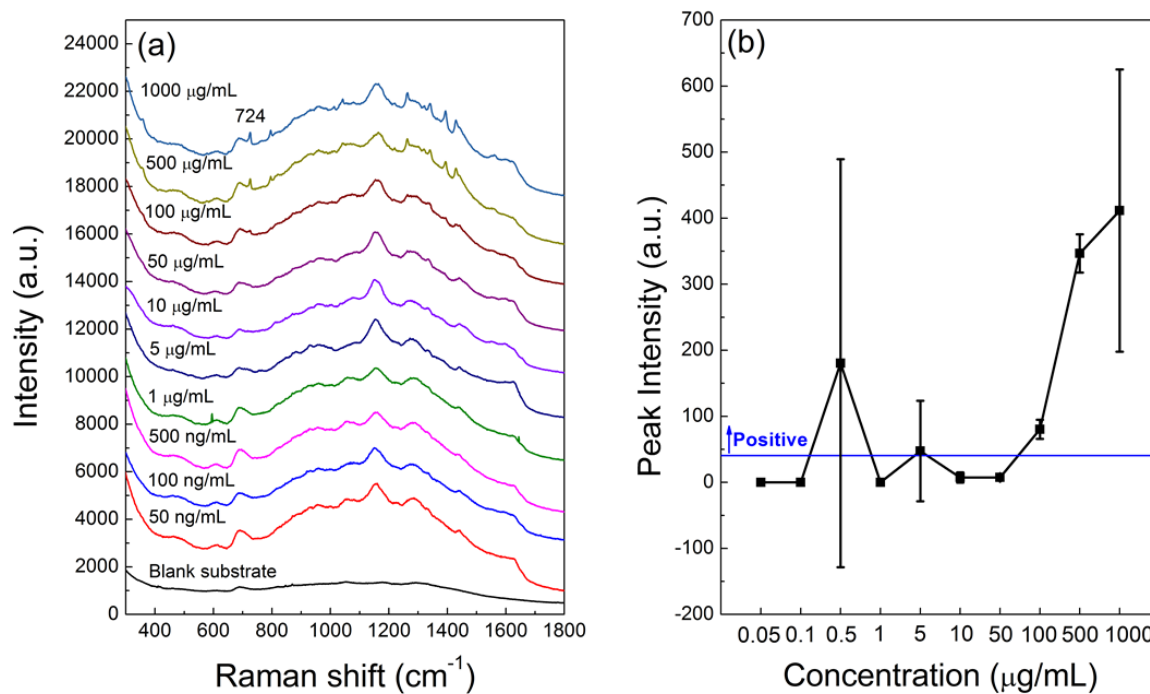


Figure B.11 (a) SERS spectra of BaA at different concentrations in methanol (b) Corresponding peak intensities at 724 cm^{-1} . SERS spectra were acquired at 60 mW, 10s. The spectra were vertically offset for clarity.

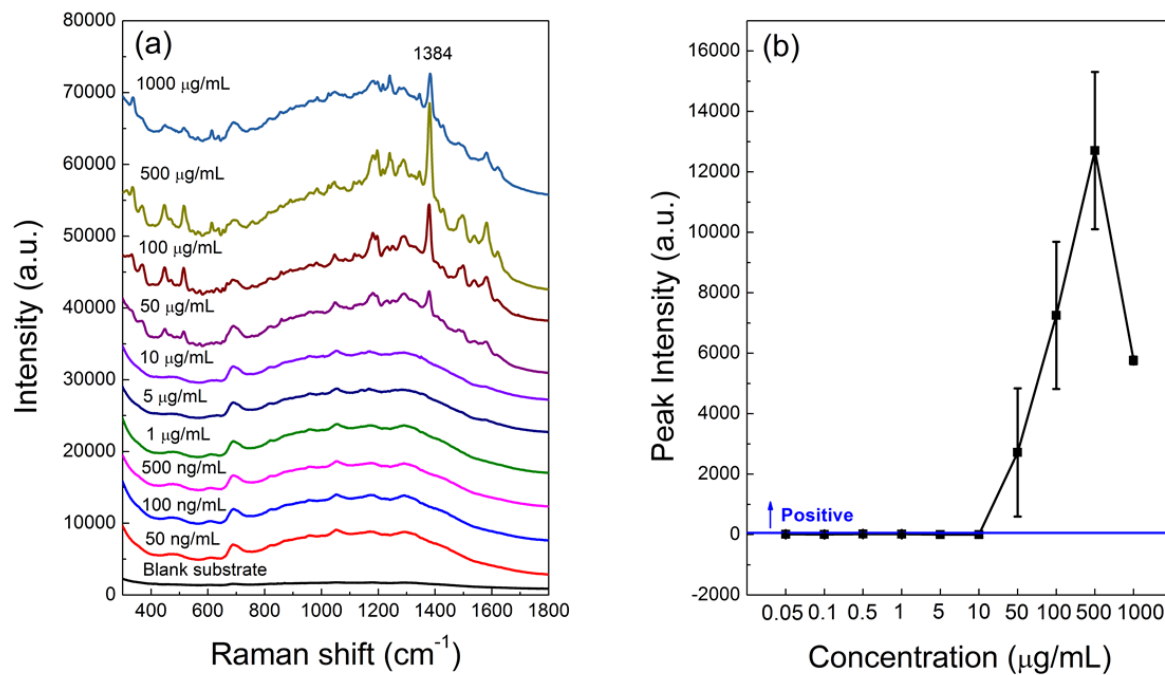


Figure B.12 (a) SERS spectra of BaP at different concentrations in methanol (b) Corresponding peak intensities at 1384 cm^{-1} . SERS spectra were acquired at 60 mW, 10s. The spectra were vertically offset for clarity.

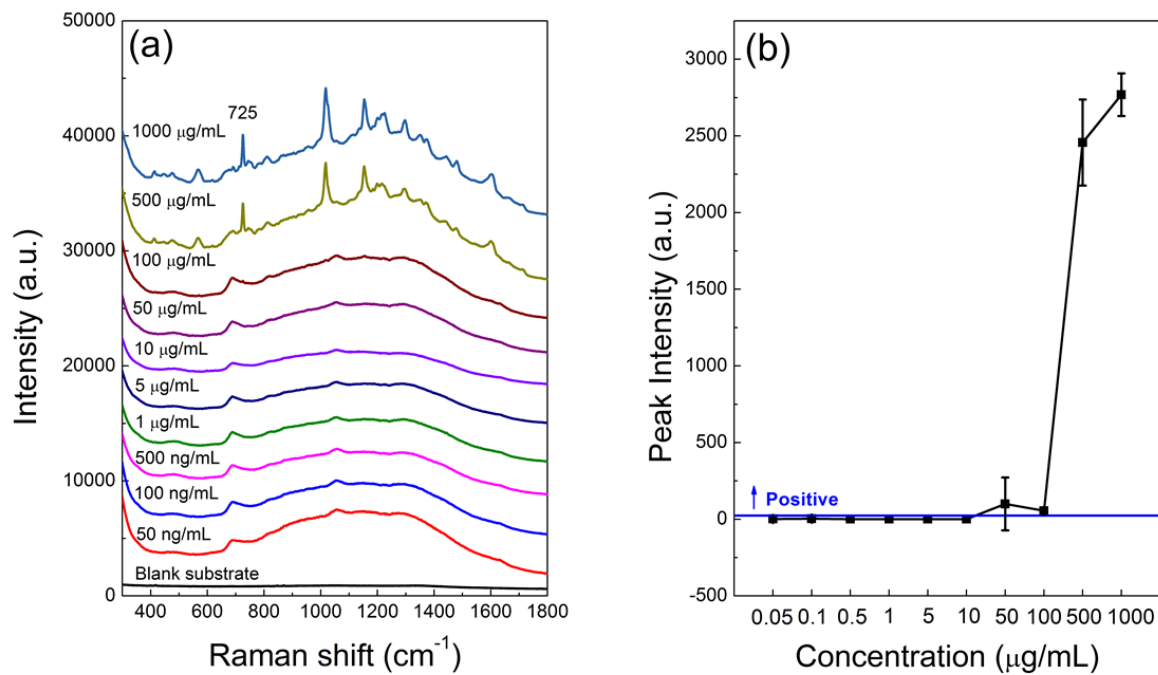


Figure B.13 (a) SERS spectra of F at different concentrations in methanol (b) Corresponding peak intensities at 725 cm^{-1} . SERS spectra were acquired at 60 mW, 10s. The spectra were vertically offset for clarity.

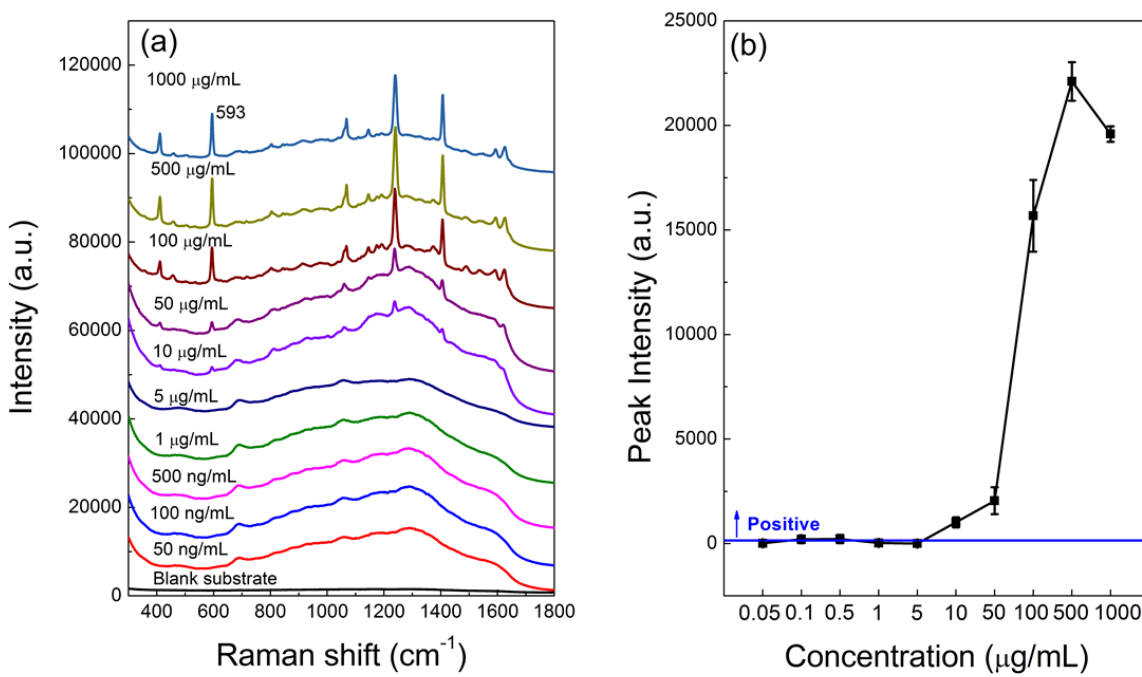


Figure B.14 (a) SERS spectra of P at different concentrations in methanol (b) Corresponding peak intensities at 593 cm^{-1} . SERS spectra were acquired at 60 mW, 10s. The spectra were vertically offset for clarity.

APPENDIX C
TOWARDS ULTRA-THIN LAYER CHROMATOGRAPHY AND SURFACE ENHANCED
RAMAN SPECTROSCOPY DETECTION OF POLYCYCLIC AROMATIC
HYDROCARBONS³

Supplementary Information

Part I. SERS spectra of PAHs on thiol modified AgNR substrates

In order to evaluate the potential influence of thiol modification on the SERS detection of target PAHs, the intensity of three model PAHs, BaA, BaP, and P, was compared on the thiol modified substrates. 0.1 μL of the PAH solutions at 200 $\mu\text{g}/\text{mL}$ were applied to the modified AgNR substrates, and the solvent was allowed to evaporate before SERS spectra were acquired at 60 mW for 10 s. The SERS spectra of PAHs on mercaptoethanol (ME), mercaptohexanol (MH), propanethiol (PT), and octanethiol (OCT) modified substrates are shown in Figures C.1-C.4, respectively. The dashed curves indicate SERS spectra of PAHs acquired on unmodified AgNR substrates.

³ Jing Chen, Yao-wen Huang, and Yiping Zhao. To be submitted to *Sensors and Actuators B*.

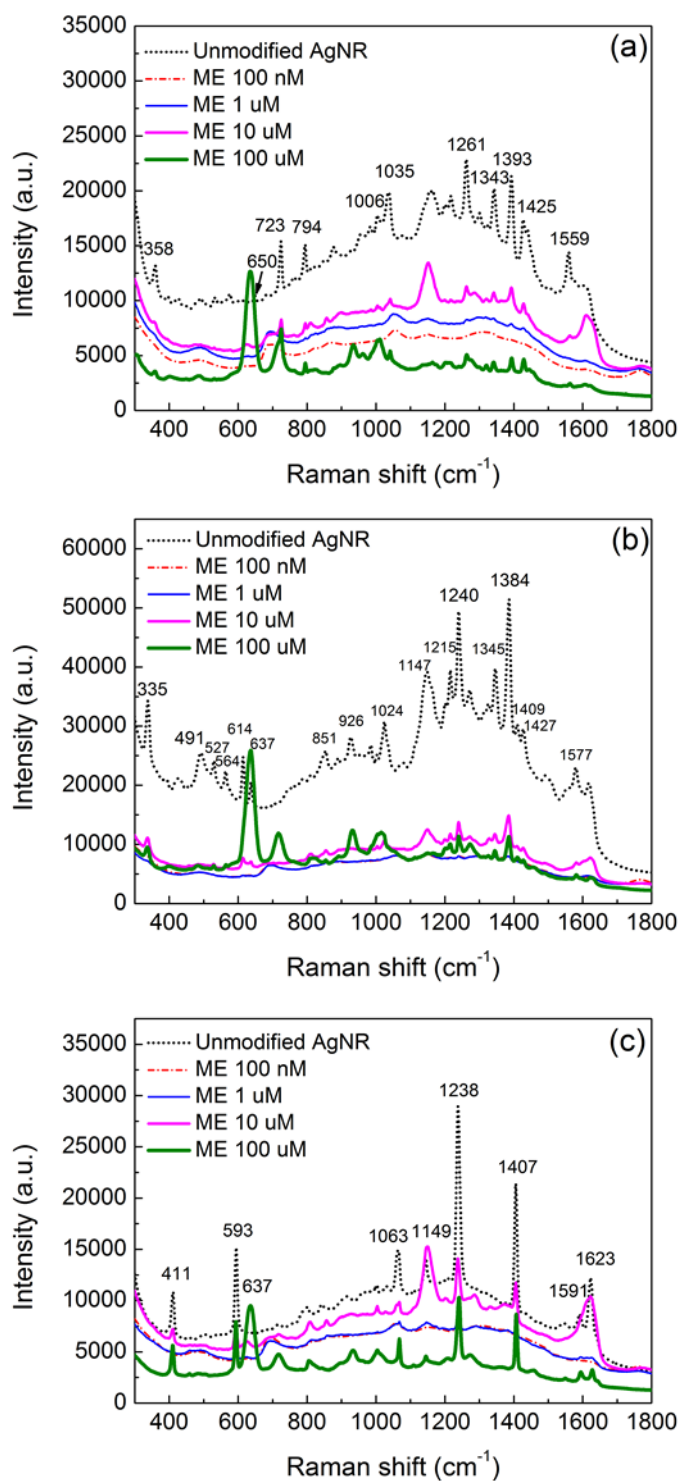


Figure C. 1 SERS spectra of (a) BaA, (b) BaP, and (c) P on difference concentrations of ME modified substrates

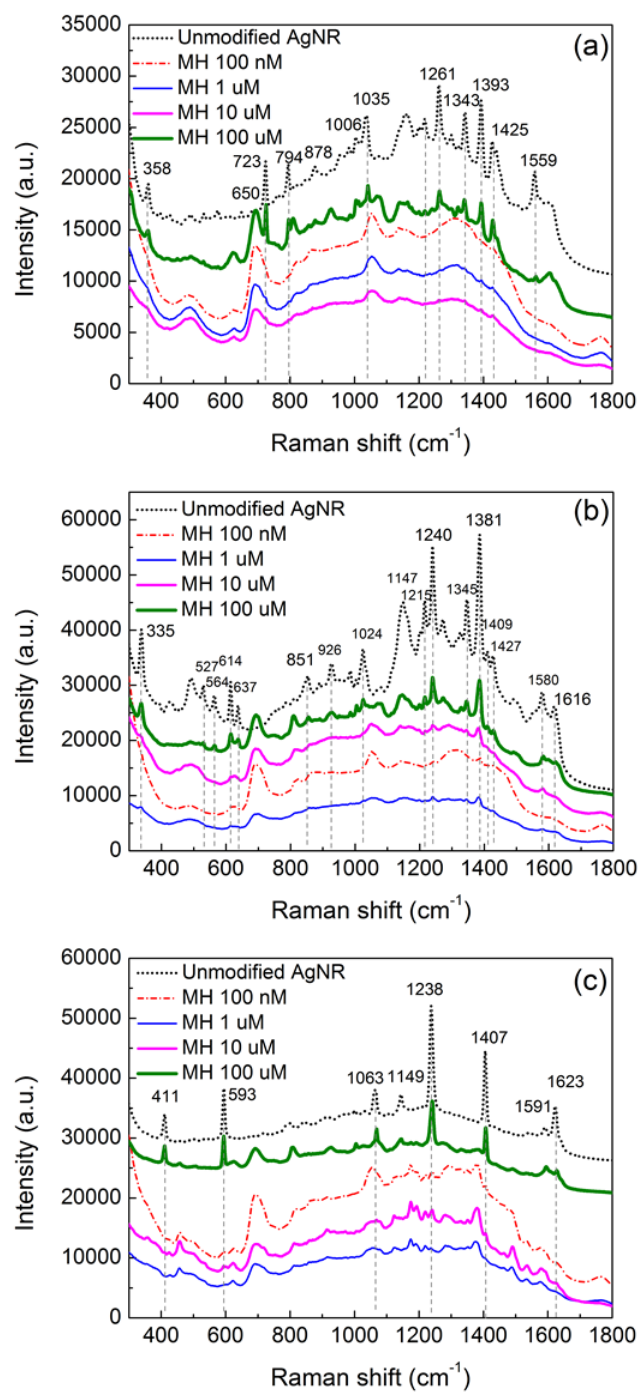


Figure C.2 SERS spectra of (a) BaA, (b) BaP, and (c) P on difference concentrations of MH modified substrates

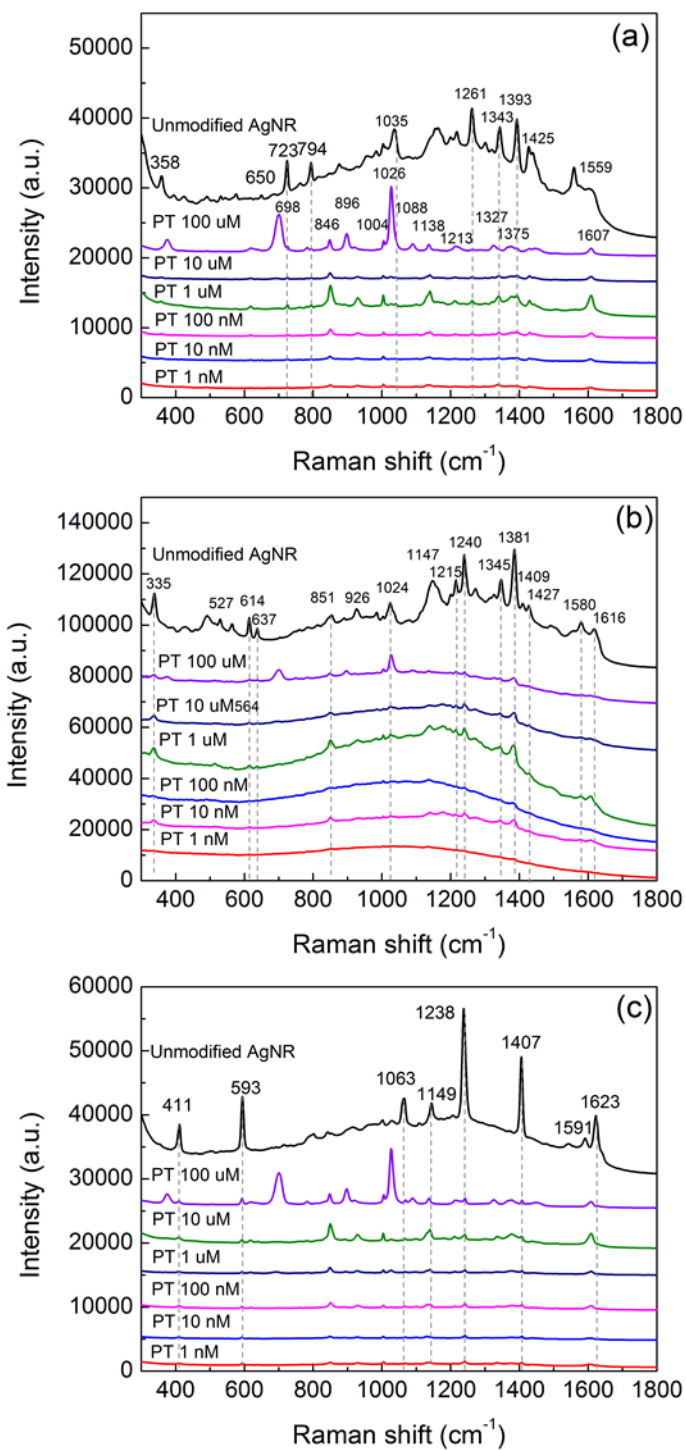


Figure C.3 SERS spectra of (a) BaA, (b) BaP, and (c) P on difference concentrations of PT modified substrates

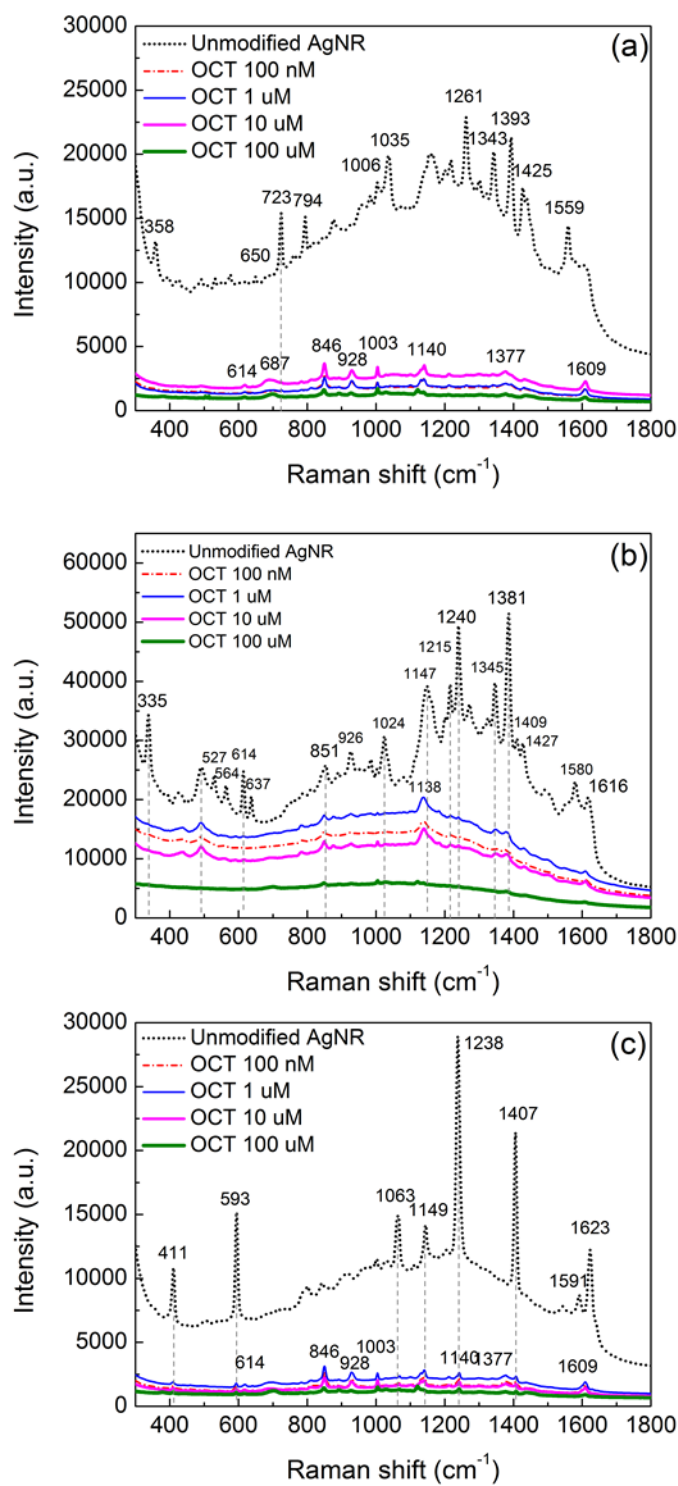


Figure C.4 SERS spectra of (a) BaA, (b) BaP, and (c) P on difference concentrations of OCT modified substrates

Part II. Mobile phase solvent selection

To screen for appropriate solvents, 0.5 μL of common lab solvents, including methanol, acetonitrile, hexane, dichloromethane, chloroform, toluene, acetone, isopropanol, and 18 M Ω ultra-pure water were added to the AgNR substrates, and the diameter of the solvent spots was recorded. In a second experiment, the AgNR substrates were placed into a 35 mL beaker containing ~ 3 mL of various organic solvents, and allowed to stand for 5 min at a $\sim 70^\circ$ tilting angle from the bottom of the beaker. The substrates were then removed from the beaker and the solvent migration distance was immediately marked on the substrate. After solvent evaporation, SERS spectra were collected from areas on the substrate which had been soaked in the solvent. According to the results shown in Table C.1, ultra-pure water demonstrated very different properties from the organic solvents, with the smallest spreading diameter (2.0 ± 0.4) and the shortest migration distance (0.9 ± 0.2 mm). In addition, the drying process of water typically required more than 30 s. In contrast, the organic solvents resulted in relatively large spots (2.7 - 5.8 mm in diameter), with the exception of dichloromethane, whose spot size was roughly the same as water. Dichloromethane was noted for its tendency to evaporate, with a remarkably high vapor pressure of 53.3 kPa at 20 $^\circ\text{C}$. Despite its low surface tension, the quick evaporation process self-limited its spot size.

In general, organic solvents migrated to longer distances than water (2.3 - 5.8 mm on average). However, there was not a direct correlation between a solvent's spot spreading diameter and its migration distance on the AgNRs. For instance, acetonitrile had the largest spot among all solvents when dropped onto the AgNR substrate, but its migration distance was only ~ 3.5 mm above the meniscus. In comparison, methanol had an average spot size of 4.2 mm, but its migration distance was considerably longer than any other solvent (5.8 ± 1.5). This implies that

solvents that create large spots on the substrate do not necessarily lead to good migration. Hence only the solvents with acceptable migration distances should be included in the mobile phase panel. On the other hand, the drying speed is mainly determined by the solvent's vapor pressure and surface tension. For example, toluene has a low vapor pressure which is equivalent to water (~ 3 kPa at 20 °C); hence it dried more slowly than most of other organic solvents (whose vapor pressures are between 15-50 kPa). However, the high surface tension of toluene (28.52 mN/m at 20 °C) makes it easier for this solvent to spread into a large area and dry faster than water.

Table C.1 Spreading area, migration distance, and drying speed of solvents on the AgNRs

Solvent	Spreading diameter (mm)	Migration distance (mm)	Drying speed
18 M Ω water	2.0 \pm 0.4	0.9 \pm 0.2	Slow
Methanol	4.2 \pm 0.3	5.8 \pm 1.5	Fast
Toluene	4.2 \pm 0.4	2.9 \pm 0.4	Less fast
Hexanes	3.2 \pm 0.3	2.6 \pm 0.4	Very fast
Acetonitrile	5.8 \pm 0.3	3.5 \pm 1.0	Fast
IPA	3.5 \pm 0.2	3.5 \pm 0.5	Fast
Dichloromethane	1.0 \pm 0.2	2.6 \pm 0.6	Very fast
Chloroform	2.7 \pm 0.2	2.3 \pm 0.4	Fast
Acetone	3.1 \pm 0.3	2.7 \pm 0.3	Fast

The SERS spectra of the AgNR surface after solvent evaporation are shown in Figure C.5. Few peaks have been identified except those typical of surface contaminant residues at 493, 690, 810, and 963 cm^{-1} , *etc.* Among the tested solvents, water (black curve in Fig. C.5) demonstrated the highest signal intensity due to its greatest surface tension, which pulled together nanorods upon evaporation and introduced SERS hot spots. Conversely, the spectrum of hexanes (pink curve in Fig. C.5) appeared to have low signal intensity, owing to its lack of surface tension to bundle the AgNRs. Other organic solvents with intermediate surface tension caused some degree of nanorod bundling, thus the resultant SERS signal intensity fell between that of hexanes and water. As an exception, the spectrum of toluene showed a striking similarity with the blank substrate, with extremely low intensity and a low signal to noise ratio. Upon examining the surface tension of toluene, it is evident that the low SERS intensity could not have been attributed to the same mechanism which causes low intensity in hexanes-treated substrate, as the surface tension of toluene is only smaller than water among all the tested solvents. When a Raman reporter molecule, BPE (dissolved in methanol) was added to toluene treated substrates, no peaks of BPE could be identified from the SERS spectra (data not shown). Literature on SERS spectrum of toluene indicates that a 3% toluene vapor in nitrogen could lead to adsorption of this benzene derivative onto SERS-active substrates that was sufficient for SERS detection [1]. When the AgNR substrate was exposed to a much higher concentration of toluene, its surface was likely to be saturated by the adsorbed molecules. At this point, it is not surprising that signal quenching of its own as well as that of BPE would occur. Failure to evaporate completely from the substrate surface thus excluded toluene from the UTLC mobile phase solvent list.

Based on the results on the solvents' ability to wet the AgNR substrates as well as their potential interference to SERS detection, four representative solvents, methanol, acetonitrile, dichloromethane, and hexane were selected for UTLC of the PAHs.

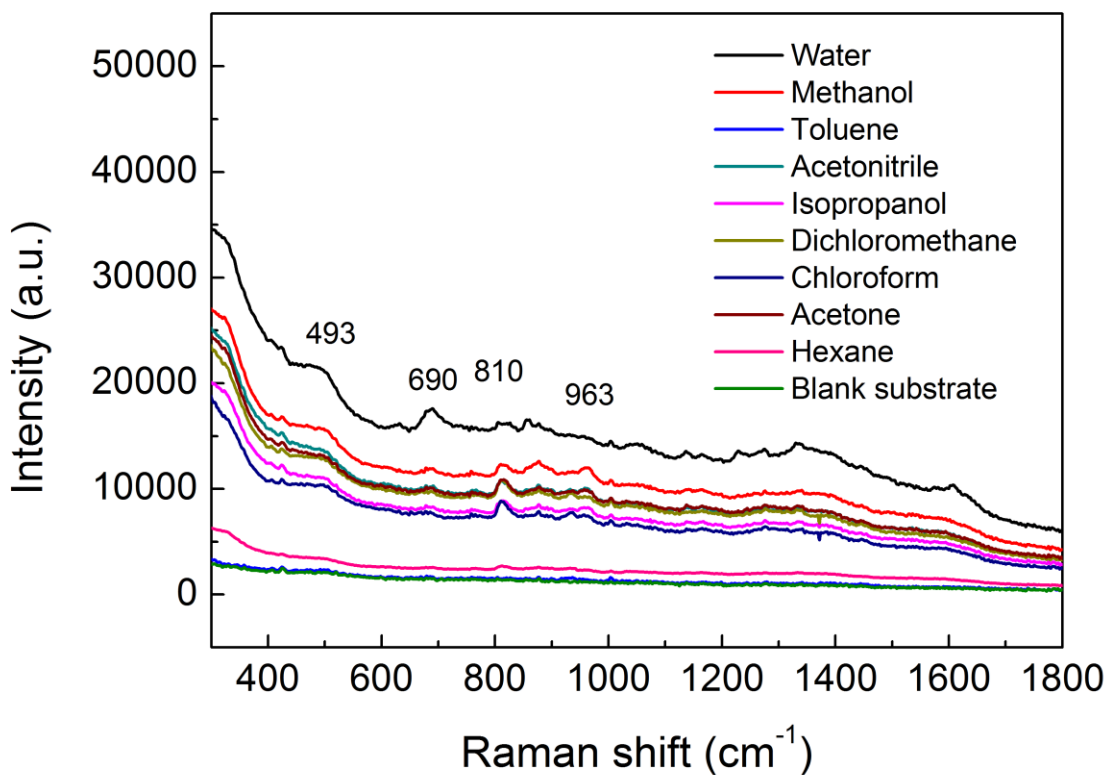


Figure C.5 SERS spectra of common lab solvents on the AgNR substrate.

Part III. UTLC separation using methanol, acetonitrile, hexanes, and dichloromethane

UTLC development using single solvents

Typical UTLC separation using methanol as the mobile phase solvent is shown in Figure C.6a, and the calculated R_f values are given in Table C.2. Satisfactory solvent migration distances of 8 - 10 mm were typically achieved, which were comparable to observations in other studies using engineered UTLC plates [2, 3]. However, little separation was achieved among the PAHs, as all three components migrate to roughly the same distance near the solvent front. The large R_f s, along with the narrow chromatographic bands (confined to a 0.5 mm region) suggest that the PAHs had a much higher affinity to methanol than to the AgNRs. Consequently, an almost complete elution of all sample components occurred. Theoretically, in TLC and HPLC, as the migration distance or elution time increases, the chromatographic bands appear broader due to higher diffusion rates [4]. In the AgNR based UTLC, however, because PAHs can only be poorly adsorbed to silver, little retention was offered by the AgNRs. As a consequence, strong eluents such as methanol could easily bring all PAHs non-selectively to the solvent front.

In contrast, when acetonitrile served as the mobile phase solvent, broader bands were found closer to the original sample spots (Fig. C.6b). This indicates the strength of acetonitrile as an eluent was not as strong as methanol. Unfortunately, the migration distance of acetonitrile was too short (~ 2.5 - 3 mm) for any conclusions to be drawn on the PAH retention behaviors. The chromatographic bands appearing at ~ 1 mm in Figure C.6b were in fact caused by the molecular distribution of the original sample spot: as the samples were first applied onto the AgNR substrate they tend to form coffee ring like spots ~ 1 - 1.5 mm in diameter, thus the SERS intensity of PAHs was expected to be the strongest at ~ 0.5 - 1 mm away from the spot center even without UTLC development. This further emphasizes the importance of choosing strong

wetting solvents for UTLC, since long solvent migration distances of greater than 5 mm was less affected by the size of the initial sample spot.

In this regard, neither dichloromethane nor hexanes could fulfill the requirement on solvent migration distance when used alone (Figs. C.6c-d). The migration distance of dichloromethane was typically 3 - 5 mm. Similar to methanol, all three PAH compounds readily migrated to near the solvent front, though the chromatographic bands appeared much broader than those developed by methanol (Fig. C.6c). Shorter migration distances were found on the hexanes developed substrates. The affinities of BaA, BaP, and P to hexanes were expected to be greater than those to methanol because of their higher solubility in nonpolar solvents. However, since the solvent barely wetted the substrate, no effective elution was achieved (Fig. C.6d).

In addition to acetonitrile, dichloromethane, and hexane, other solvents, such as acetone, tetrahydrofuran, and water also yield poor migration distances which range from 0.5 mm to ~ 4 mm (data not shown). Consequently, in order to ensure an acceptable migration distance, methanol was selected as a primary solvent in the UTLC mobile phase and other solvents were mixed with methanol to adjust the elution strength.

Development using two-component organic mobile phases on unmodified AgNRs

As anticipated, when acetonitrile, hexanes, and dichloromethane were mixed with methanol in the mobile phase, the solvent migration distance was significantly improved from 3 - 5 mm to 6 - 10 mm (representative separation chromatograms are shown in Fig. C.7a-c). The retention of PAHs in these modified mobile phases also demonstrated some differences from that in the one-component mobile phase systems. For example, acetonitrile: methanol 1:1 (v/v) appeared to provide more retention of BaA, and possibly BaP, compared with developing with only methanol (Fig. C.7a vs Fig. C.6a). On the other hand, the R_f values of BaA and BaP in the

binary mobile phase were also consistently greater than those found with acetonitrile alone (Fig. C.7a vs Fig. C.6b). Of course, the total solvent distance could also affect the final calculated R_f values, and the R_f s obtained in acetonitrile might have been higher had the migration distance been longer. Nevertheless, influence of methanol on the chromatographic band width was also obvious: the BaA, BaP, and P bands all appeared narrower in the mixture mobile phase than in acetonitrile alone (Fig. C.7a vs Fig. C.6b). However, these new bands, especially BaA and BaP, still tended to overlap. Band overlapping suggests that the chromatographic separation was still rather poor.

Similar phenomena were found with the mixture of methanol and dichloromethane, although the migration distances were only improved slightly by addition of methanol (4-6 mm in the binary mobile phase vs 4-5 mm in dichloromethane alone). The elution strength of the solvent mixture was not as strong as that of methanol, due to the presence of dichloromethane (Fig. C.7b vs Fig. C.6a). Meanwhile, the BaA and BaP bands also appeared narrower than those developed by dichloromethane alone (Fig. C.7b vs Fig. C.6c). However, band tailing was also observed in P, which made the bands elongate and span a large portion of the migration distance. Furthermore, the PAH bands still overlapped, indicating unsatisfactory separation.

Finally, UTLC development with a mobile phase consisting of methanol and hexane showed significantly improved total migration to 8.5 - 10 mm (Fig. C.7c), compared with 2 - 2.5 developed in hexane only (Fig. C.6d). Retention of the PAHs was consistent with that in hexanes, as P migrated to near the solvent front ($R_f = 0.82$) and BaA and BaP lag behind ($R_f = 0.71$). Interestingly, PAH retention was quite opposite to that observed when methanol alone was used as the mobile phase solvent, in which BaA and BaP migrated to the solvent front and P followed ~ 0.5 mm behind (Fig. C.6a). This suggests that 50% of hexane in the mobile phase

served as a strong modifier that could alter the retention behaviors to a great extent compared with methanol. Still, band elongation was observed in the chromatogram, and the overlapping of BaA and BaP remained unresolved.

In general, it is learned from these experiments that firstly, incorporation of methanol into the mobile phase solvents is necessary for UTLC on the AgNRs, since methanol can significantly improve the overall migration distance as well as narrowing the chromatographic bands. Secondly, the retention behaviors can be manipulated by using binary mobile phase systems instead of a single solvent, but the improvement in UTLC band resolution is minimal.

Table C.2 Retention factors of BaA, BaP, and P on unmodified AgNRs

Solvent	BaA	BaP	P
Methanol	0.94	0.94	0.88
Acetonitrile	0.30	0.20	0.30
Dichloromethane	0.30	0.30	0.40
Hexanes	0.63	0.56	0.56
Methanol: acetonitrile 50:50 (v/v)	0.90	0.93	0.87
Methanol: dichloromethane 67:33 (v/v)	0.71	0.71	0.82
Methanol: hexane 50:50 (v/v)	0.85	0.81	0.77
Methanol: water 50:50 (v/v)	0.06	0.06	0.09
Methanol: water 70:30 (v/v)	0.13	0.13	0.38
Methanol: water 90:10 (v/v)	0.80	0.45	0.80
Methanol: water 95:5 (v/v)	0.74	0.60	0.79

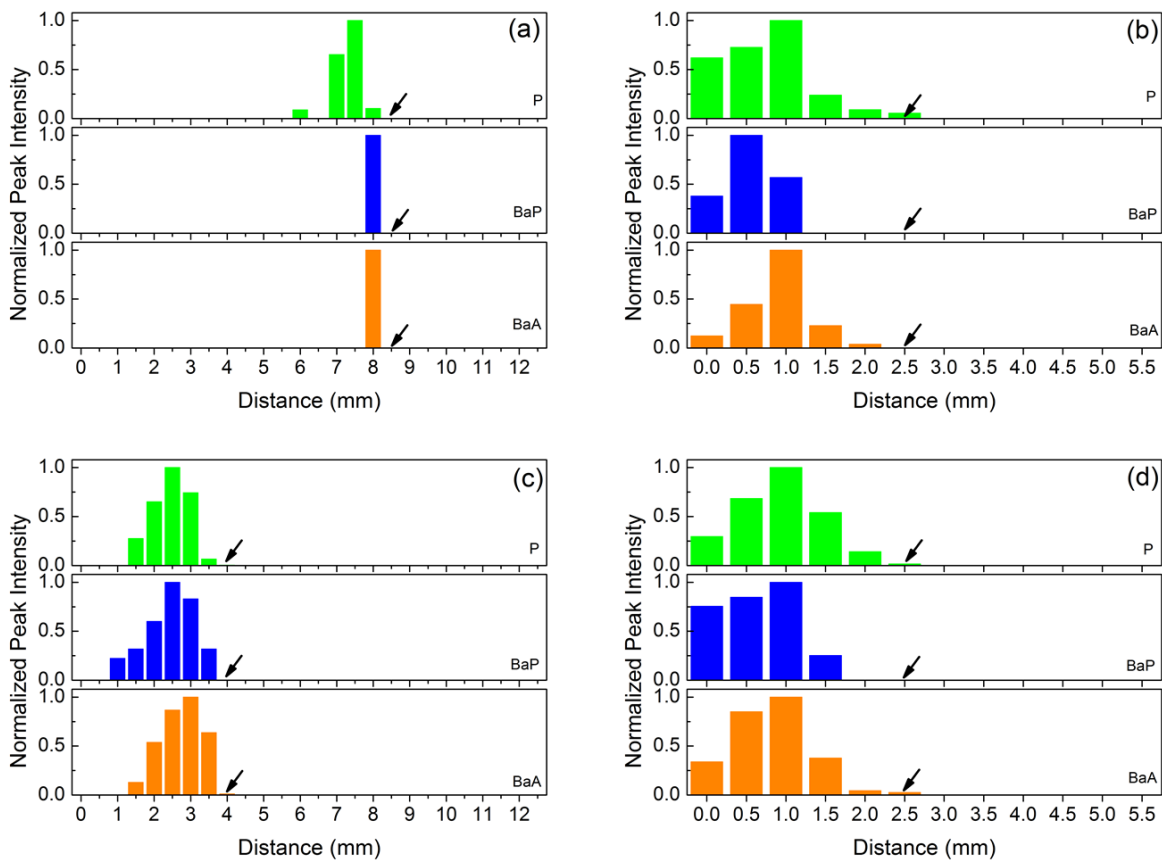


Figure C.6 UTLC separation of BaA, BaP, and P on unmodified AgNR substrates using single solvent systems (a) methanol (b) acetonitrile (c) dichloromethane and (d) hexane as the mobile phase. Black arrows indicate the solvent front measured for each sample spot.

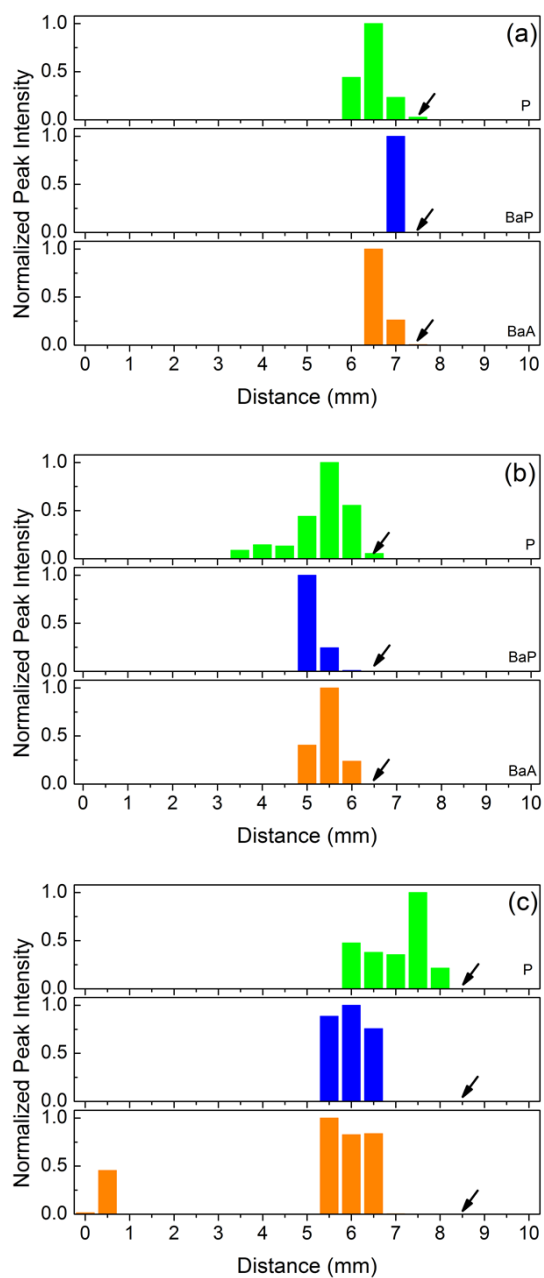


Figure C.7 UTLC separation of BaA, BaP, and P on unmodified AgNR substrates using binary mobile phases (a) methanol: acetonitrile (1:1, v/v) (b) methanol: dichloromethane (2:1, v/v) (c) methanol: hexane (1:1, v/v). Black arrows indicate the solvent front measured for each sample spot.

References

1. Chang, A.S., M. Bora, H.T. Nguyen, E.M. Behymer, C.C. Larson, J.A. Britten, J.C. Carter, and T.C. Bond. *Nanopillars array for surface enhanced Raman scattering*. in *SPIE Defense, Security, and Sensing*. 2011. International Society for Optics and Photonics.
2. Bezuidenhout, L.W. and M.J. Brett, *Ultrathin layer chromatography on nanostructured thin films*. *Journal of Chromatography A*, 2008. **1183**(1-2):179-185.
3. Jim, S.R., M.T. Taschuk, G.E. Morlock, L.W. Bezuidenhout, W. Schwack, and M.J. Brett, *Engineered anisotropic microstructures for ultrathin-layer chromatography*. *Analytical Chemistry*, 2010. **82**(12):5349-5356.
4. Sherma, J. and B. Fried (Eds), *Handbook Of Thin-Layer Chromatography*. Vol. 89. 2003: CRC press.

APPENDIX D

DETECTION OF POLYCYCLIC AROMATIC HYDROCARBONS FROM COOKING OIL USING ULTRA-THIN LAYER CHROMATOGRAPHY AND SURFACE ENHANCED RAMAN SPECTROSCOPY⁴

Supplementary Information

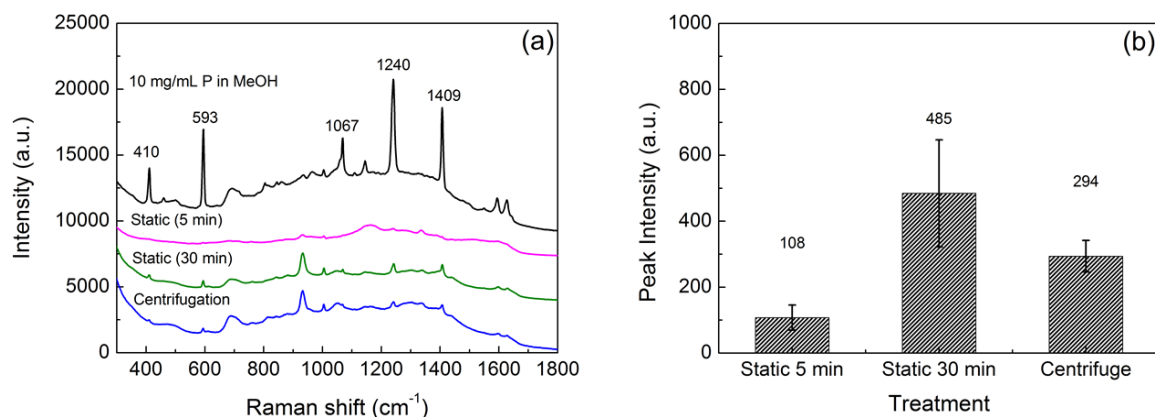


Figure D.1 Effect of partitioning conditions on the SERS intensity of extracted P. (a) SERS spectra of P in standard solution and after extraction and settling under different conditions: static settling for 5 and 30 min, and centrifugation for 1 min at 3000 rpm (b) Corresponding peak intensity at 593 cm⁻¹.

⁴ Jing Chen, Yao-wen Huang, and Yiping Zhao. To be submitted to *Sensors and Actuators B*.

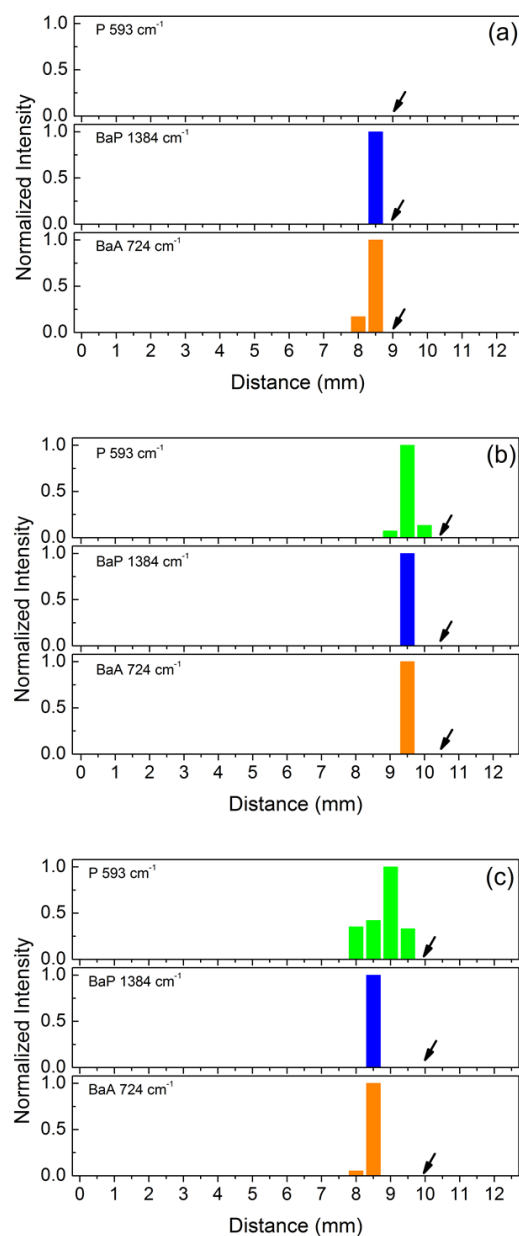


Figure D.2 UTLC-SERS detection of PAHs using methanol on 10 μM ME modified substrates.

(a) UTLC separation of 100 $\mu\text{g/mL}$ PAHs extracted from vegetable oil (b) Separation of 500 $\mu\text{g/mL}$ PAHs extracted from vegetable oil (c) Separation of 1 mg/mL PAHs extracted from vegetable oil

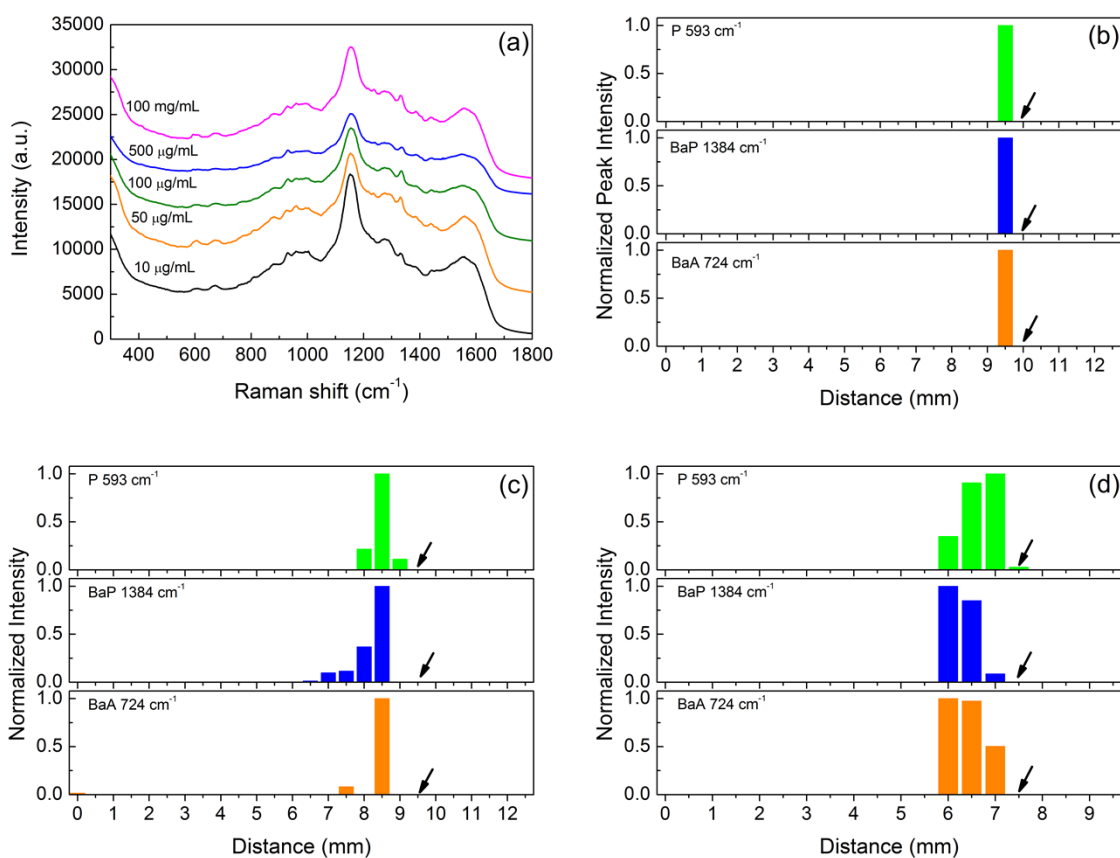


Figure D.3 UTLC-SERS detection of PAHs using methanol: water (80:20, v/v) on unmodified substrates. (a) SERS spectra of PAH extracts from vegetable oil before UTLC (b) UTLC separation of 100 µg/mL PAHs extracted from vegetable oil (c) Separation of 500 µg/mL PAHs extracted from vegetable oil (d) Separation of 1 mg/mL PAHs extracted from vegetable oil